

**DOT/FAA/AR-03/75**

Office of Aviation Research  
Washington, D.C. 20591

# **Damage Resistance and Tolerance of Composite Sandwich Panels— Scaling Effects**

February 2004

Final Report

This document is available to the U.S. public  
through the National Technical Information  
Service (NTIS), Springfield, Virginia 22161.



U.S. Department of Transportation  
**Federal Aviation Administration**

## **NOTICE**

This document is disseminated under the sponsorship of the U.S. Department of Transportation in the interest of information exchange. The United States Government assumes no liability for the contents or use thereof. The United States Government does not endorse products or manufacturers. Trade or manufacturer's names appear herein solely because they are considered essential to the objective of this report. This document does not constitute FAA certification policy. Consult your local FAA aircraft certification office as to its use.

This report is available at the Federal Aviation Administration William J. Hughes Technical Center's Full-Text Technical Reports page: [actlibrary.tc.faa.gov](http://actlibrary.tc.faa.gov) in Adobe Acrobat portable document format (PDF).

1. Report No. DOT/FAA/AR-03/75		2. Government Accession No.		3. Recipient's Catalog No.	
4. Title and Subtitle DAMAGE RESISTANCE AND TOLERANCE OF COMPOSITE SANDWICH PANELS—SCALING EFFECTS				5. Report Date February 2004	
				6. Performing Organization Code	
7. Author(s) John S. Tomblin, K. Suresh Raju, and Gabriel Arosteguy				8. Performing Organization Report No.	
9. Performing Organization Name and Address Wichita State University 1845 North Fairmount Wichita, KS 67260-0093				10. Work Unit No. (TRAIS)	
				11. Contract or Grant No.	
12. Sponsoring Agency Name and Address U.S. Department of Transportation Federal Aviation Administration Office of Aviation Research Washington, DC 20591				13. Type of Report and Period Covered Final Report	
				14. Sponsoring Agency Code ACE-110	
1. Supplementary Notes The FAA William J. Hughes Technical Monitor was Peter Shyprykevich.					
16. Abstract <p>The impact responses and the damage states in flat sandwich panels with thin facesheets are known to be dependent on the diameter of the spherical steel impactor. The residual strength of impact-damaged sandwich panels under static in-plane compressive loads was dependent on the nature of the damage state. The coupon sizes used in these investigations were relatively small, and the finite size effects may be embedded in the observed trends. The effects of scaling the planar dimensions of sandwich specimens on the damage resistance were studied by conducting experiments and finite element analysis. The impact force and the damage size were observed to decrease as both the planar dimensions were increased. These effects were negligible when only a single dimension was scaled. The off-center impacts indicated that for a given energy level, the impacts occurring closer to the boundary supports were more severe compared to those farther away from the boundaries. The impacts on sandwich specimens supported by a rigid base proved to be the most severe case in terms of the impact behavior and the resulting damage metrics. The parametric study conducted using the finite element model confirmed the observed experimental trends and further indicated that the damage formation is the dominant energy dissipation mechanism when the ratio of the impactor mass to that of the target is greater than 2 and vibrational energy transfer is dominant for ratios less than 2.</p> <p>The effects of the ratio of specimen width to planar damage size on the compressive residual strength and failure modes were investigated for two sandwich configurations. A subsurface damage state was considered for the study and inflicted using a 3" diameter impactor. The scaling effects were characterized in terms of the residual strength and strain distributions in the vicinity of the damage region. The latter was measured using a photogrammetry method. The residual strength was found to increase by 12% when the ratio of the specimen size to damage size was increased from 4.6 to 12.4 for sandwich specimens with two-ply facesheets. No trends were, however, observed for sandwich specimens with four-ply facesheets. The strain and displacement distributions indicated bending of the facesheet within the damage region leading to a strain concentration-driven failure mode resembling an open hole configuration for the two-ply facesheet sandwich panels. The 6.5" wide sandwich specimens with four-ply facesheets failed by global buckling initiated by an unstable dimple propagation. For wider specimens, there was a dimple growth-arrest mechanism that lead to eventual facesheet fracture. The increase of the specimen height resulted in a slight decrease in residual strength.</p> <p>This study showed that the results obtained from small specimens are valid as far as the compressive residual strength obtained experimentally. However, larger specimen sizes will sustain less impact damage for equivalent impact energy levels. Thus, it is valid to test smaller panels if the damage is simulated correctly from the larger specimens. The effects of specimen height were not investigated but could effect the buckling response of the panels.</p>					
17. Key Words Composites, Sandwich, Scaling, Damage resistance, Damage tolerance, Testing			18. Distribution Statement This document is available to the public through the National Technical Information Service (NTIS), Springfield, Virginia 22161.		
19. Security Classif. (of this report) Unclassified		20. Security Classif. (of this page) Unclassified		21. No. of Pages 70	22. Price

## TABLE OF CONTENTS

	Page
EXECUTIVE SUMMARY	ix
1. INTRODUCTION	1
2. IMPACT TESTING OF SANDWICH PANELS	6
2.1 Characterization of Scaling Effects Based on Impact Event	9
2.1.1 Impacts at the Geometric Center	9
2.1.2 Off-Center Impacts	13
2.2 Characterization of Scaling Effects Based on Impact Damage	13
3. FINITE ELEMENT ANALYSIS OF SCALING EFFECTS ON IMPACT RESISTANCE	18
3.1 FINITE ELEMENT MODELING OF SANDWICH IMPACT	19
3.1.1 Contact Behavior of Sandwich Panels and Contact Laws	20
3.1.2 Comparison With Experimental Data	22
3.2 Parametric Study	24
4. SCALING EFFECTS ON THE CAI STRENGTH OF SANDWICH PANELS	27
4.1 Compression Testing of Sandwich Panels	29
4.2 Results	34
4.2.1 Analysis of Displacement and Strain Distributions in [(90/45)/CORE] <sub>s</sub> Sandwich Panels	35
4.2.2 Analysis of Displacement and Strain Distributions in [(90/45) <sub>2</sub> /CORE] <sub>s</sub> Sandwich Panels	38
5. CONCLUSIONS	41
6. REFERENCES	42
APPENDICES	
A—Force-Time Histories	
B—Displacement and Strain Profiles Using ARAMIS	

## LIST OF FIGURES

Figure		Page
1	Typical Coupon Sizes Used by Previous Investigators	1
2	Compressive Residual Strength Behavior of Impact-Damaged Sandwich Panels	3
3	Normalized Compression-After-Impact Strengths of Sandwich Panels With Different Levels of Impact Damage and Associated Width to Damage Size Ratios	3
4	Comparison of Normalized Residual Indentation as a Function of $b/2R_{damage}$ Ratios in Different Sandwich Configurations Impacted With 1" and 3" Impactors	4
5	Geometric Scaling Associated With the Impact on Sandwich Panels and Geometric Scaling Addressed in the Present Investigation	6
6	Specimen Geometry and Impact Locations Used in the Study	7
7	(a) Test Fixture for Specimen Size 16" × 16" Showing Off-Center Impact, (b) Test Fixture for Specimen Size 12" × 24", and (c) Test Fixture for Specimen Size 12" × 48"	8
8	Force-Time History for [(90/45)/CORE] <sub>s</sub> Sandwich Panels Impacted at Energy Level E <sub>1</sub> , When Both Planar Dimensions are Scaled	9
9	Force-Time History for [(90/45)/CORE] <sub>s</sub> Sandwich Panels Impacted at Energy Level E <sub>1</sub> , When One Planar Dimension Is Scaled	10
10	Force-Time History for [(90/45) <sub>2</sub> /CORE] <sub>s</sub> Sandwich Panels Impacted at Energy Level E <sub>1</sub> , When Both Planar Dimensions Are Scaled	10
11	Force-Time History for [(90/45) <sub>2</sub> /CORE] <sub>s</sub> Sandwich Panels Impacted at Energy Level E <sub>1</sub> , When One Planar Dimension Is Scaled	11
12	Peak Impact Force for [(90/45)/CORE] <sub>s</sub> Sandwich Panels at Different Energy Levels	11
13	Peak Impact Force for [(90/45) <sub>2</sub> /CORE] <sub>s</sub> Sandwich Panels at Different Energy Levels	12
14	Variation of Fundamental Frequency for Sandwich Panels as a Function of Planar Dimensions Showing the Relative Frequencies of the Panel Sizes Used in This Study	12
15	Summary of Peak Impact Force for Off-Center Impacts	13

16	Summary of TTU C-Scan Planar Damage Size for [(90/45)/CORE] <sub>s</sub> Sandwich Panels at Different Energy Levels	14
17	Summary of Residual Indentations for [(90/45)/CORE] <sub>s</sub> Sandwich Panels at Different Energy Levels	14
18	Summary of TTU C-Scan Planar Damage Size for [(90/45) <sub>2</sub> /CORE] <sub>s</sub> Sandwich Panels at Different Energy Levels	15
19	Summary of Residual Indentations for [(90/45) <sub>2</sub> /CORE] <sub>s</sub> Sandwich Panels at Different Energy Levels	15
20	Summary of TTU C-Scan Planar Damage Size for Off-Center Impacts	16
21	Summary of Residual Indentations for Off-Center Impacts	16
22	TTU C-Scan Plots for [(90/45)/CORE] <sub>s</sub> Sandwich Panels Impacted at Different Locations With an Impact Energy of 58 lbf-in	17
23	TTU C-Scan Plots for [(90/45)/CORE] <sub>s</sub> Sandwich Panels Impacted at Different Locations With an Impact Energy of 135 lbf-in	17
24	TTU C-Scan Plots for [(90/45) <sub>2</sub> /CORE] <sub>s</sub> Sandwich Panels Impacted at Different Locations With an Impact Energy of 58 lbf-in	17
25	TTU C-Scan Plots for [(90/45) <sub>2</sub> /CORE] <sub>s</sub> Sandwich Panels Impacted at Different Locations With an Impact Energy of 135 lbf-in	18
26	Representation of the Contact-Impact Problem Using Contact Laws	20
27a	Typical Loading Response of Sandwich Panels Subjected to Static Indentation Using Spherical Indentors	21
27b	Typical Unloading Response of Sandwich Panels Subjected to Static Indentation Using Spherical Indentors	22
28	Comparison of FE Model and Dobyns Model Predictions With Experimental Data	23
29	Linearized Contact Behavior Used in the Parametric Study	24
30	Finite Element Model Predictions for Fraction of Impact Energy Absorbed for Sandwich Panels With Different Contact Energy Dissipation Fractions	26
31	Finite Element Model Predictions for Energy Absorbed by Sandwich Panels Due to Creation of Damage With Different Contact Energy Dissipation Fractions	26

32	Typical Impact Damage and Associated Metrics in Sandwich Panels With Thin Facesheets Impacted With Blunt Impactors	27
33	General Scaling of Metrics in Damage Tolerance Problem of Sandwich Panels and Scaling Problem Addressed in this Study	28
34	Compression Test Fixture With Sandwich Specimen 16.5" Wide by 10.5" High	30
35	Compression Test Fixture With Sandwich Specimen 12.5" Wide by 16.5" High	30
36	Typical Aramis System and Aramis Arrangement for Compression Testing	31
37	Location of Strain Gages and Scan Region for Photogrammetry Measurements	31
38	Typical Out-of-Plane Displacement Distribution, $w(x,y)$ , and In-Plane Strain Distributions, $\epsilon_{Yy}(x,y)$ , Measured Using Aramis Photogrammetry System	32
39	Measured Displacement and Strain Distributions Across a Horizontal Section Passing Through the Damage Region for $[(90/45)/CORE]_s$ Sandwich Specimens With Width, $b = 6.5"$ , at Different Load Levels	33
40	Plot of Compressive Residual Strength as a Function of $b/2R_{damage}$	34
41	Plot of Compressive Residual Strength as a Function of $h/2R_{damage}$	35
42a	Strain Distribution in $[(90/45)/CORE]_s$ Sandwich Panels at Nominal Load of 450 lbf/in	36
42b	Strain Distribution in $[(90/45)/CORE]_s$ Sandwich Panels at Nominal Load of 550 lbf/in	36
42c	Strain Distribution in $[(90/45)/CORE]_s$ Sandwich Panels at Nominal Load of 650 lbf/in	37
42d	Strain Distribution in $[(90/45)/CORE]_s$ Sandwich Panels at Nominal Load of 730 lbf/in	37
42e	Out-of-Plane Displacement Distribution in $[(90/45)/CORE]_s$ Sandwich Panels at Nominal Load of 730 lbf/in	38
43a	Strain Distribution in $[(90/45)_2/CORE]_s$ Sandwich Panels at Nominal Load of 800 lbf/in	39
43b	Strain Distribution in $[(90/45)_2/CORE]_s$ Sandwich Panels at Nominal Load of 1000 lbf/in	39

43c	Strain Distribution in $[(90/45)_2/\text{CORE}]_s$ Sandwich Panels at Nominal Load of 1200 lbf/in	40
43d	Strain Distribution in $[(90/45)_2/\text{CORE}]_s$ Sandwich Panels at Nominal Load of 1600 lbf/in	40

## LIST OF TABLES

Table		Page
1	Test Matrix to Study the Scaling Effects on Damage Resistance	7
2	Test Matrix for Scaling Effects on Damage Tolerance of Sandwich Panels	29
3	Damage Metrics for Sandwich Specimens	29

## EXECUTIVE SUMMARY

The impact responses and the damage states in flat sandwich panels with thin facesheets are known to be dependent on the diameter of the spherical steel impactor. The residual strength of impact-damaged sandwich panels under static in-plane compressive loads was dependent on the nature of the damage state. The coupon sizes used in these investigations were relatively small, and the finite size effects may be embedded in the observed trends. The effects of scaling the planar dimensions of sandwich specimens on the damage resistance were studied by conducting experiments and finite element (FE) analysis. The impact force and the damage size were observed to decrease as both the planar dimensions were increased. These effects were negligible when only a single dimension was scaled. The off-center impacts indicated that for a given energy level, the impacts occurring closer to the boundary supports were more severe compared to those farther away from the boundaries. The impacts on sandwich specimens supported by a rigid base proved to be the most severe case in terms of the impact behavior and the resulting damage metrics. The parametric study conducted using the FE model confirmed the observed experimental trends and further indicated that the damage formation is the dominant energy dissipation mechanism when the ratio of the impactor mass to that of the target is greater than 2 and vibrational energy transfer is dominant for ratios less than 2.

The effects of the ratio of specimen width to planar damage size on the compressive residual strength and failure modes were investigated for two sandwich configurations. A subsurface damage was considered that was inflicted using a 3" diameter impactor. The scaling effects were characterized in terms of the residual strength and strain distributions in the vicinity of the damage region. The latter was measured using a photogrammetry method. The residual strength was found to increase by 12% when the ratio of the specimen size to damage size was increased from 4.6 to 12.4 for sandwich specimens with two-ply facesheets. No trends were, however, observed for sandwich specimens with four-ply facesheets. The strain and displacement distributions indicated bending of the facesheet within the damage region leading to a strain concentration-driven failure mode resembling an open-hole configuration for the two-ply facesheet sandwich panels. The 6.5" wide sandwich specimens with four-ply facesheets failed by global buckling initiated by an unstable dimple propagation. For wider specimens, there was a dimple growth-arrest mechanism that lead to eventual facesheet fracture. The increase of the specimen height resulted in a slight decrease in residual strength.

This study showed that the results obtained from small specimens are valid as far as the compressive residual strength obtained experimentally. However, larger specimen sizes will sustain less impact damage for equivalent impact energy levels. Thus, it is valid to test smaller panels if the damage is simulated correctly from the larger specimens. The effects of specimen height were not investigated but could affect the buckling response of the panels.

## 1. INTRODUCTION.

The damage sustained due to localized accidental loadings has been shown to be a limiting constraint in the design of a sandwich airframe structure. Thin facesheets with relatively compliant cores make these sandwich structures vulnerable to impact damage. The low-velocity impact events have been shown [1] to produce very distinct damage states which are governed by the impactor size. The damage states may vary from clearly visible, severe, localized skin damage to extensive core damage without any external indications, making it difficult to detect [1]. The latter damage states, which are typical of blunt impactors, were found to degrade the residual strength under compressive loading by up to 60% [1].

Even though the previous experimental investigations provided the overall trends associated with the behavior of sandwich panels under impact loads, resulting damage states, and residual strength properties, the observations have been limited to laboratory coupons with idealized boundary conditions. Most previous experimental investigations used coupons of arbitrary planar dimensions, the maximum size being limited by the laboratory test equipment and the high cost associated with prototypes. The typical test sections (for impact testing) used for sandwich coupons by several investigators are summarized in figure 1. The damage resistance characteristics exhibited by these laboratory coupons within the range of impact energy levels investigated may not reflect that of airframe structures, which are typically several times larger than these coupons. The boundary conditions used in these investigations make the coupons much stiffer in global bending, thereby, the local contact stiffness dictated the impact behavior. Thus, the behavior was more representative of laminates and sandwich panels with a substructure (stiffener, frame, etc.) behind (or in the vicinity of) the point of impact and may not adequately describe the behavior of monocoque sandwich structures prevalent in new generation general aviation airframes. Further, it is important to understand if the damage states existing for a given impact energy range, in the small coupons, translate to those which would have occurred in a larger structure.

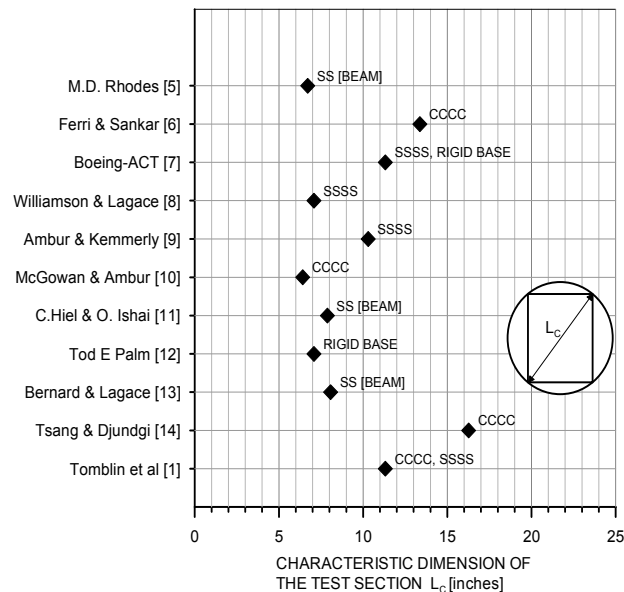


FIGURE 1. TYPICAL COUPON SIZES USED BY PREVIOUS INVESTIGATORS

Morton [2] investigated the scaling effects on the impact responses for laminated beams using dimensional analysis. The classical scaling laws were shown to apply for elastic behavior of transversely impacted carbon fiber-reinforced epoxy beams. Morton found that the impact duration scaled as the scale factor and the impact force as the scale factor squared. Swanson [3] reported that the knowledge of the failure mechanisms involved was required to predict the scaling of impact damage. Based on the impact tests on laminated plates and cylinders, Swanson observed complex scaling behavior of impact damage. Delamination was found to depend on the absolute specimen size, whereas the fiber breakage depended only on the applied stresses, independent of the specimen size. Qian, et al. [4] conducted an experimental investigation to determine the accuracy of scaling rules for impact damage in carbon/epoxy laminated plates. The results indicated that the overall structural response prior to substantial damage followed the scaling rules quite closely. The formation of damage was found to be more complicated, demonstrating an apparent dependence on scale consistent with fracture mechanics. Unlike laminated plates, the sandwich structures, especially those with thin quasi-isotropic facesheets [1], have been reported to suffer extensive core damage with little or no facesheet delaminations when impacted with blunt impactors. The scaling effects associated with the behavior of sandwich structures have to be addressed to leverage the application of the existing knowledge base to the design of airframe structures.

The damage tolerance of sandwich structures has been typically quantified using in-plane compression tests. The residual strength has been observed [1] to be a strong function of the planar damage area, as shown in figure 2. The residual strength was reported to approach an asymptote with increasing planar damage size. The specimens impacted with a larger-diameter (3") impactor populated the asymptotic region of the residual strength degradation curve, whereas the specimens impacted with a smaller-diameter (1") impactor populated the initial region of the curve. It should be noted that the specimen width  $b$  (and height  $h$ ) were held constant for all the tests, irrespective of the damage size. Thus, the ratio  $b/2R_{damage}$  (where  $2R_{damage}$  is the average (through-the-thickness) planar diameter of the impact-damaged region) may vary between specimens with different damage sizes that are caused by different energy levels. The variation of  $b/2R_{damage}$  for different sandwich configurations investigated in a previous study is illustrated in figure 3. The relative values of  $b/2R_{damage}$  are illustrated using different symbol sizes. The larger symbols shown in figure 3 represent the higher  $b/2R_{damage}$  ratio. The initial portion of the residual strength distributions are typically populated by specimens with higher  $b/2R_{damage}$  ratios, and this ratio decreases as the asymptotic region is approached. The logical question arising is whether the residual strength asymptote is a conservative estimate based on the existing experimental data. The finite width effects or the scaling of  $b/2R_{damage}$  ratio on the residual strength of sandwich structures, especially in the asymptotic region, will be of particular interest to the designer when using the existing residual strength data.

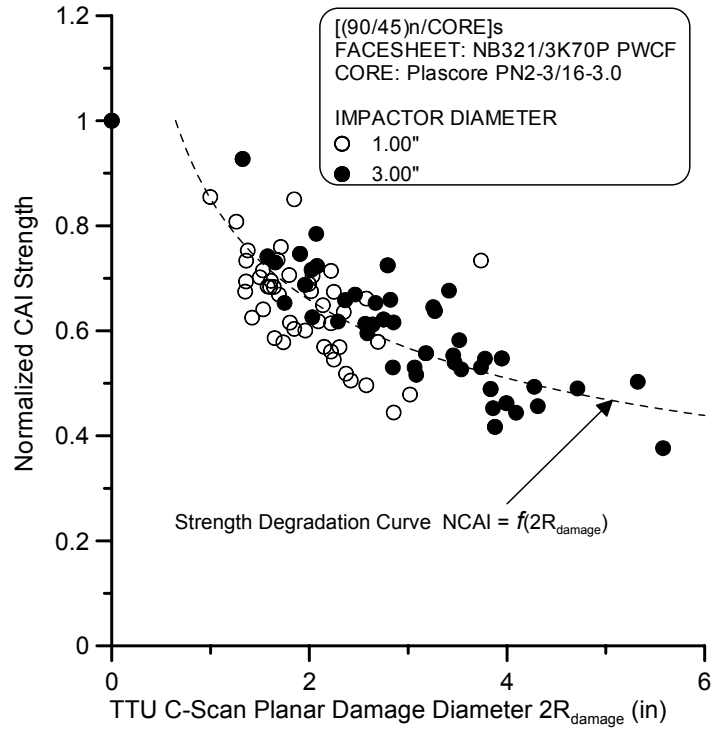


FIGURE 2. COMPRESSIVE RESIDUAL STRENGTH BEHAVIOR OF IMPACT-DAMAGED SANDWICH PANELS [1]

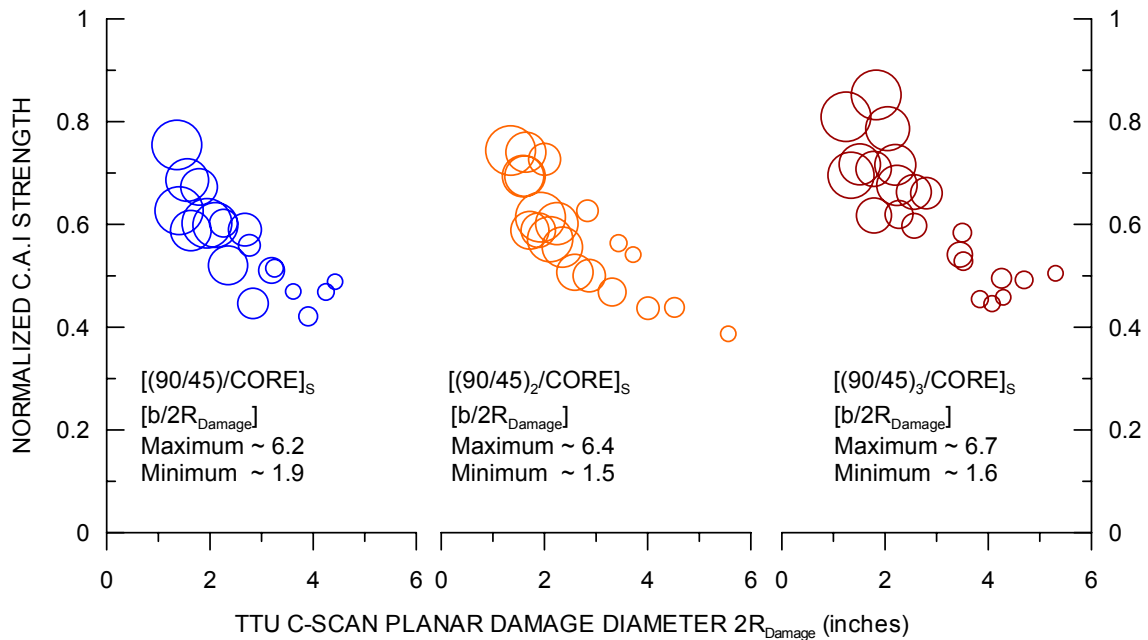


FIGURE 3. NORMALIZED COMPRESSION-AFTER-IMPACT STRENGTHS OF SANDWICH PANELS WITH DIFFERENT LEVELS OF IMPACT DAMAGE AND ASSOCIATED WIDTH TO DAMAGE SIZE RATIOS

The scaling effects associated with the damage tolerance of impact-damaged sandwich panels have not been well addressed in open literature. Previous investigations [15 and 16] on open-hole laminates have indicated that the ratio of specimen width to hole diameter ( $w/D$ ) would influence the residual strength under in-plane tensile and compressive loads. The studies indicated that the strength of the laminates were sensitive to the  $w/D$  ratios, for  $w/D \leq 4$ . The observations on solid laminates may not be easily extended to sandwich structures with subsurface damage states, as the facesheet within the damaged region may facilitate a significant amount of load transfer unlike the open-hole configuration. The amount of residual indentation can influence the fraction of load that can be transferred through the damaged region and dictate the final failure mode [1]. It can be observed from figure 4 that most of the impact damage states due to the 1" impactor possesses a  $b/2R_{damage}$  ratio of 4 or higher, while the ratio for impact damage states due to the 3" impactor were observed to be less than 4 in most cases. However, the key difference between these two damaged states was the amount of associated residual indentation depth, which is presented in terms of the ratio  $t_{facesheet}/\Delta_{RMAX}$ , where  $t_{facesheet}$  is the facesheet thickness and  $\Delta_{RMAX}$  is the maximum residual indentation depth. The impact damage due to a 1" impactor was typically accompanied by indentation depths that were up to ten times the facesheet thickness, indicating significant loss of load-carrying capability through the damage zone and, thus, may more closely represent an open-hole configuration. Thus, it can be argued that the initial portions of the residual strength curves are free of finite width effects. The residual indentation depths associated with impact damage due to a larger impactor were in most cases less than the facesheet thickness, except in cases where facesheet fractures were observed [1]. Since the width to damage size ratio for most of these damage states is less than 4, additional test data with higher  $b/2R_{damage}$  ( $> 4$ ) may be necessary to establish the conservatism associated with existing data. Thus, the 3" impactor was selected for the scaling study.

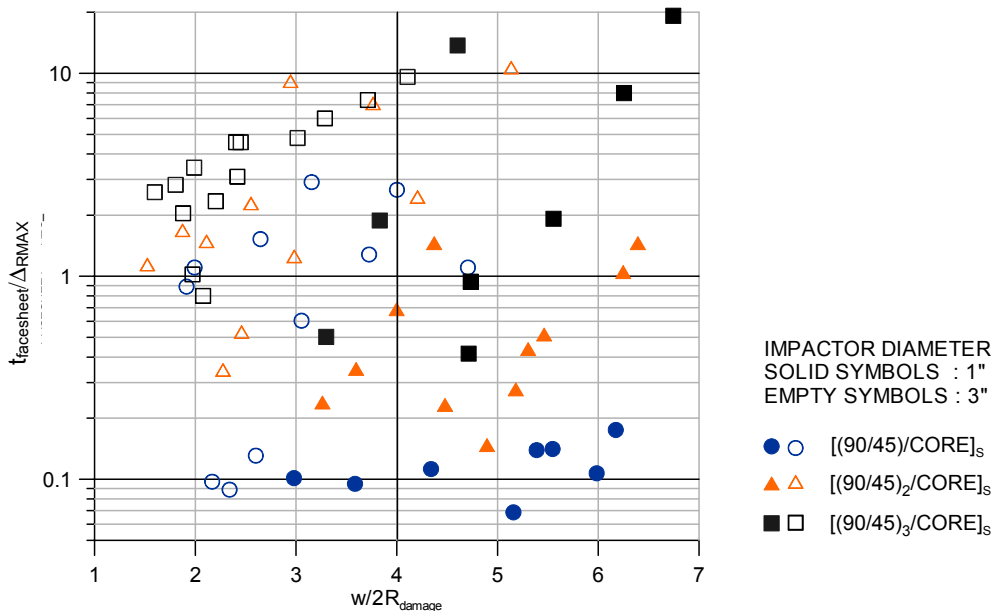


FIGURE 4. COMPARISON OF NORMALIZED RESIDUAL INDENTATION AS A FUNCTION OF  $b/2R_{damage}$  RATIOS IN DIFFERENT SANDWICH CONFIGURATIONS IMPACTED WITH 1" AND 3" IMPACTORS [1]

In an effort to augment the existing test data for use in the design, the scaling issues associated with the impact resistance and damage tolerance of sandwich structures were undertaken. The effect of geometric scaling of the planar dimensions of sandwich panels on the impact resistance of sandwich panels was studied experimentally. Sandwich configurations  $[(90/45)/CORE]_s$  and  $[(90/45)_2/CORE]_s$  with a 0.75" thick Nomex honeycomb core were impacted at four energy levels with a 3" diameter impactor. The experimental study indicated that the peak impact force, planar damage size, and residual indentation depth decrease with increasing panel dimensions. However, the above quantities were quite insensitive when only one of the planar dimensions was changed. Further, off-center impact tests indicated increasing damage metrics and loss of symmetry of the damage region as the impact location approached the boundary supports. The experimental trends were further corroborated using finite element (FE) models, which used experimentally determined contact laws, reported by Raju [17]. The model was also used along with linearized contact laws to study the energy dissipation in sandwich panels. The energy dissipation was observed to be dominated by the damage process for smaller coupons, while the kinetic energy transfer governed the energy absorption as the panel size increased.

A limited number of compression-after-impact (CAI) tests were conducted on the aforementioned sandwich configurations to study the finite width and height effects. The sandwich specimens were subjected to impact damage at a fixed energy level using a 3" diameter impactor. The planar damage size was held constant, while the width of the specimens were varied from 6.5" to 16.5", which provided specimen width to damage size ratios between 4.2 and 12 for  $[(90/45)/CORE]_s$  and 3.2 and 8 for  $[(90/45)_2/CORE]_s$  sandwich panels. A full-field displacement and strain measurement photogrammetry system was used to monitor the displacement and strain distributions during the tests. In summary, the following issues were addressed in this investigation:

- a. What are the effects of planar geometric scaling on the impact resistance and resulting damage metrics in sandwich panels with thin facesheets impacted by a 3" impactor?
- b. How does the impact location affect the impact resistance?
- c. Damage Tolerance: What are the scaling effects associated with the geometric scaling of the panel width and height with respect to a fixed impact damage state?

The effects of geometric scaling on the impact behavior of sandwich panels and the resulting damage metrics were investigated by conducting a limited number of experiments and FE modeling. The geometric scaling of sandwich structures strictly implies that all the geometric quantities, i.e., facesheet thickness, core thickness, and the planar dimensions, are scaled proportionally, as shown in figure 5. However, in most airframe structures employing sandwich construction with thin facesheets, the scaling is associated with the planar dimensions only. Therefore, in the present investigation, the effects of scaling the planar dimensions of the sandwich panels were addressed. The present investigation on damage resistance was divided into two parts. In the first part, the scaling effects on the impact resistance and damage metrics were studied by conducting experiments on sandwich specimens. In the following study, an FE

model was assembled and used to study the effects of panel sizes beyond the current test capabilities. The details and the results of these two studies are described and summarized in the following sections.

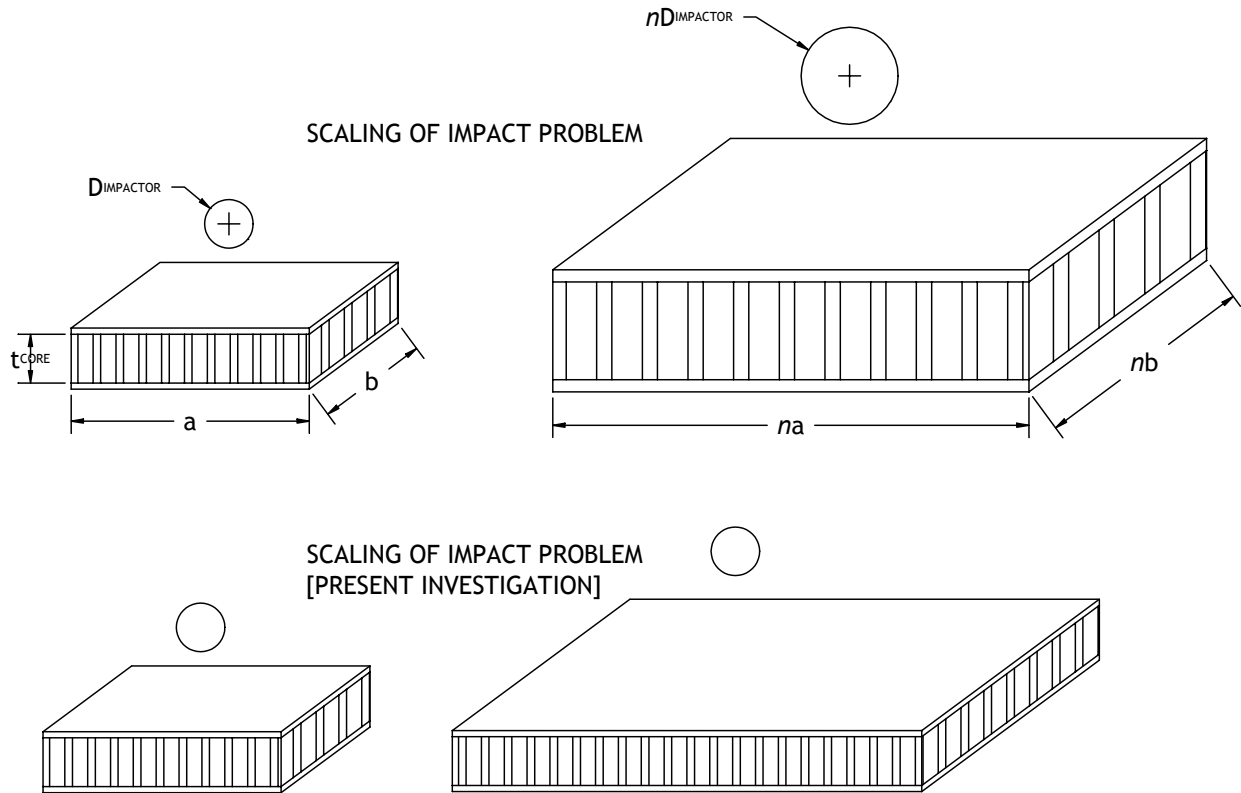


FIGURE 5. GEOMETRIC SCALING ASSOCIATED WITH THE IMPACT ON SANDWICH PANELS AND GEOMETRIC SCALING ADDRESSED IN THE PRESENT INVESTIGATION

## 2. IMPACT TESTING OF SANDWICH PANELS.

The impact testing of sandwich panels of different planar sizes was carried out to investigate the scaling effects on impact responses and damage metrics. The sandwich panels were fabricated using a Newport NB321/3K70 plain weave carbon fabric prepreg for the facesheets and a Plascore® PN2-3/16-3.0 Nomex™ 0.75" thick honeycomb material for the sandwich core. The sandwich lay-up configurations used in the study were  $[(90/45)/CORE]_S$  and  $[(90/45)_2/CORE]_S$ . The facesheets were bonded to the core using Hysol 9628.060 PSF NW film adhesive and cured using a cocure-cobond autoclave process [1].

The test matrix for studying the scaling effects on the impact resistance is summarized in table 1. The specimens were impacted at their geometric centers and at other locations, as illustrated in figure 6. Four distinct energy levels based on previous experience [1] were used to produce subsurface damage states. The sandwich panel geometries included square test sections as well as rectangular test sections. Clamped edge boundary conditions were used along the four edges

for all specimen sizes, and an additional rigid-base support condition was included to represent impact on the sandwich structure in the immediate vicinity or on top of a frame or a bulkhead. The rigid-base support represents the extreme case of infinite global-bending stiffness, resulting in an impact response that is governed completely by the local contact mechanism. The test program also included off-center impacts for the 16" × 16" test section to study the influence of the presence of boundary supports close to the impact location. A total of 28 impact tests were conducted per sandwich configuration (56 tests overall).

TABLE 1. TEST MATRIX TO STUDY THE SCALING EFFECTS ON DAMAGE RESISTANCE

Test Section a × b (inches)		8 × 8	12 × 12	16 × 16	12 × 24	12 × 48
Boundary Condition		Clamped & Rigid Base	Clamped	Clamped	Clamped	Clamped
Impact Location	(a/2,b/2)	4 clamped & 4 Rigid Base	4	4	4	4
	(a/4,b/2)			2		
	(a/8,b/2)			2		

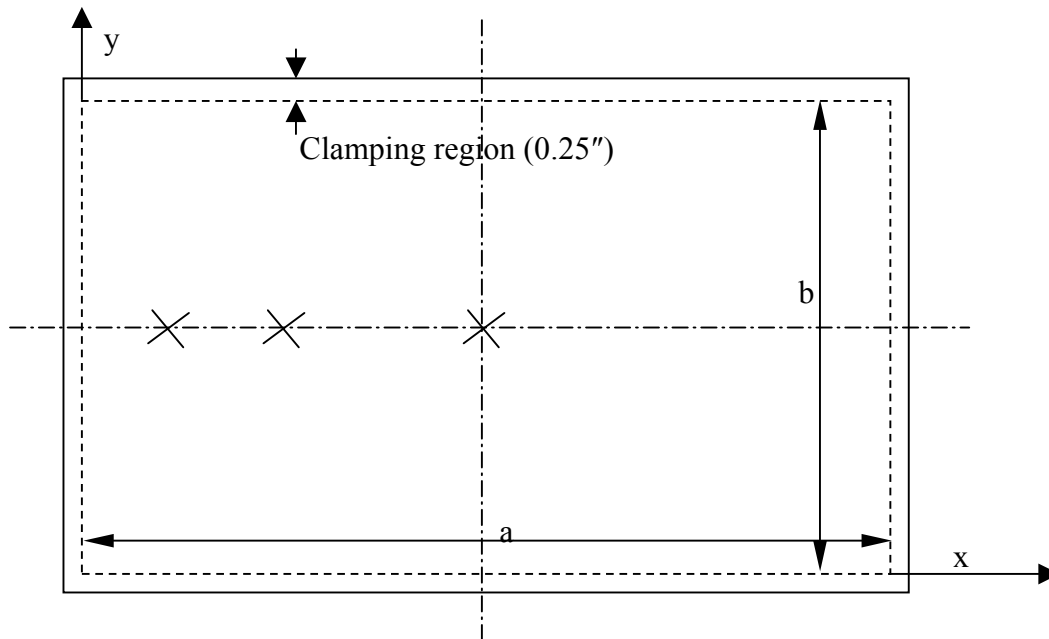
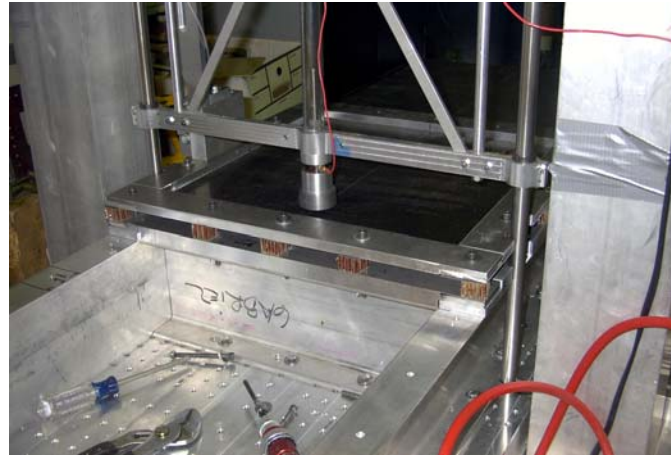


FIGURE 6. SPECIMEN GEOMETRY AND IMPACT LOCATIONS USED IN THE STUDY

The sandwich panels were impacted using a drop-weight impact tester with a nominal impact velocity of 96.6 in/sec (12" drop height). The impact test fixtures used in this study for different specimen sizes are shown in figure 7. Since the impact velocity was fixed, the different energy levels were achieved by changing the impactor mass. The ratio of the impactor mass to the

sandwich panel mass (referred to as the mass ratio) was, therefore, not constant for all the tests. The mass ratios ranged between 4 and 59 for sandwich panels with two-ply facesheets and between 1.57 and 38 for sandwich panels with four-ply facesheets. Thus, the impact tests in this investigation represent quasi-static impacts rather than wave-controlled impacts.



(a)



(b)



(c)

FIGURE 7. (a) TEST FIXTURE FOR SPECIMEN SIZE 16" × 16" SHOWING OFF-CENTER IMPACT, (b) TEST FIXTURE FOR SPECIMEN SIZE 12" × 24", AND (c) TEST FIXTURE FOR SPECIMEN SIZE 12" × 48"

The sandwich specimens were impacted with predetermined energy levels, based on previous studies. The sandwich panels were impacted with nominal impact energy levels of 58, 96, 135, and 157 lbf-in. The impact force history was recorded during each test and the data analyzed to obtain the time histories of displacement, velocity, and energy. The impacted sandwich panels were then subjected to nondestructive damage inspections using Through-Transmission

Ultrasonic (TTU) C-scan equipment and residual indentation depth measurement. The effects of scaling were characterized in terms of the peak impact force, duration of impact, planar damage size, and maximum residual indentation depth, with the results summarized in the following sections.

## 2.1 CHARACTERIZATION OF SCALING EFFECTS BASED ON IMPACT EVENT.

### 2.1.1 Impacts at the Geometric Center.

The effect of scaling the planar dimensions of sandwich panels was characterized using the force-time histories at the four energy levels. The typical force-time histories for  $[(90/45)/CORE]_s$  and  $[(90/45)_2/CORE]_s$  sandwich panels at the first energy level ( $E_1 = 58$  lbf-in) are presented in figures 8 through 11. The force-time history plots for square specimens and rectangular specimens have been plotted separately for clarity. The plots indicate that the specimens with rigid-base supports induce the highest impact force and the lowest contact duration for both sandwich configurations. The impact forces reduce with the increasing specimen planar size (both dimensions) with a corresponding increase in duration of impact. The change of specimen dimension along a single direction, however, did not introduce significant differences in responses, as illustrated in figures 9 and 11. The no time histories of force for all impact tests can be found in appendix A.

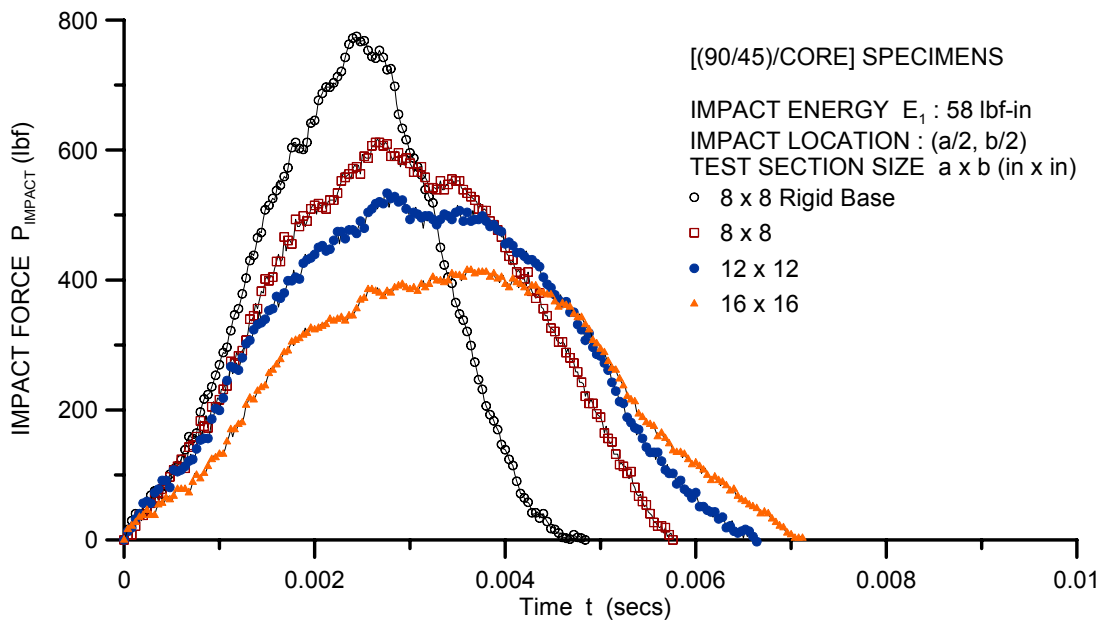


FIGURE 8. FORCE-TIME HISTORY FOR  $[(90/45)/CORE]_s$  SANDWICH PANELS IMPACTED AT ENERGY LEVEL  $E_1$ , WHEN BOTH PLANAR DIMENSIONS ARE SCALED

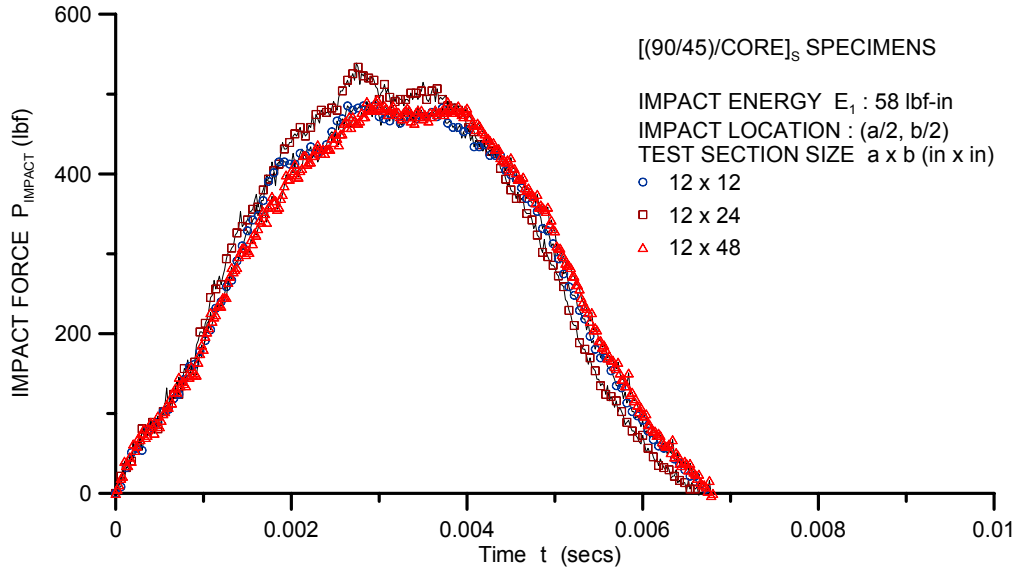


FIGURE 9. FORCE-TIME HISTORY FOR  $[(90/45)/CORE]_s$  SANDWICH PANELS IMPACTED AT ENERGY LEVEL  $E_1$ , WHEN ONE PLANAR DIMENSION IS SCALED

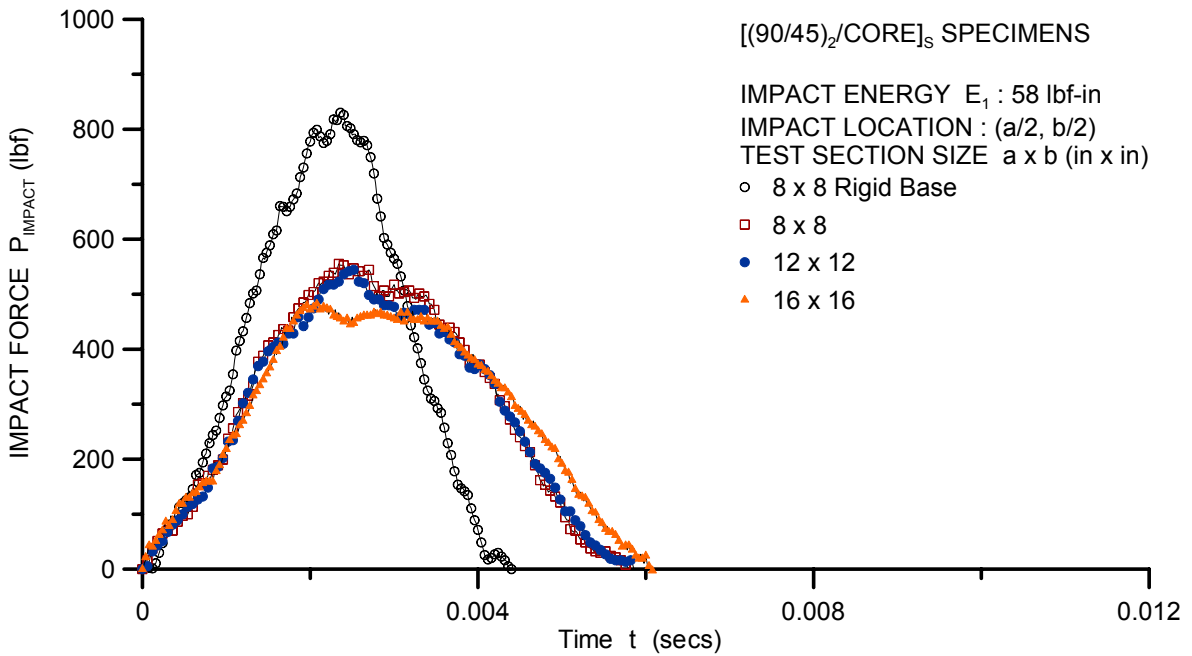


FIGURE 10. FORCE-TIME HISTORY FOR  $[(90/45)_2/CORE]_s$  SANDWICH PANELS IMPACTED AT ENERGY LEVEL  $E_1$ , WHEN BOTH PLANAR DIMENSIONS ARE SCALED

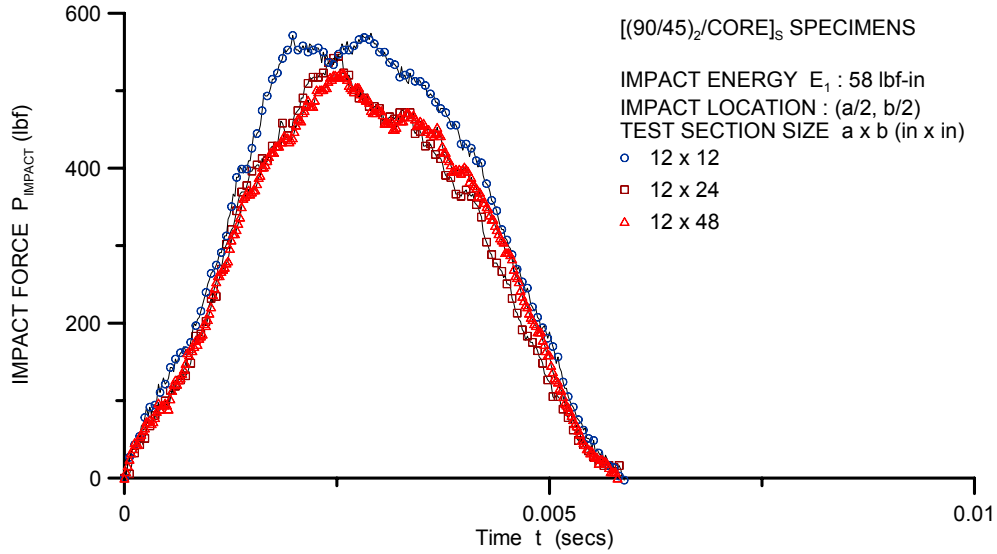


FIGURE 11. FORCE-TIME HISTORY FOR  $[(90/45)_2/CORE]_s$  SANDWICH PANELS IMPACTED AT ENERGY LEVEL  $E_1$ , WHEN ONE PLANAR DIMENSION IS SCALED

The peak impact forces recorded during the tests for different specimen sizes under each sandwich configuration are summarized in figures 12 and 13. The peak impact force was observed to decrease with increasing panel size when both the planar dimensions were changed. The peak impact force for the specimens supported on a rigid base was considerably higher than the rest of the specimen sizes.

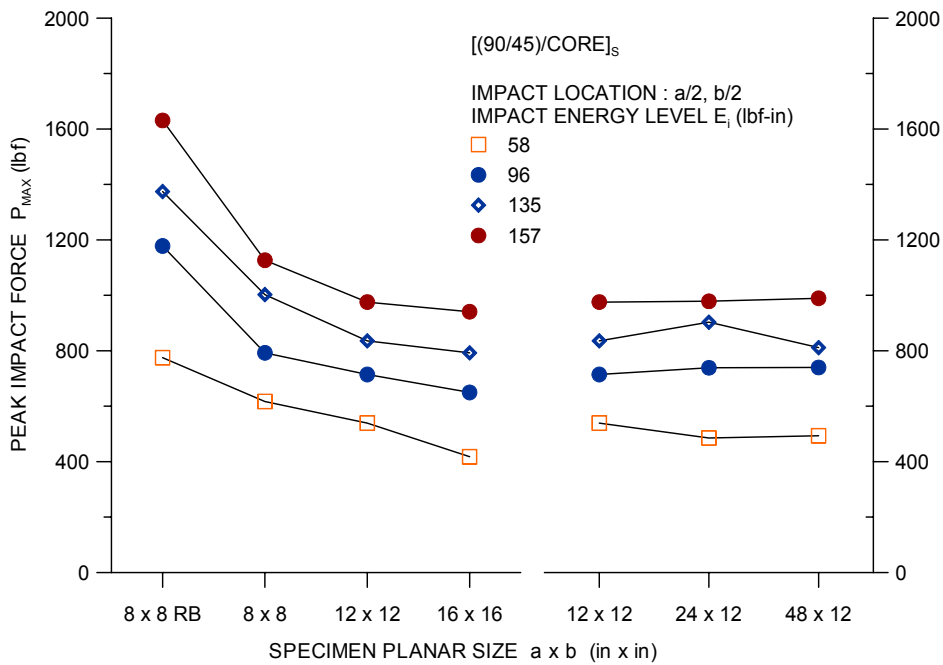


FIGURE 12. PEAK IMPACT FORCE FOR  $[(90/45)/CORE]_s$  SANDWICH PANELS AT DIFFERENT ENERGY LEVELS

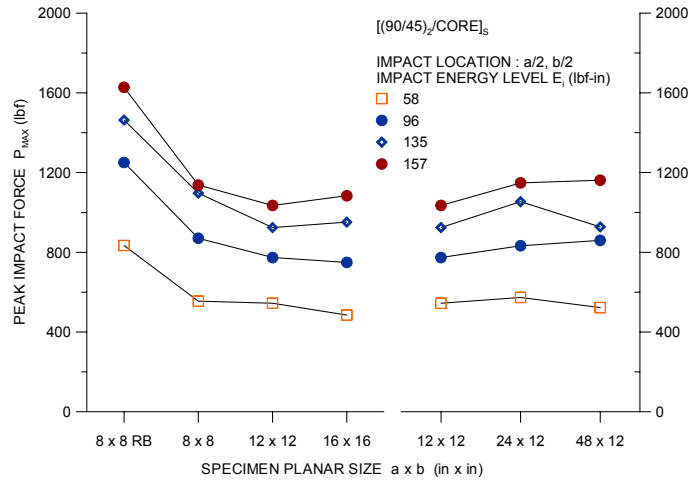


FIGURE 13. PEAK IMPACT FORCE FOR  $[(90/45)_2/CORE]_s$  SANDWICH PANELS AT DIFFERENT ENERGY LEVELS

The peak impact force was found to be fairly insensitive when only one of the planar dimensions was changed. Even though slight differences existed between the peak impact force levels at each energy level, no trend could be established. This observation can be explained by considering the variation of the fundamental frequency of the sandwich plates as a function of the planar dimensions, see figure 14. The increment of frequency when both the planar dimensions are altered (i.e.,  $8 \times 8 \rightarrow 12 \times 12 \rightarrow 16 \times 16$ ) is higher than that associated with the change in a single planar dimension (i.e.,  $12 \times 12 \rightarrow 12 \times 24 \rightarrow 12 \times 48$ ). The natural frequency was computed using a solution for a simply supported plate by classical laminated plate theory. Thus, if the impact response is dominated by the fundamental mode, it can be inferred that the peak impact force is proportional to the fundamental frequency. The lack of a trend in the experimental data for sandwich panels, for which a single planar dimension was scaled, may also be due to the differences between the mass of the impactor and the panel.

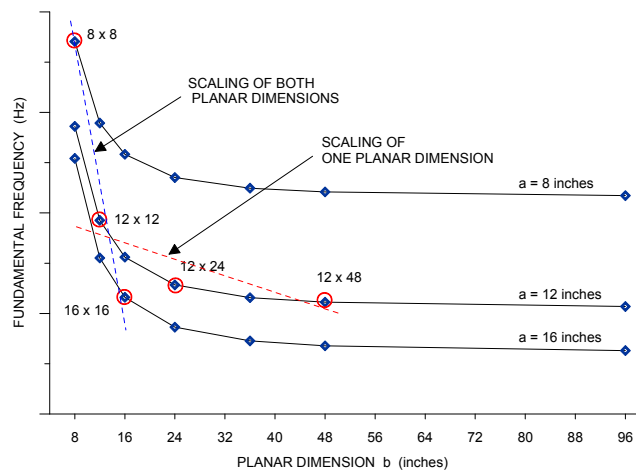


FIGURE 14. VARIATION OF FUNDAMENTAL FREQUENCY FOR SANDWICH PANELS AS A FUNCTION OF PLANAR DIMENSIONS SHOWING THE RELATIVE FREQUENCIES OF THE PANEL SIZES USED IN THIS STUDY

### 2.1.2 Off-Center Impacts.

A limited number of impact tests were conducted on 16" × 16" sandwich specimens to study the effects of impacts at locations other than the geometric center. This study was warranted by the argument that the impact events in an airframe structure may occur at locations other than the geometric center. The impact testing was conducted at two energy levels, 58 and 135 lbf-in, using a 3" diameter impactor. The off-center impacts were conducted at distances of 2" (a/8) and 4" (a/4) from the supported edge. The peak impact forces recorded during the impact tests on  $[(90/45)/CORE]_S$  and  $[(90/45)_2/CORE]_S$  sandwich panels at two energy levels are summarized in figure 15. The time history of force for individual tests can be found in appendix A. It can be observed that the peak impact force increases as the impact location approaches the boundary supports due to the increased flexural stiffness of the panel closer to the supports. Thus, in an airframe, the locations close to the underlying frames or bulkheads will increase the stiffness of the panel, resulting in higher impact forces.

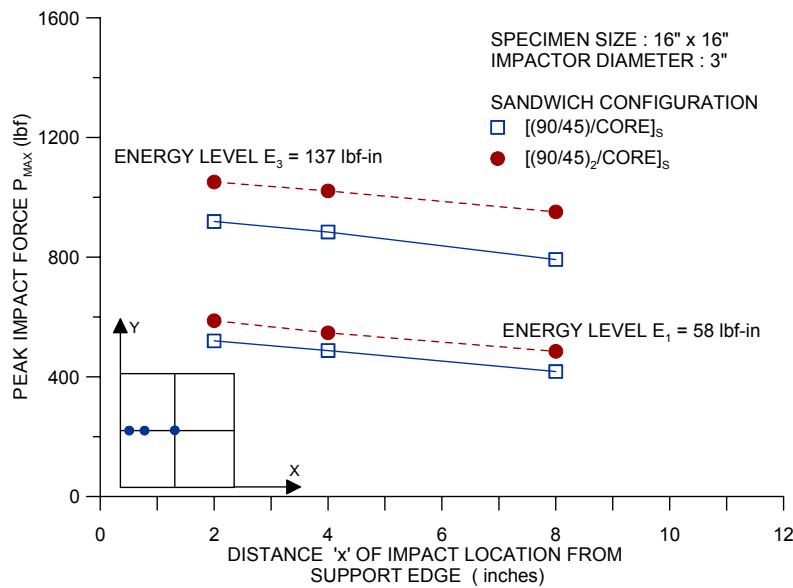


FIGURE 15. SUMMARY OF PEAK IMPACT FORCE FOR OFF-CENTER IMPACTS

## 2.2 CHARACTERIZATION OF SCALING EFFECTS BASED ON IMPACT DAMAGE.

The impact damage in sandwich panels with thin facesheets has been characterized using nondestructive techniques in terms of a planar damage diameter,  $2R_{damage}$  and the maximum residual indentation depth  $\Delta_{RMAX}$ . The planar damage diameters and residual indentation depths for  $[(90/45)/CORE]_S$  sandwich panels at different energy levels are shown in figures 16 and 17 respectively, while the same for  $[(90/45)_2/CORE]_S$  sandwich panels are shown in figures 18 and 19 respectively. The planar damage diameter was observed to decrease when both the planar dimensions of the panels were increased. The above trend was more pronounced in  $[(90/45)_2/CORE]_S$  sandwich panels when compared to  $[(90/45)/CORE]_S$  for which some scatter existed at lower energy levels.

The planar damage diameter was consistently smaller for the sandwich panels with rigid-base supports at all energy levels. The residual indentation depths were, however, larger for the specimens supported by a rigid base at all energy levels. Thus, core crushing is propagated in the thickness direction when the specimens are supported on a rigid-base, whereas the core damage propagation occurs along the lateral directions in specimens that have boundary supports that allow some flexural deformation. Visible skin fractures were also observed in sandwich specimens with rigid-base supports at the highest energy levels.

The larger damage sustained, when the panel has rigid support underneath, has implications for real structure with internal framing. Special attention during inspection should be focused on the areas under or near such supports, as one would expect the damage to be more visible there.

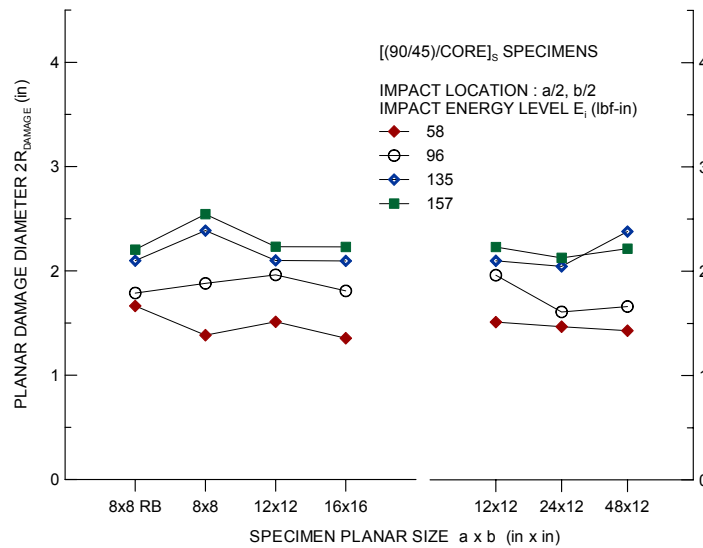


FIGURE 16. SUMMARY OF TTU C-SCAN PLANAR DAMAGE SIZE FOR  $[(90/45)/CORE]_s$  SANDWICH PANELS AT DIFFERENT ENERGY LEVELS

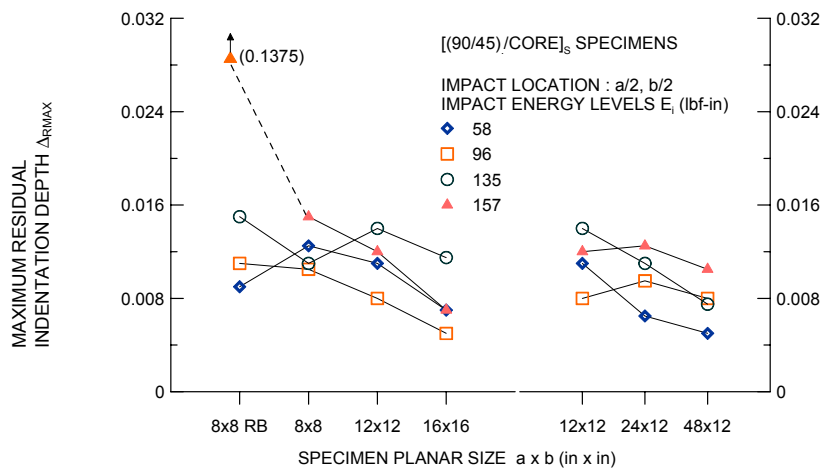


FIGURE 17. SUMMARY OF RESIDUAL INDENTATIONS FOR  $[(90/45)/CORE]_s$  SANDWICH PANELS AT DIFFERENT ENERGY LEVELS

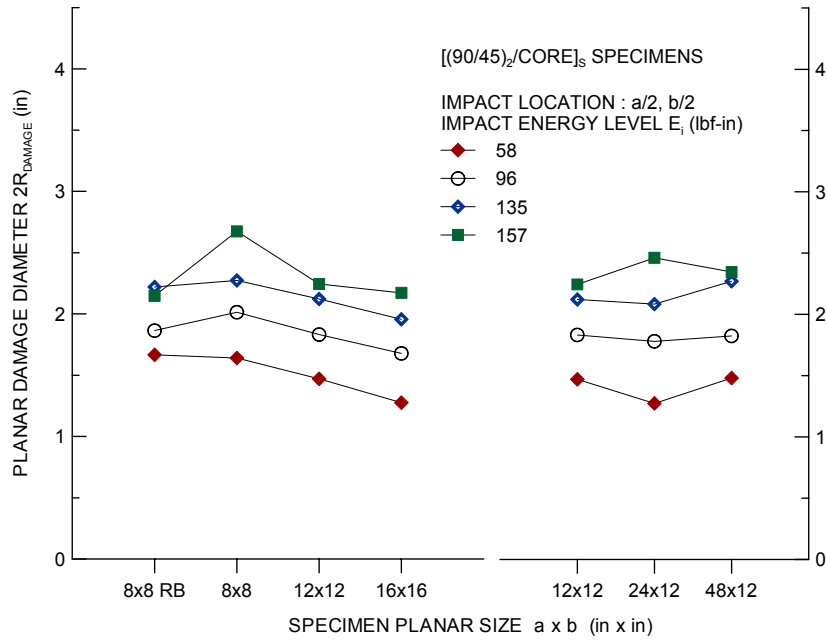


FIGURE 18. SUMMARY OF TTU C-SCAN PLANAR DAMAGE SIZE FOR  $[(90/45)_2/CORE]_s$  SANDWICH PANELS AT DIFFERENT ENERGY LEVELS

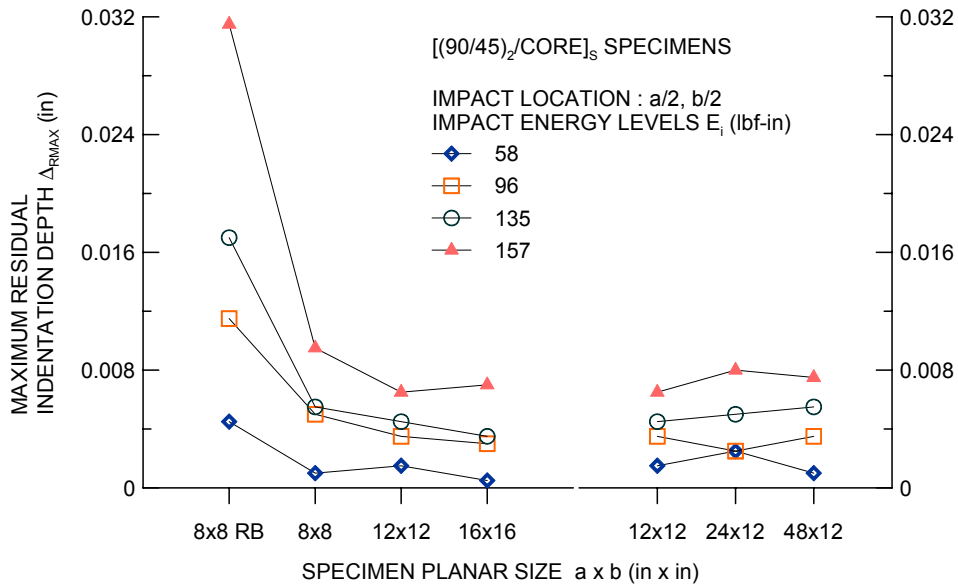


FIGURE 19. SUMMARY OF RESIDUAL INDENTATIONS FOR  $[(90/45)_2/CORE]_s$  SANDWICH PANELS AT DIFFERENT ENERGY LEVELS

The planar damage diameter did not exhibit any particular trend when a single planar dimension of the panel was scaled for both sandwich configurations. The residual indentation depth was found to decrease with increasing panel size (scaling of one dimension) for the  $[(90/45)/CORE]_s$  specimens at two energy levels.

The planar damage diameter and residual indentation depth for off-center impacts are summarized in figures 20 and 21 respectively. As expected, the planar damage diameter and residual indentation depths increased as the impact location moved closer to the support edge. The TTU C-scan plots for off-center impacts are shown in figures 22 through 25. These figures show that as the impact location approaches the support edge, the shape of the damage region becomes more asymmetrical at the higher-energy level (135 lbf-in).

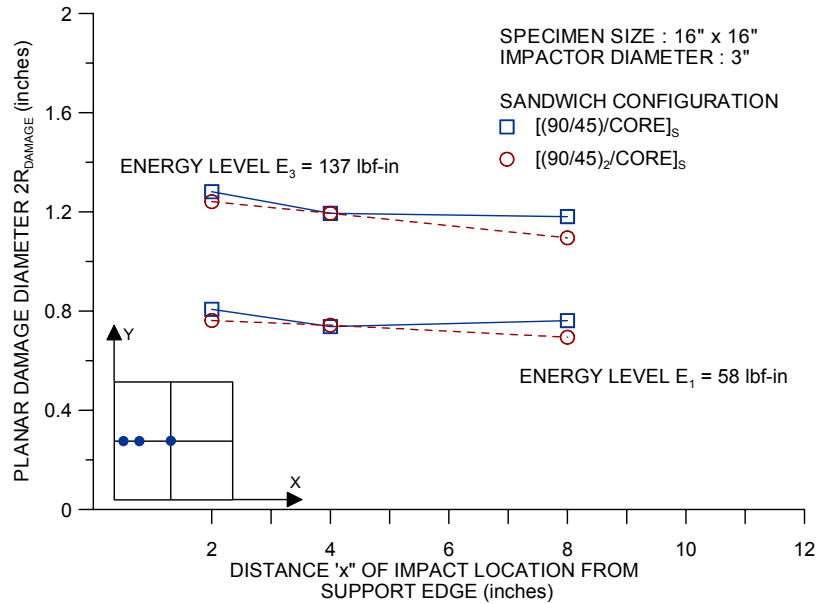


FIGURE 20. SUMMARY OF TTU C-SCAN PLANAR DAMAGE SIZE FOR OFF-CENTER IMPACTS

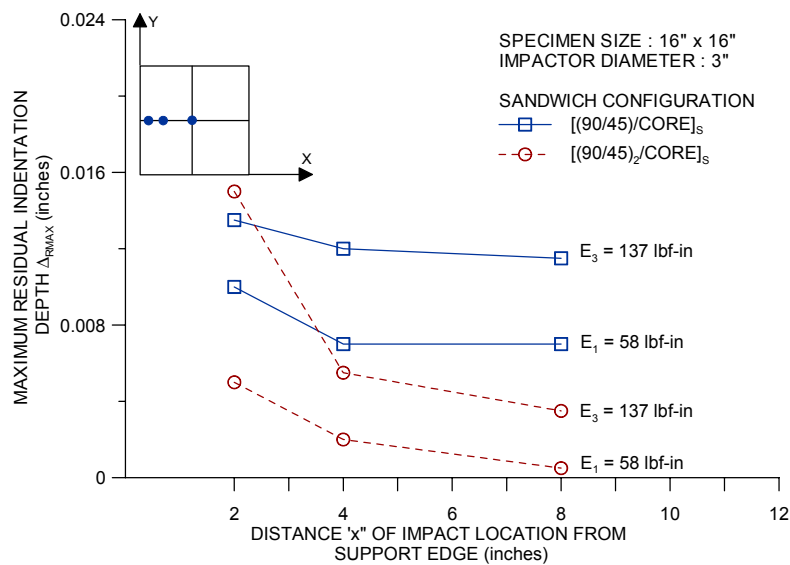


FIGURE 21. SUMMARY OF RESIDUAL INDENTATIONS FOR OFF-CENTER IMPACTS

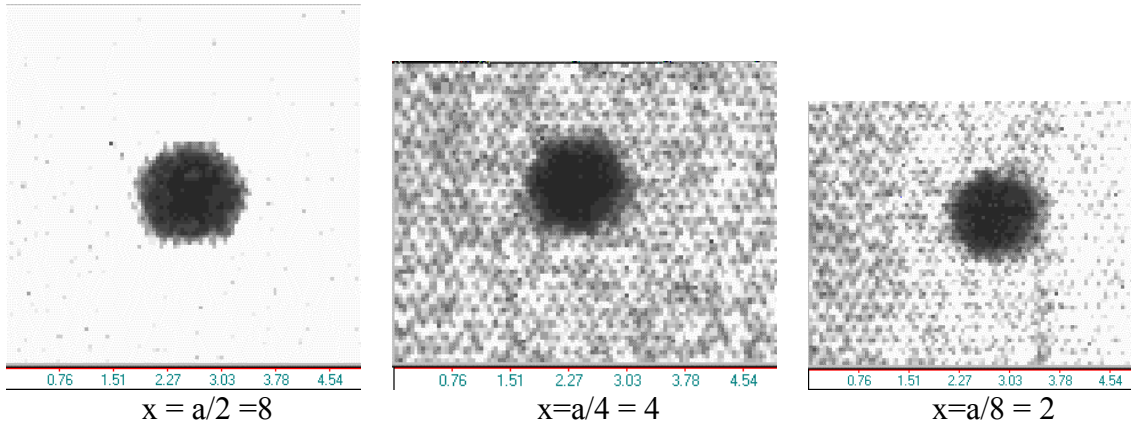


FIGURE 22. TTU C-SCAN PLOTS FOR  $[(90/45)/CORE]_s$  SANDWICH PANELS IMPACTED AT DIFFERENT LOCATIONS WITH AN IMPACT ENERGY OF 58 lbf-in

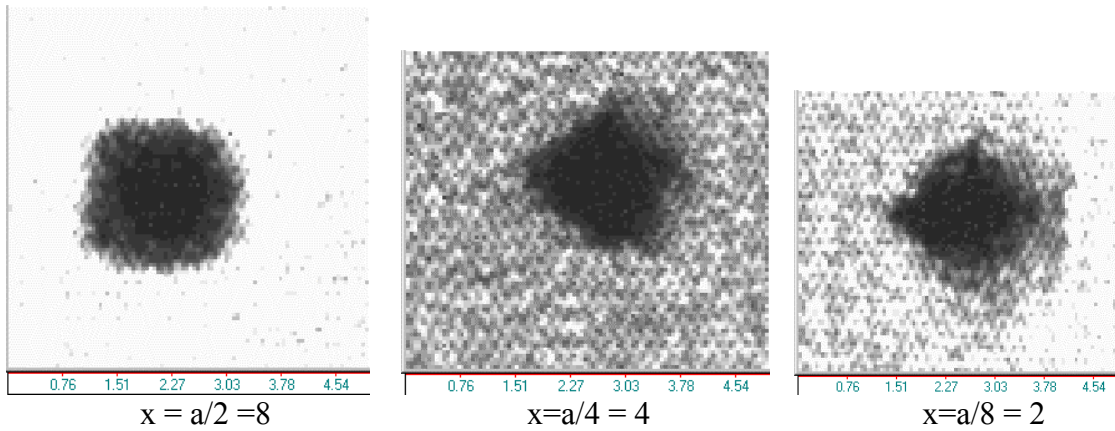


FIGURE 23. TTU C-SCAN PLOTS FOR  $[(90/45)/CORE]_s$  SANDWICH PANELS IMPACTED AT DIFFERENT LOCATIONS WITH AN IMPACT ENERGY OF 135 lbf-in

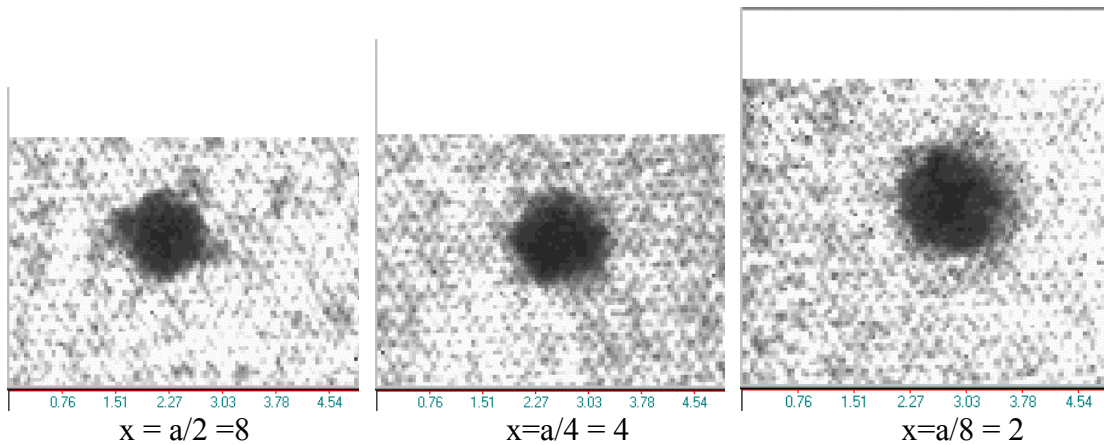


FIGURE 24. TTU C-SCAN PLOTS FOR  $[(90/45)_2/CORE]_s$  SANDWICH PANELS IMPACTED AT DIFFERENT LOCATIONS WITH AN IMPACT ENERGY OF 58 lbf-in

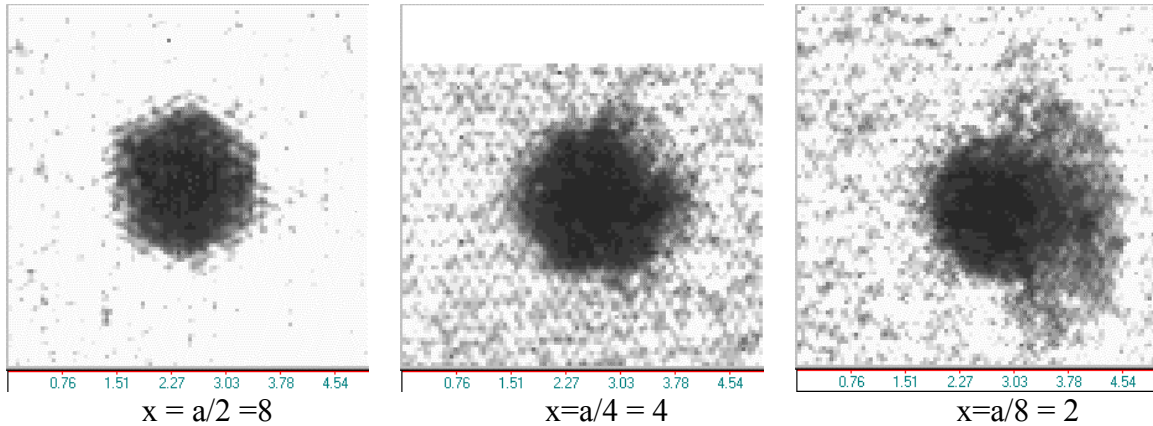


FIGURE 25. TTU C-SCAN PLOTS FOR  $[(90/45)_2/\text{CORE}]_s$  SANDWICH PANELS IMPACTED AT DIFFERENT LOCATIONS WITH AN IMPACT ENERGY OF 135 lbf-in

In summary, the impact responses and the resulting damage metrics of sandwich panels were found to be affected by the scaling of the planar dimensions and the location of impact relative to the boundary supports. The impact forces and the damage metrics decreased as both the planar dimensions of the sandwich panel were increased simultaneously. The scaling of a single planar dimension did not produce any significant differences in impact response and damage metrics. The impact of sandwich panels supported on a rigid base proved to be the most severe case causing facesheet fractures at the higher-energy levels used in this study (but not necessarily yielding the highest planar damage area). The planar damage size for specimens supported on a rigid base was consistently smaller than specimens with clamped-edge boundary conditions. The residual indentations in specimens supported on a rigid base were, however, larger than the rest of the specimen sizes at all energy levels. The location of the impact relative to the boundary supports was found to alter the impact response and the damage metrics. The planar damage region became asymmetrical as the impact location was moved closer to the boundary supports.

### 3. FINITE ELEMENT ANALYSIS OF SCALING EFFECTS ON IMPACT RESISTANCE.

The experimental results on the effects of geometric scaling of the planar dimensions reported in section 2.2 indicated that the peak impact force and the resulting impact damage size were inversely proportional to the planar size of the sandwich panel. The experimental results also indicated the dependence of the impact force and the resulting damage size and shape on the location of the impact with respect to the support edges. The maximum panel size was, however, limited to 16" due to the practical limitations on the impact-testing machine. Further, it was observed that the increase of planar dimension in one direction alone would not significantly alter the impact response and the resulting damage metrics, implying the dependence on the smallest planar dimension of the sandwich plate. In an effort to extend the experimental observations to panel sizes that are much larger than those investigated experimentally, an FE model was assembled. The FE model was used to study the planar scaling effects on the response of sandwich panels and the energy dissipation characteristics under low-velocity impacts. The details of the FE modeling, comparisons with experimental data, and the details of a parametric study are discussed in the following sections.

### 3.1 FINITE ELEMENT MODELING OF SANDWICH IMPACT.

The low-velocity impacts of laminated and sandwich plates have been modeled using analytical and numerical methods by past researchers. The impact models range from simple spring-mass models, which assume that the low-velocity impact process is quasi-static in nature, to beam and plate models that incorporate the effects of higher-frequency modes [18 and 19]. The plate models used for studying the impact of laminated plates typically use the solutions developed by Whitney and Pagano [20] for static loading and follow the procedure developed by Sun and Chattopadhyay [21] to analyze the impact problem. The models used for laminated plates were extended to sandwich plates by considering the core as just another layer [14, 18, and 22]. Dobyns [22] has used this approach to study the response of sandwich panels subjected to different kinds of transient load and impact loading. However, in view of the dominant core deformations in sandwich panels with low-density cores, additional models [18] have been developed to account for the out-of-plane core deformations. Both 2-D and three-dimensional FE models have also been used to study the impact responses of sandwich plates [18].

The central feature of most plate models and 2-D FE models is the use of an experimentally obtained contact law. The contact law establishes the relation where the change in thickness of the beam and plate at the contact point and the resulting contact force is being tracked between the beam and plate and the impactor. Using experimentally obtained static-contact indentation laws to address the problem of spherical and cylindrical objects impacting on composite laminates and sandwich panels has been widely reported [14, 18, 22, and 23]. The contact law is necessary to couple the equations of motion of the target and the projectile, if the contact process is not explicitly represented in the model. The use of a contact law in effect decouples the local indentation and global bending, thus simplifying the problem. The contact laws are valid for low-velocity impacts, where in the contact process can be approximated by its static equivalent. The implementation of the contact law further assumes that the effects of impact damage on the primary vibrational modes of the target structure to be negligible [18, 24, and 25].

In this investigation, the FE modeling of sandwich impact was accomplished using the MSC Marc nonlinear FE computer program [26]. The sandwich plates were modeled using bilinear 8-noded thick shell elements (Marc Element 22) with displacement and rotation degrees of freedom [27]. Second-order interpolations are used for coordinates, displacements, and rotations, and the effects of transverse shear are also included. The impactor was approximated by a point mass. The impactor and sandwich plate contact interaction were modeled using a nonlinear inelastic spring, as shown in figure 26. The nonlinear spring behavior was implemented using an external subroutine. The inputs for the subroutine were obtained from a previous experimental investigation of the contact behavior of sandwich panels [17]. The contact behavior of sandwich panels under quasi-static loading is discussed in the following section.

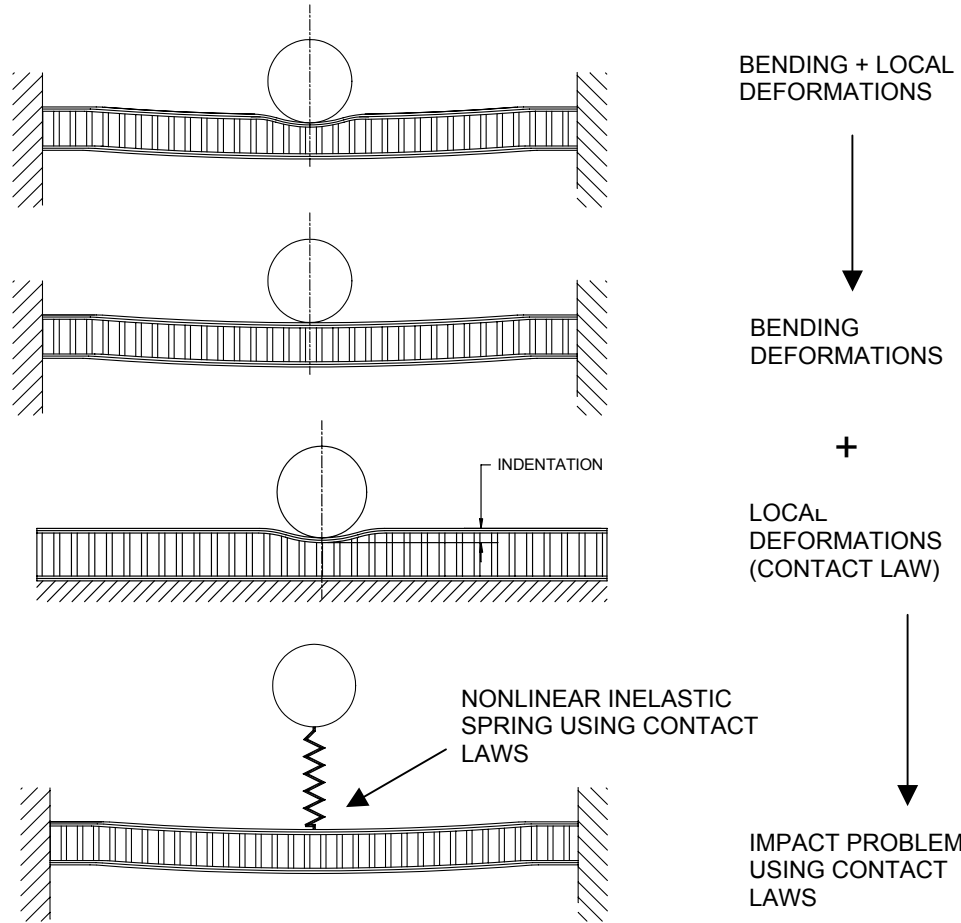


FIGURE 26. REPRESENTATION OF THE CONTACT-IMPACT PROBLEM USING CONTACT LAWS

### 3.1.1 Contact Behavior of Sandwich Panels and Contact Laws.

The contact behavior of sandwich panels indented by spherical indentors has been investigated experimentally and by using FE methods [17, 18, and 23]. The indentation in sandwich panels has been typically investigated by using a rigid-base support condition [17]. The typical load-indentation behavior of a sandwich panel is illustrated in figure 27a. The figure shows the behavior of  $[(90/45)_2/\text{CORE}]_S$  sandwich panel indented by a 3" diameter indenter. The load-indentation response consists of initial linear elastic region up to a critical indentation depth  $u_{CR}$ . The behavior is nonlinear and inelastic beyond the critical depth, and the specimen may be indented to depths that are several times the facesheet thickness before a facesheet fracture occurs. The nonlinear region is highly dissipative in nature, the energy being absorbed by the initiation and propagation of core crushing and delaminations in the facesheet [17 and 28]. The loading behavior of the sandwich panels is modeled using the following equations:

$$P(u) = \begin{cases} C_0 u_z & 0 \leq u_z \leq u_{CR} \\ C_1 + C_2 u_z^3 & u_{CR} < u_z \leq u_{FRACT} \end{cases} \quad (1)$$

where,  $C_0$ ,  $C_1$ ,  $C_2$ , and  $C_3$  are coefficients obtained by curve fitting the experimental data. In general, these coefficients are functions of the facesheet properties, core properties, and the indenter size [17]. The response of the sandwich panels during the unloading process is illustrated in figure 27b. The response is modeled using Crook's model [29], which is given by

$$P_{UL}(u) = P_{MAX} \left[ \frac{u_z - u_{RES}}{u_{MAX} - u_{RES}} \right]^m \quad u_{CR} \leq u_z < u_{FRACT} \quad (2)$$

where  $u_{MAX}$  and  $P_{MAX}$  are the maximum indentation and the corresponding force before unloading begins. The preceding equation requires knowledge of the residual indentation  $u_{RES}$  and the unloading index  $m$ . The residual indentation depth and the unloading index may be functions of the maximum indentation  $u_{MAX}$  before unloading. The unloading index  $m$  is obtained by conducting multiple indentation experiments where the unloading is initiated at different  $u_{MAX}$ . The energy dissipated during the contact process is given by the area enclosed between the loading and the unloading portion of the curves.

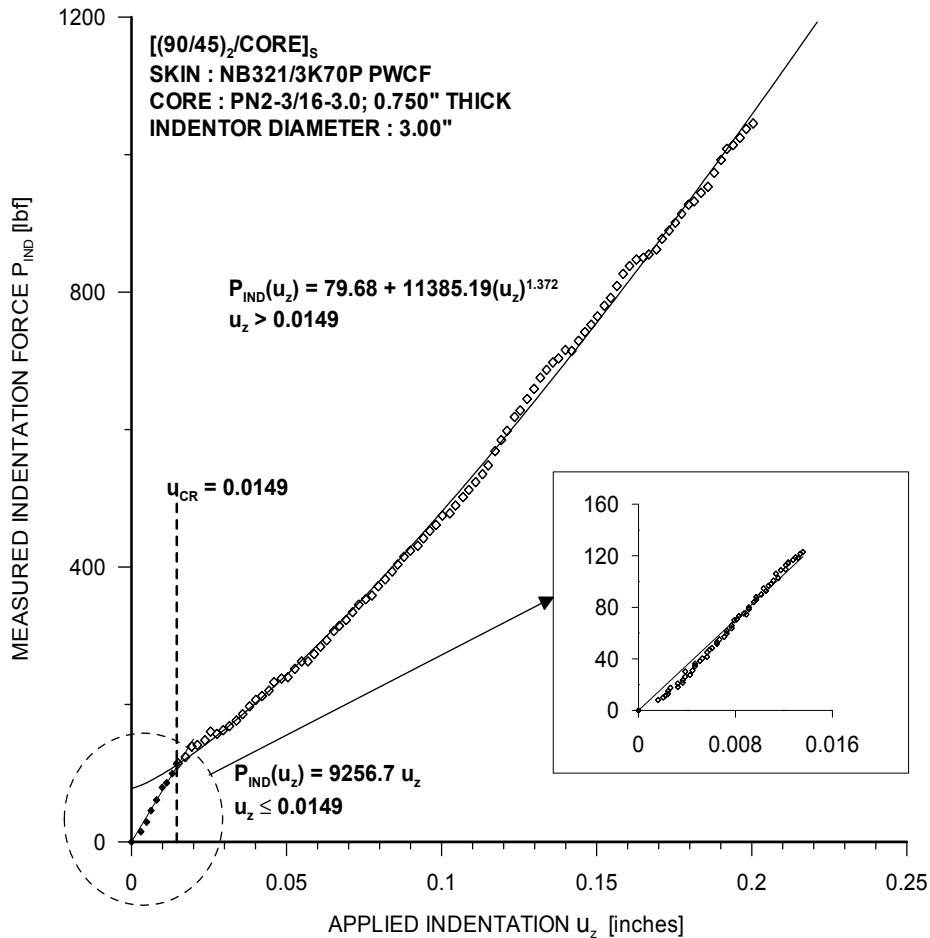


FIGURE 27a. TYPICAL LOADING RESPONSE OF SANDWICH PANELS SUBJECTED TO STATIC INDENTATION USING SPHERICAL INDENTORS [17]

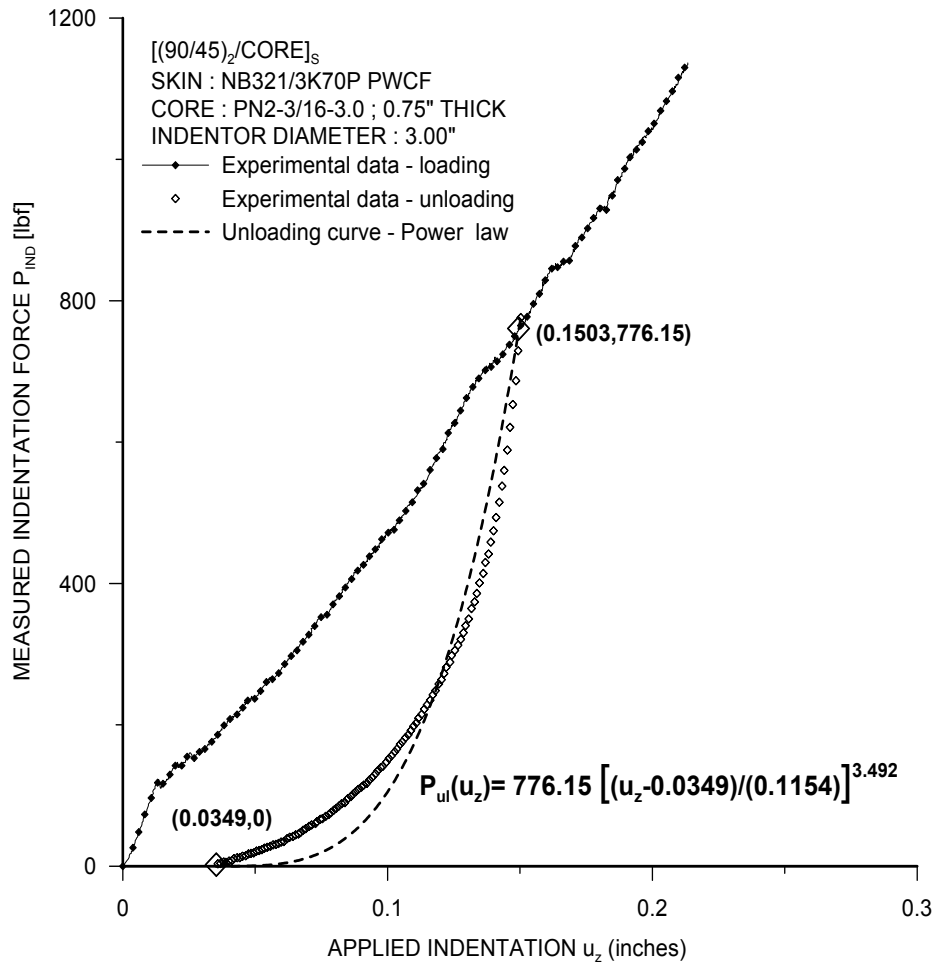


FIGURE 27b. TYPICAL UNLOADING RESPONSE OF SANDWICH PANELS SUBJECTED TO STATIC INDENTATION USING SPHERICAL INDENTORS [17]

The contact laws reported in reference 17 were used in the FE simulation of the impact response of [(90/45)<sub>2</sub>/CORE]<sub>s</sub> sandwich panels impacted by a 3" diameter impactor. The FE predictions were compared with the experimental data and the predictions of an analytical model developed by Dobyns [22]. The FE model was then used with linearized contact laws to conduct a parametric study addressing the scaling effects on impact responses. The FE model was also used to study the energy dissipation in sandwich panels. Even though the model cannot predict the failure mechanisms explicitly, the energy dissipated during the impact process can be used as a measure of damage.

### 3.1.2 Comparison With Experimental Data.

To assess the validity of the FE model, a comparison was made between the force-time histories obtained from experiments and the FE model prediction. Another numerical model, developed by Dobyns, was also used for comparison. The experimental data for the [(90/45)<sub>2</sub>/CORE]<sub>s</sub> sandwich specimen impacted with a 3" diameter impactor, with an impact energy of 55 lbf-in, and an impact velocity of 96 in/sec were used for testing the model predictions. The facesheets

were made of NB321/3K70 P plain weave carbon fabric/epoxy prepreg material, and the sandwich core was made of 0.75" thick Plascore Nomex PN2-3/16-3.0. The sandwich specimen was supported using clamped-edge boundary conditions, which did not restrict the in-plane translation degree of freedom. The edges of the sandwich panel in the FE model were constrained for rotations and out-of-plane displacement. The Dobyns model, however, is formulated for simply supported boundary conditions. The coefficients of the contact law were obtained from a previous study [17] and are as follows:

$$\begin{aligned}
 C_0 &= 9256.7 \text{ lbf/in} \\
 u_{CR} &= 0.0149 \text{ in} \\
 C_1 &= 79.68 \text{ lbf} \\
 C_2 &= 11385.2 \\
 C_3 &= 1.372
 \end{aligned}$$

The force-time histories predicted by the FE and Dobyns model are compared with the experimental data in figure 28. The FE model slightly overpredicted the peak impact force, while it predicted the impact duration very closely. The predictions of the FE and Dobyns model follow the experimental data very closely during the loading phase. However, both models overpredicted the impact forces during the unloading phase. It should be noted that the contact behavior used in the FE model is inelastic while the Dobyns model is elastic. The differences in the force histories during the unloading phase indicated that energy dissipation mechanisms other than those due to contact and vibration may be present in the experiments.

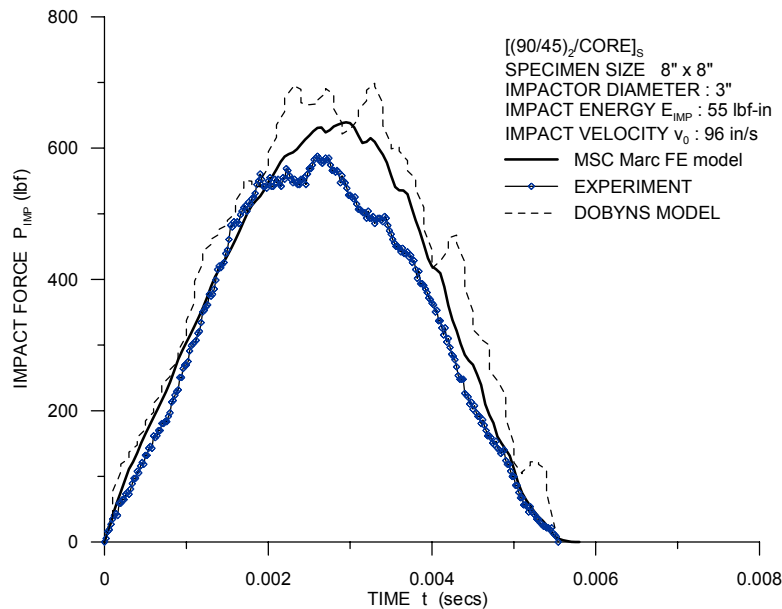


FIGURE 28. COMPARISON OF FE MODEL AND DOBYNS MODEL PREDICTIONS WITH EXPERIMENTAL DATA

Since the FE model compared reasonably well with the experimental data, the model was subsequently used for conducting a parametric study using linearized inelastic contact laws. The details of the parametric studies and the pertinent results are discussed in the following section.

### 3.2 PARAMETRIC STUDY.

The FE model using experimentally determined contact laws was shown to predict the impact response satisfactorily. The FE model can be used to study the energy dissipated during the impact process, and the dissipated energy can be resolved into kinetic energy and damage energy. The results of the experimental investigation discussed in section 2 showed the dependence of impact responses and resulting damage metrics on the sandwich planar size. The sandwich specimen sizes were, however, limited by the physical limits on the impact-testing machine. The FE model can also be used to study specimen sizes that may be prohibitive in practice. Further, the contact behavior of sandwich panels, which in general depends on the properties of the sandwich constituents and the indenter size, can be varied arbitrarily to study their effects on the impact response. In this study, the effects of the sandwich planar size and contact properties on the energy dissipation characteristics of sandwich panels subjected to low-velocity impacts were addressed. Linearized contact laws were used to further simplify the problem and are discussed in the following paragraph.

The linearized contact law assumes linear loading and unloading responses, as shown in figure 29. The linearized laws retain all the characteristics of the actual contact laws while being relatively simple. The linearized laws can be cast in terms of two parameters, the loading and unloading stiffnesses,  $K_L$  and  $K_{UL}$ . The energy dissipated during the contact process is given by the area enclosed between the loading and unloading curves. The relative values of the loading and unloading stiffness dictate the fraction of contact energy that is dissipated. The energy dissipation fraction,  $\phi$ , which defined as the ratio of dissipated energy to the indentation energy, is dependent on the ratio  $K_L/K_{UL}$ . The behavior is elastic when  $K_L/K_{UL} = 1$ , plastic when the ratio  $K_L/K_{UL} = 0$ .

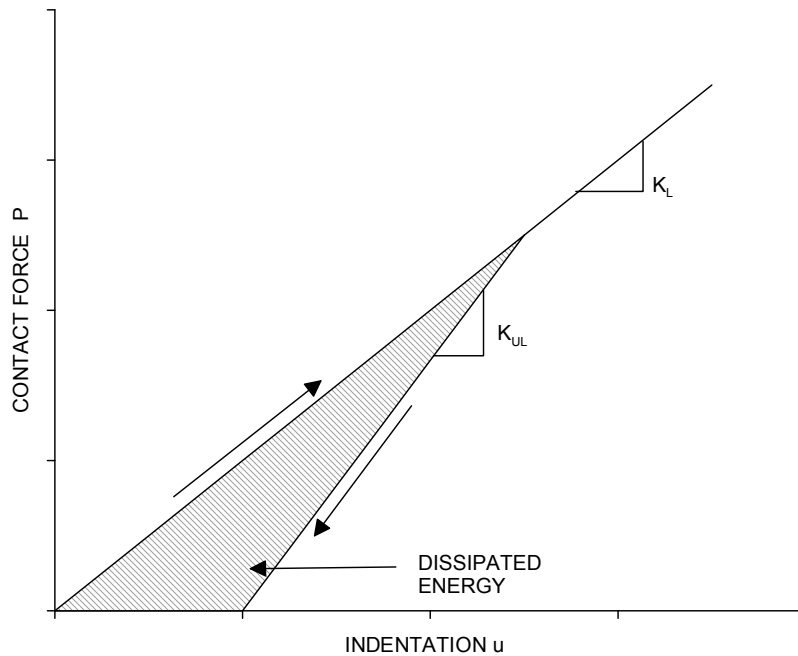


FIGURE 29. LINEARIZED CONTACT BEHAVIOR USED IN THE PARAMETRIC STUDY

In this study, the effects of energy dissipation fraction and the scaling of specimen planar size were investigated using linearized contact laws. Dissipation fractions of 0, 0.25, 0.5, 0.75, and 0.9 were used to simulate contact behaviors ranging from totally elastic to near plastic behavior. A loading stiffness,  $K_L = 8000$  lbf/in was used to define the contact behavior. The sandwich configuration used in this study was  $[(90/45)_2/\text{CORE}]_S$ . The sandwich panels were modeled using the properties for facesheets made of NB321/3K70P plain weave carbon fabric/epoxy prepreg material, and the sandwich core was made of 0.75" thick Plascore Nomex PN2-3/16-3.0. Square sandwich plates with side dimensions of 4", 8", 16", 32", 48", 64", 96", and 128" were used in this study. The sandwich specimens were impacted with an impact energy of 50 lbf-in at an impact velocity of 100 in/sec. The FE data were analyzed for the total energy dissipated,  $E_{ABS}$ , which is the difference in the energy of the impactor prior to impact,  $E_{IMP}$  and at the cessation of contact,  $E_{REBOUND}$ , (equation 3); the energy dissipated due to contact  $E_{DISSIP}$ ; and the vibrational energy transferred,  $E_{VIBR}$ . The energy dissipated due to the contact process was obtained from the force-indentation response during the impact, and the vibrational energy transfer was obtained as the difference between the rebound energy of the impactor and the dissipated contact energy (equation 4)

$$E_{ABS} = E_{IMP} - E_{REBOUND} \quad (3)$$

$$E_{VIBR} = E_{ABS} - E_{DISSIP} \quad (4)$$

The plot of the total energy absorption ratio ( $E_{ABS}/E_{IMP}$ ) as a function of plate size predicted by the FE model is shown in figure 30 for different levels of contact energy dissipation fraction,  $\phi$ . The total energy absorbed, initially, decreases up to a certain plate size, after which the absorbed energy increases at a rapid rate with respect to the plate size. The amount of total energy absorbed by the plate in the initial region is proportional to  $\phi$ . The ratio of the impactor mass to the plate mass, ( $m_{IMP}/m_{PLATE}$ ), or the mass ratio, is shown as a function of the plate size in the same figure. It can be observed that for plate sizes corresponding to mass ratios less than 1, a sharp increase in absorbed energy occurs, irrespective of  $\phi$ . Past researchers have indicated that a mass ratio of 2 corresponds to the transition between a quasi-static impact and flexure wave-controlled impacts [18 and 30].

The total energy transferred to the sandwich plate was further resolved into the contact energy and kinetic or vibrational energy of the plate. The variation of contact energy dissipated (due to formation of damage) as a function of the plate size is shown in figure 31. The energy lost in creating damage decreases as the plate size increases, which is in agreement with the experimental observations in section 2, where the damage size was observed to decrease with increasing plate size. It can be seen in the same figure that the energy dissipated due to damage falls sharply around a mass ratio of 2. Further, the damage energy appears to have reached a lower limit for  $\phi = 0.25$  and 0.50, indicating that a lower bound exists for very large plates on the amount of damage that can be created at a given impact energy level. Thus, it can be inferred that the energy absorption in sandwich plates is dominated by the creation of damage for mass ratios greater than 2, and the energy is transferred to the plate in the form of vibrational energy for mass ratios less than 2.

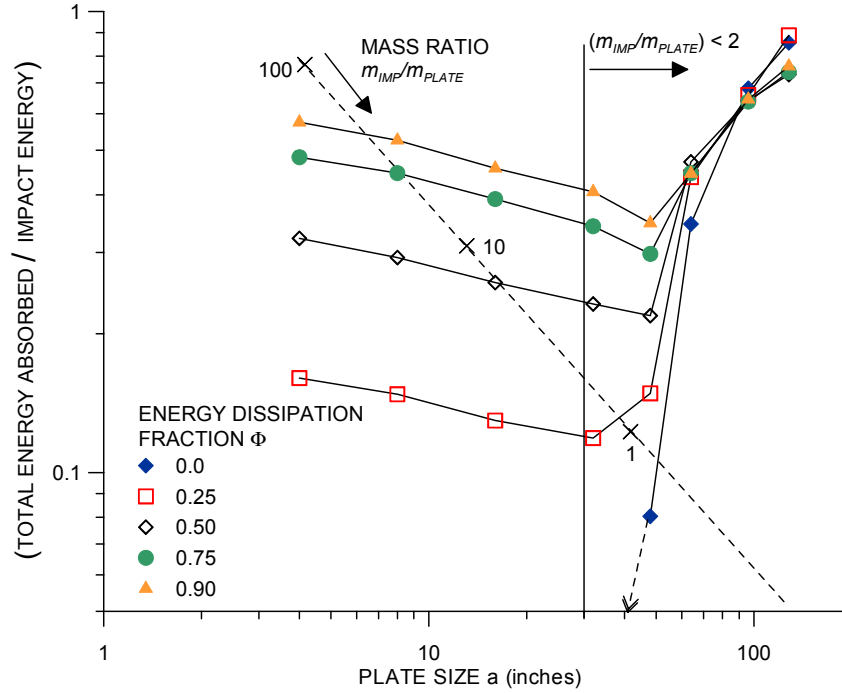


FIGURE 30. FINITE ELEMENT MODEL PREDICTIONS FOR FRACTION OF IMPACT ENERGY ABSORBED FOR SANDWICH PANELS WITH DIFFERENT CONTACT ENERGY DISSIPATION FRACTIONS

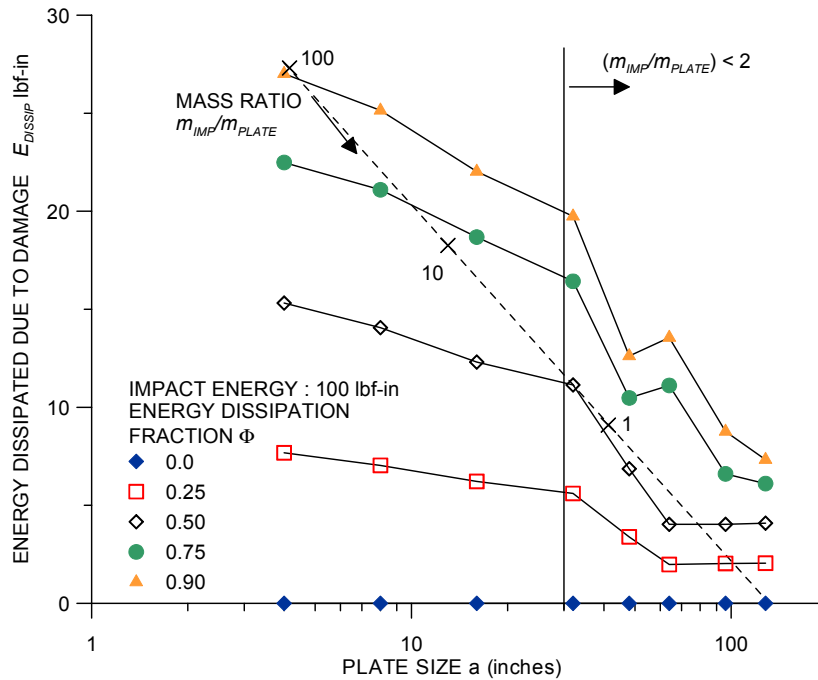


FIGURE 31. FINITE ELEMENT MODEL PREDICTIONS FOR ENERGY ABSORBED BY SANDWICH PANELS DUE TO CREATION OF DAMAGE WITH DIFFERENT CONTACT ENERGY DISSIPATION FRACTIONS

In summary, the FE model using experimentally determined contact laws, predicted the impact force history reasonably well. Even though the model cannot predict the damage explicitly, the energy absorbed by the inelastic contact spring can be used as a measure of damage. The results from the parametric study indicated that the energy absorption in sandwich panels depends on the panel size and the dissipativeness of the contact behavior. The energy transferred to the sandwich plate decreases with increasing plate size and is dominated by the formation of damage, for mass ratios greater than 2. However, the energy transfer was observed to increase when the mass ratio was less than 2 and was dominated by the vibrational energy of the sandwich plate.

#### 4. SCALING EFFECTS ON THE CAI STRENGTH OF SANDWICH PANELS.

The impact damage in sandwich structures is dependent on the facesheet, core, and the impactor size [1]. The typical impact damage in sandwich structures may consist of facesheet damage (matrix cracking, delaminations, and fractures), core damage (core crushing and cell wall fractures), and a residual indentation distribution, which is an equilibrium state between the degraded facesheet and core [1 and 31]. The damage metrics associated with impact damage are illustrated in figure 32. The damage metrics amenable to nondestructive inspection are the planar damage diameter,  $2R_{damage}$ , and the maximum residual indentation depth,  $\Delta_{RMAX}$ . The residual strength has been shown to correlate well with the planar damage size, especially for the blunt impactors where the residual indentation is of the order of the facesheet thickness or less [1].

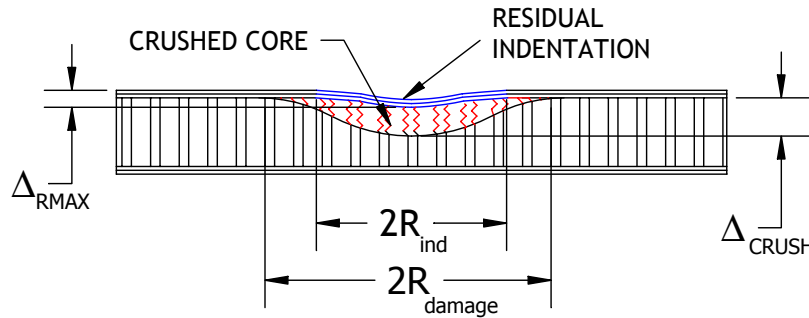


FIGURE 32. TYPICAL IMPACT DAMAGE AND ASSOCIATED METRICS IN SANDWICH PANELS WITH THIN FACESHEETS IMPACTED WITH BLUNT IMPACTORS [31]

The scaling of the damage tolerance problem associated with sandwich panels involved the scaling of geometric dimensions and the damage metrics, as illustrated in figure 33. The scaling of core thickness seldom occurs in airframe applications, and the thickness scaling alters the core behavior in the transverse direction [17]. Thus, the scaling of core thickness was not addressed in this investigation. Further, when the core thickness is held constant, the scaling of the panel height will introduce the possibility of global buckling, precluding (or coupling) the failure driven by the impact damage. Thus, in this study, both the core thickness and the specimen height  $h$  were held constant, even though limited tests were conducted to study the scaling of panel height alone. The scaling of the damage metric  $2R_{damage}$ , in general, implies the scaling of associated residual indentation depth. The proportional scaling of both these damage metrics is not feasible without introducing facesheet damage, which further complicates the problem under

study. Thus, in the present investigation, the planar damage size was held constant, and the width of the panel was scaled to provide different ratios of  $b/2R_{damage}$ , which is of particular interest for leveraging the existing data into practical use.

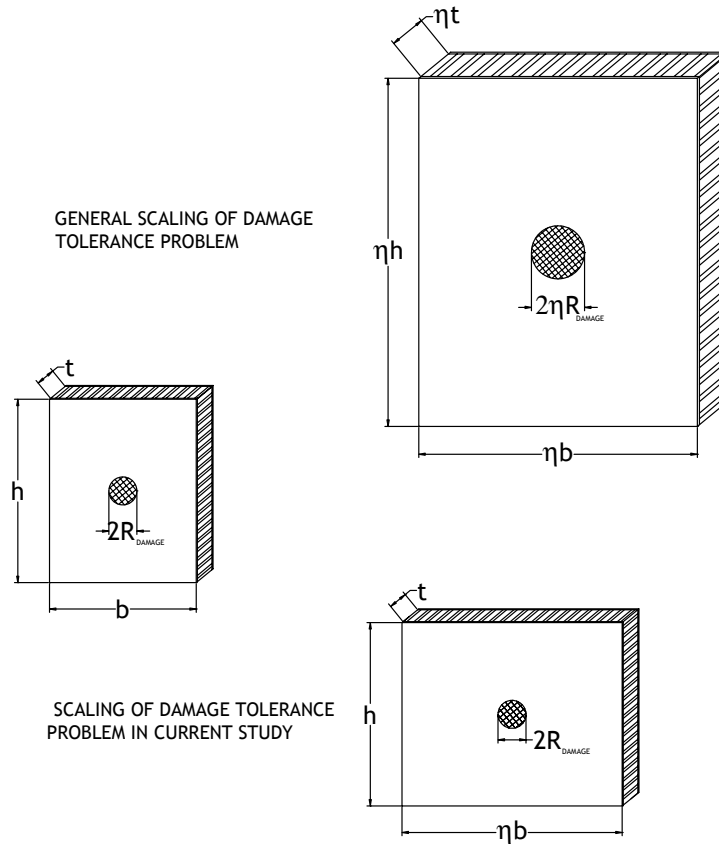


FIGURE 33. GENERAL SCALING OF METRICS IN DAMAGE TOLERANCE PROBLEM OF SANDWICH PANELS AND SCALING PROBLEM ADDRESSED IN THIS STUDY

The effect of scaling of  $b/2R_{damage}$ , for a fixed damage size, on the behavior of two sandwich configurations was studied experimentally. The sandwich configurations studied were  $[(90/45)/CORE]_s$  and  $[(90/45)_2/CORE]_s$ . The sandwich panels were fabricated using a Newport NB321/3K70 Plain weave carbon fabric prepreg for the facesheets and Plascore® PN2-3/16-3.0 Nomex™ 0.75" thick honeycomb material for the sandwich core. The combination of panel widths and heights tested are summarized in table 2. A total of 12 compression tests were conducted in this study, 6 for each sandwich configuration which only differed by facesheet thickness.

The impact damage in the above sandwich panels was introduced by supporting the panels on a rigid base and impacting them with a 3" diameter impactor. The rigid-base support was used to generate equal levels of damage in all specimens. The impact energy level was chosen such that a subsurface damage was created in the panels. The planar damage diameter, the maximum residual indentation depth, and the associated ratios,  $b/2R_{damage}$  and  $h/2R_{damage}$ , for the sandwich specimens are summarized in table 3.

TABLE 2. TEST MATRIX FOR SCALING EFFECTS ON DAMAGE TOLERANCE OF SANDWICH PANELS

	Specimen Width $b$ (inches)			
	6.5	8.5	12.5	16.5
Specimen Height $h$ (inches)	10.5	10.5	10.5	10.5
			12.5	
			16.5	

TABLE 3. DAMAGE METRICS FOR SANDWICH SPECIMENS

Sandwich Configuration	Size $b \times h$ (inches $\times$ inches)	$2R_{damage}$ (inches)	$b/2R_{damage}$	$h/2R_{damage}$	$\Delta_{RMAX}$ (inch)
[(90/45)/CORE] <sub>s</sub>	6.5 $\times$ 10.5	1.406	4.621	7.46	0.004
	8.5 $\times$ 10.5	1.495	5.683	7.02	0.005
	12.5 $\times$ 10.5	1.313	9.516	7.99	0.004
	16.5 $\times$ 10.5	1.334	12.362	7.86	0.005
	12.5 $\times$ 12.5	1.304	9.585	8.05	0.006
	12.5 $\times$ 16.5	1.325	9.448	7.93	0.003
[(90/45) <sub>2</sub> /CORE] <sub>s</sub>	6.5 $\times$ 10.5	1.859	3.494	5.65	0.013
	8.5 $\times$ 10.5	1.864	4.559	5.63	0.011
	12.5 $\times$ 10.5	1.833	6.819	5.73	0.013
	16.5 $\times$ 10.5	1.944	8.486	5.40	0.009
	12.5 $\times$ 12.5	1.843	6.782	5.69	0.010
	12.5 $\times$ 16.5	1.836	6.808	5.71	0.011

#### 4.1 COMPRESSION TESTING OF SANDWICH PANELS.

The impact-damaged sandwich panels were subjected to compression testing to obtain the residual properties and to observe the damage propagation and final failure modes. The compression tests were conducted using the procedures and fixturing reported in reference 1 with modifications to accommodate taller specimens. The typical test-fixturing arrangements are shown in figures 34 and 35. The sandwich specimens were instrumented with four far-field strain gages [1 and 31] to facilitate balancing of the loading platen to introduce uniform loading and to record the failure strains.

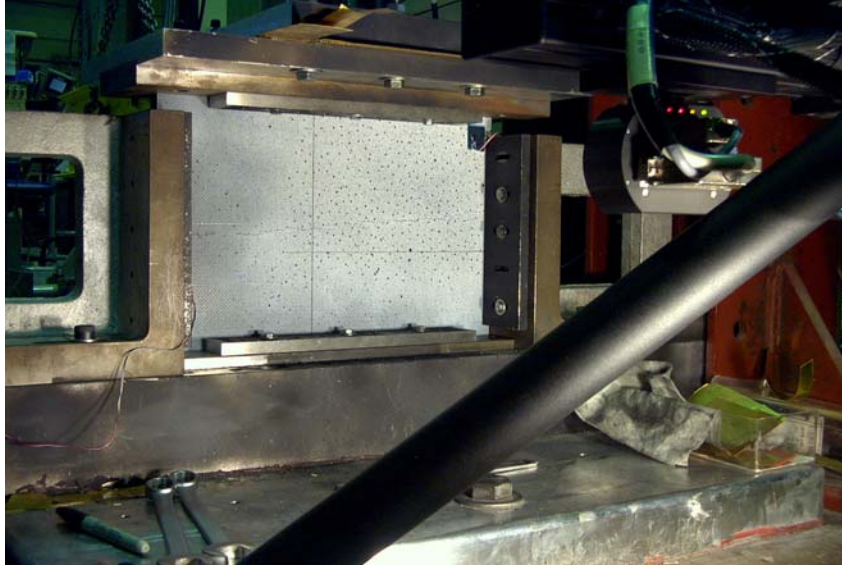


FIGURE 34. COMPRESSION TEST FIXTURE WITH SANDWICH SPECIMEN 16.5" WIDE BY 10.5" HIGH

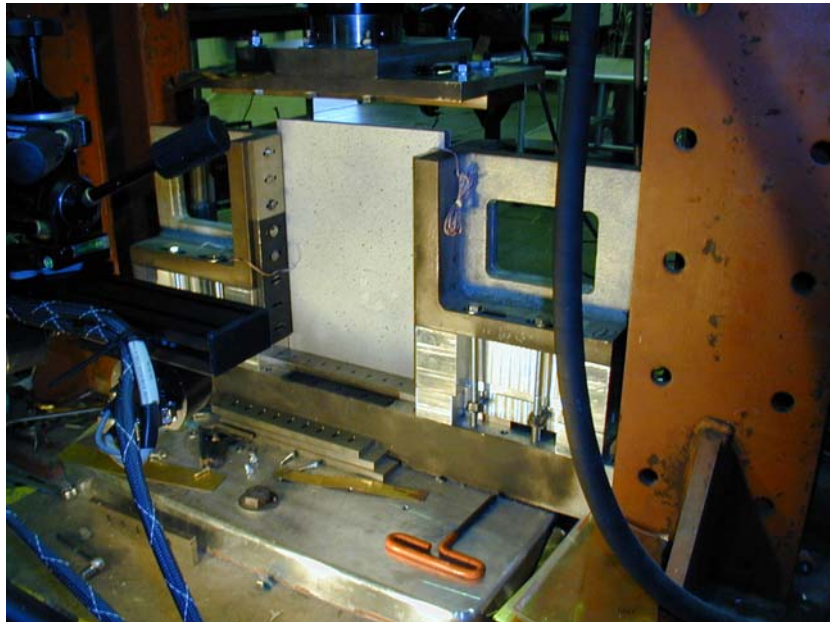


FIGURE 35. COMPRESSION TEST FIXTURE WITH SANDWICH SPECIMEN 12.5" WIDE BY 16.5" HIGH

A full-field strain and displacement measurement photogrammetry system, ARAMIS [32], was used in this investigation. The system consists of two high-resolution cameras and an image analysis computer program, as shown in figure 36. The system is capable of measuring large displacements and strains (up to 100%) over regions of maximum size 39"  $\times$  39". The sandwich specimen is coated with a flat white spray paint, with a stochastic black speckle pattern applied on top of the coating. The photogrammetry system captures high-resolution images of the

deforming object or specimen at predefined intervals of load or time. The series of images are then analyzed sequentially to obtain the cumulative displacements and strains at each load increment. The displacement and strain fields can then be analyzed to obtain displacement and strain distributions across desired sections of interest.



FIGURE 36. TYPICAL ARAMIS SYSTEM AND ARAMIS ARRANGEMENT FOR COMPRESSION TESTING

The ARAMIS system was used to measure the strains and displacement over one quadrant of the sandwich specimens. The scan region extended about an inch outside the boundaries defining the quadrant of interest, as shown in figure 37. The typical distributions of out-of-plane displacement,  $w(x,y)$ , and in-plane strains,  $\epsilon_{yy}(x,y)$ , along the loading direction are shown in figure 38. The deformation fields were then analyzed across a horizontal section passing through the center of the damage region.

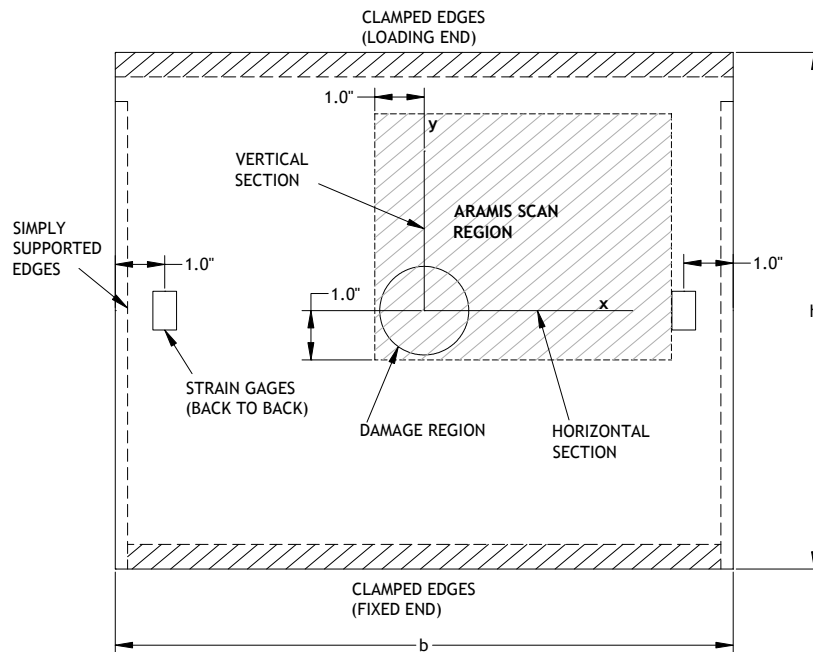


FIGURE 37. LOCATION OF STRAIN GAGES AND SCAN REGION FOR PHOTOGRAMMETRY MEASUREMENTS

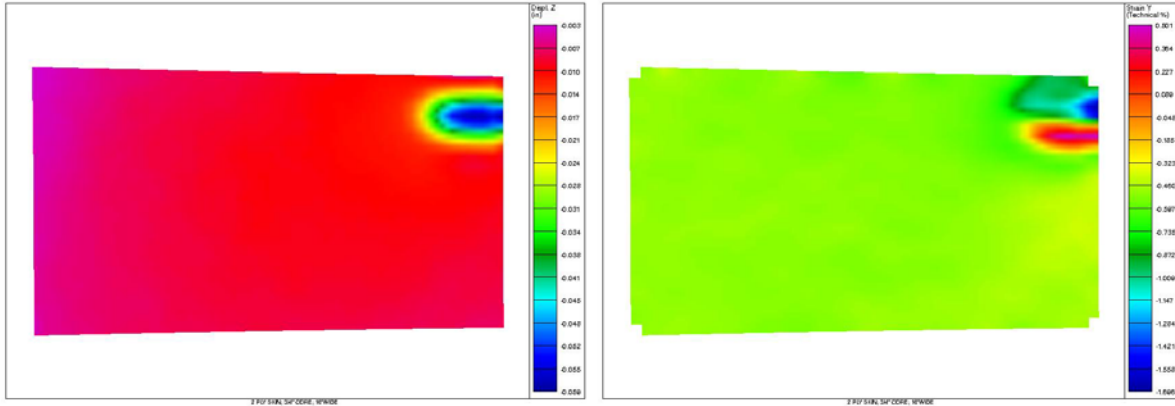


FIGURE 38. TYPICAL OUT-OF-PLANE DISPLACEMENT DISTRIBUTION,  $w(x,y)$ , AND IN-PLANE STRAIN DISTRIBUTIONS,  $\epsilon_{YY}(x,y)$ , MEASURED USING ARAMIS PHOTOGRAMMETRY SYSTEM

The typical out-of-plane displacement and in-plane strain distribution for 6.5" sandwich panels are shown in figure 39. These section plots can be used to study the kinematics of impact damage under remote compressive stress fields. The effects of  $b/2R_{damage}$  ratio can, thus, be interpreted in terms of the strain and displacement distributions. The strain distribution in the figure indicates higher strains in the damage region at lower loads, which can be attributed to the combination of strains due to in-plane compression and bending. However, at higher loads, a distinct peak in the strain distribution can be seen at the edge of the damage region, even though the displacement distribution appears to be self-similar at each load level. At low load levels, a significant amount of compressive load can be transferred through the damage region, whereas at higher loads, the additional bending of the facesheet within the damage region creates a compliant zone that diverts the load to the adjoining undamaged facesheet, creating a strain concentration similar to an open hole. The high strains indicate an imminent facesheet fracture initiation at the edge of the damage region. The displacement and strains along the horizontal section for the other specimens can be found in appendix B.

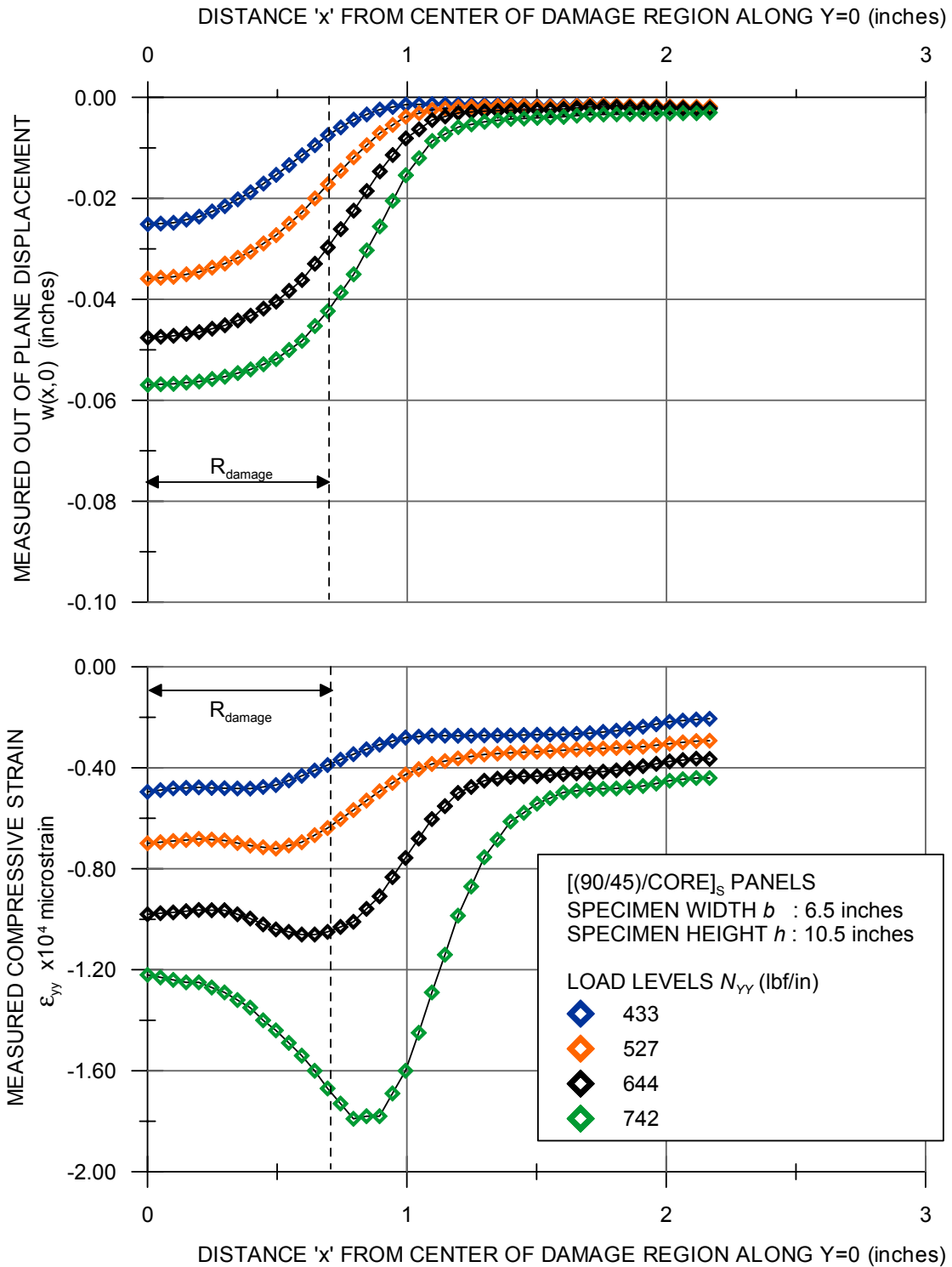


FIGURE 39. MEASURED DISPLACEMENT AND STRAIN DISTRIBUTIONS ACROSS A HORIZONTAL SECTION PASSING THROUGH THE DAMAGE REGION FOR [(90/45)/CORE]<sub>s</sub> SANDWICH SPECIMENS WITH WIDTH,  $b = 6.5''$ , AT DIFFERENT LOAD LEVELS

## 4.2 RESULTS.

The data obtained from the compression tests conducted on the sandwich specimens were analyzed to quantify the effects of the width-to-damage size ratio on the residual strength. The residual strength behavior was characterized in terms of the compressive strength and the strain distributions obtained using the photogrammetry method. The residual strength of the impact-damaged sandwich panels as a function of the ratio  $b/2R_{damage}$  is shown in figure 40. The actual damage sizes corresponding to each sandwich specimen is shown by the labels on top of the symbols in the figure. The residual strength of  $[(90/45)/CORE]_s$  sandwich panels was observed to increase with the ratio  $b/2R_{damage}$ , while the  $[(90/45)_2/CORE]_s$  exhibited this trend between specimen widths of 8.5" and 16.5". The strength of the 6.5" wide specimen for  $[(90/45)_2/CORE]_s$  configuration was higher than the rest of the widths. This can be attributed to the existence of a scatter band, and additional tests would be required before any conclusion can be drawn. The figure also shows the CAI strength of 8.5" wide specimens from a previous study [1] with different levels of impact damage. It can be concluded that the CAI strength tends to increase slightly with the ratio  $b/2R_{damage}$  for both the sandwich configurations.

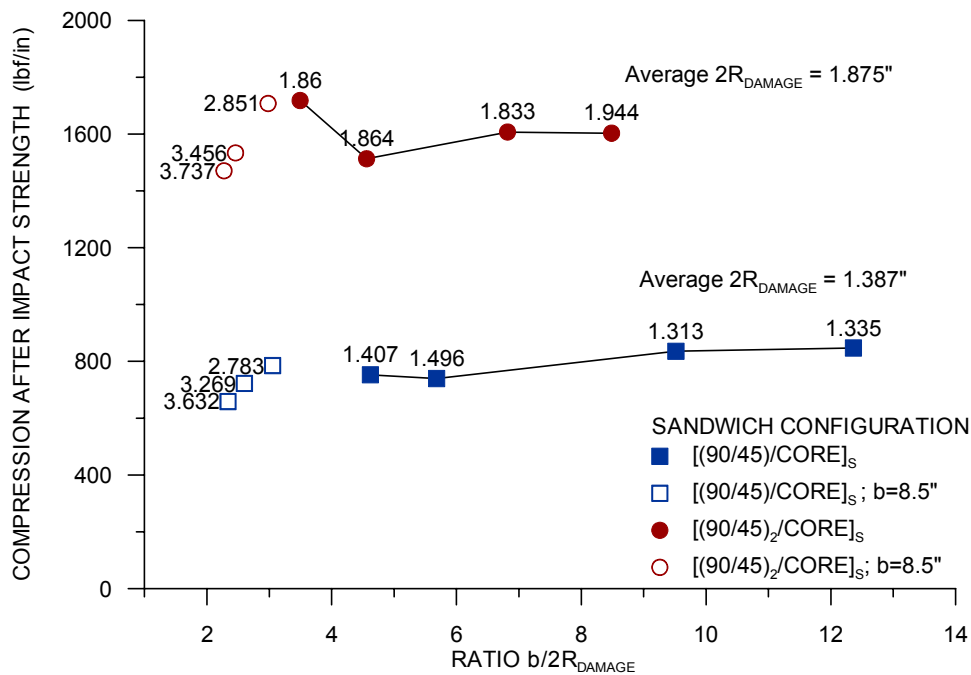


FIGURE 40. PLOT OF COMPRESSIVE RESIDUAL STRENGTH AS A FUNCTION OF  $b/2R_{damage}$

The effects of varying the height of the specimen on the compressive residual strength are shown in figure 41. The labels next to the symbols indicate the actual damage diameter for each specimen. A slight reduction in residual strength was observed for both sandwich configurations. This may be attributed to the interaction of global buckling with the impact damage acting as a geometric imperfection. Additional tests may be necessary to statistically strengthen this observation.

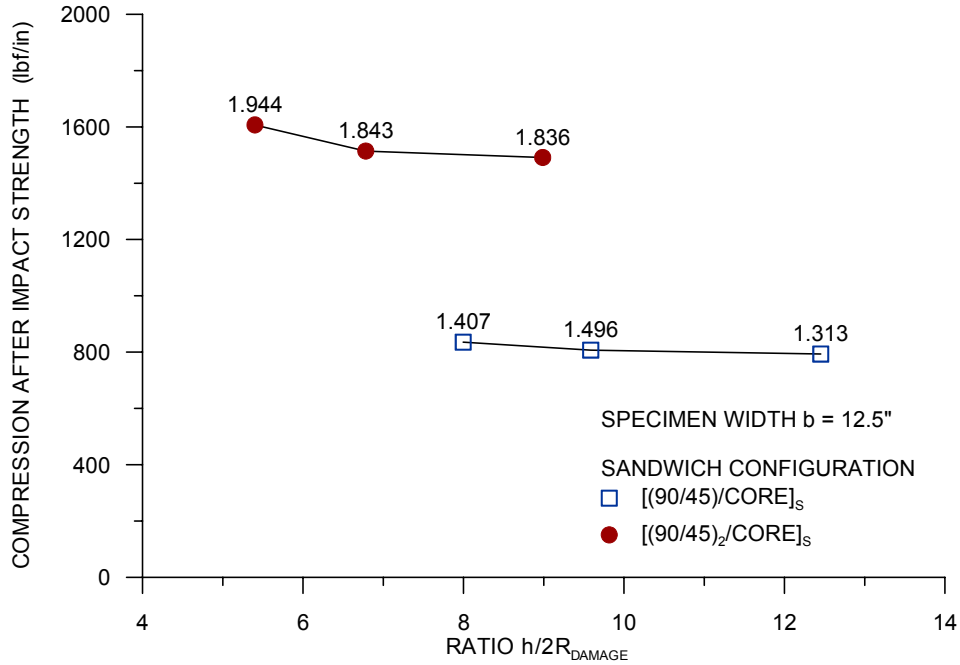


FIGURE 41. PLOT OF COMPRESSIVE RESIDUAL STRENGTH AS A FUNCTION OF  $h/2R_{damage}$

#### 4.2.1 Analysis of Displacement and Strain Distributions in $[(90/45)/CORE]_s$ Sandwich Panels.

In an effort to explain the increase in strength as the ratio  $b/2R_{damage}$  was increased, the distribution of strains along the horizontal sections for  $[(90/45)/CORE]_s$  sandwich panels of different widths was compared at different load levels. The strain distributions at four nominal load levels are shown in figures 42a through 42d. It must be noted that the measurements using ARAMIS could not be taken at precisely the same loads for each specimen. Therefore, the actual loads for specimens with different widths are indicated in each figure. The strain distributions indicated contrasting behavior as the specimen width was increased. It was observed that the facesheet within the damaged region was strained more in narrower specimens compared to wider specimens, indicating higher facesheet bending. This is supported by the out-of-plane displacements across the horizontal sections shown in figure 42e. The out-of-plane displacements are consistently higher for narrow specimens. A strain peak was observed at the edge of the damage region as the load was increased. The strain concentration effects were more pronounced in narrow specimens and tended to decrease with increase of specimen width. This implies that for narrow specimens, a greater percentage of load is carried through the facesheet within the damage region, causing increased bending of the facesheet. As the facesheet bends, the compressive stiffness of the damage region reduces, and the load is diverted across the undamaged portion of the panel. The damage region tends to behave as an open-hole region resulting in a strain concentration, as shown in figures 42c and 42d. The final failure mode for all  $[(90/45)/CORE]_s$  sandwich specimens was by facesheet fracture originating at the edge of the damage region.

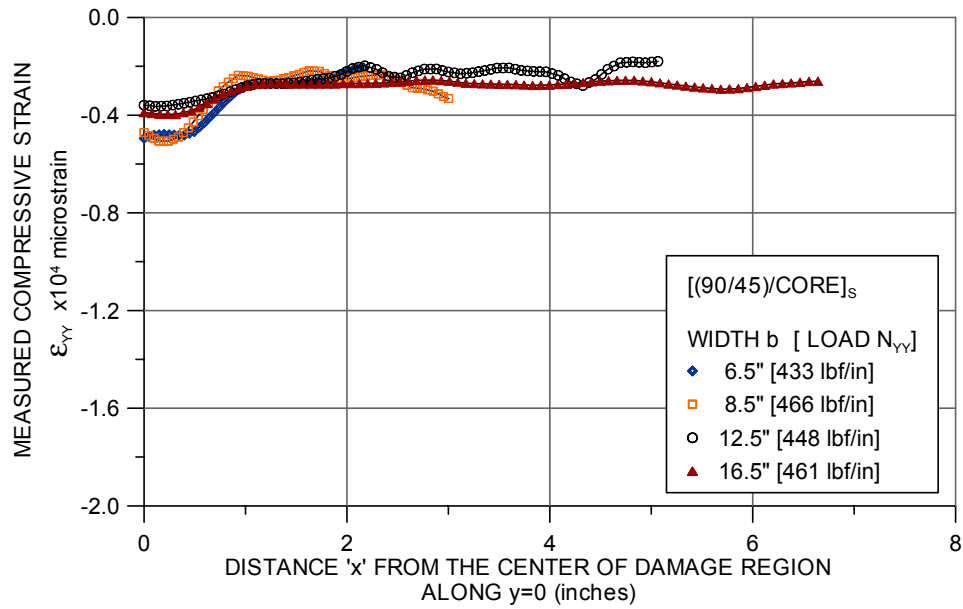


FIGURE 42a. STRAIN DISTRIBUTION IN [(90/45)/CORE]<sub>s</sub> SANDWICH PANELS AT NOMINAL LOAD OF 450 lbf/in

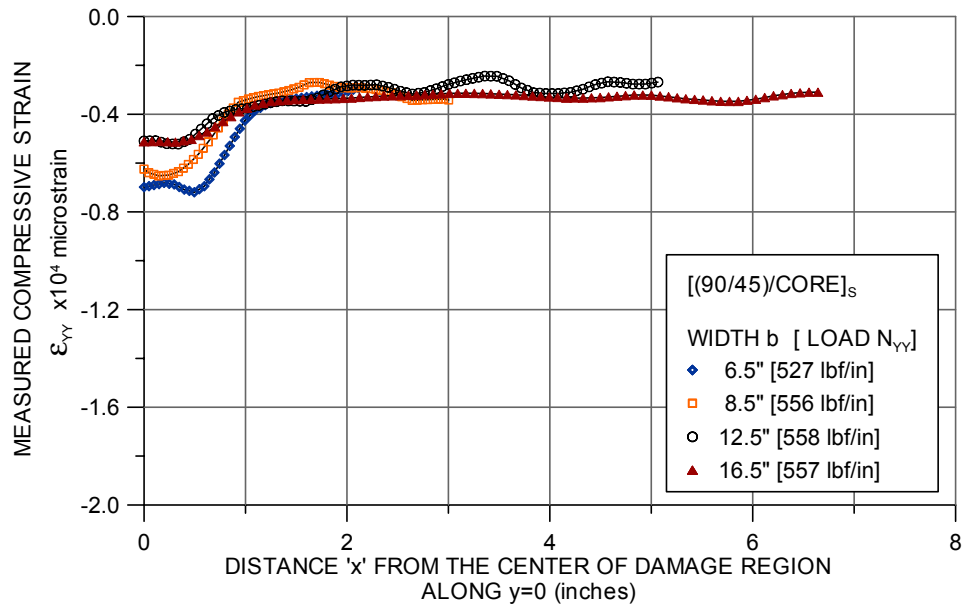


FIGURE 42b. STRAIN DISTRIBUTION IN [(90/45)/CORE]<sub>s</sub> SANDWICH PANELS AT NOMINAL LOAD OF 550 lbf/in

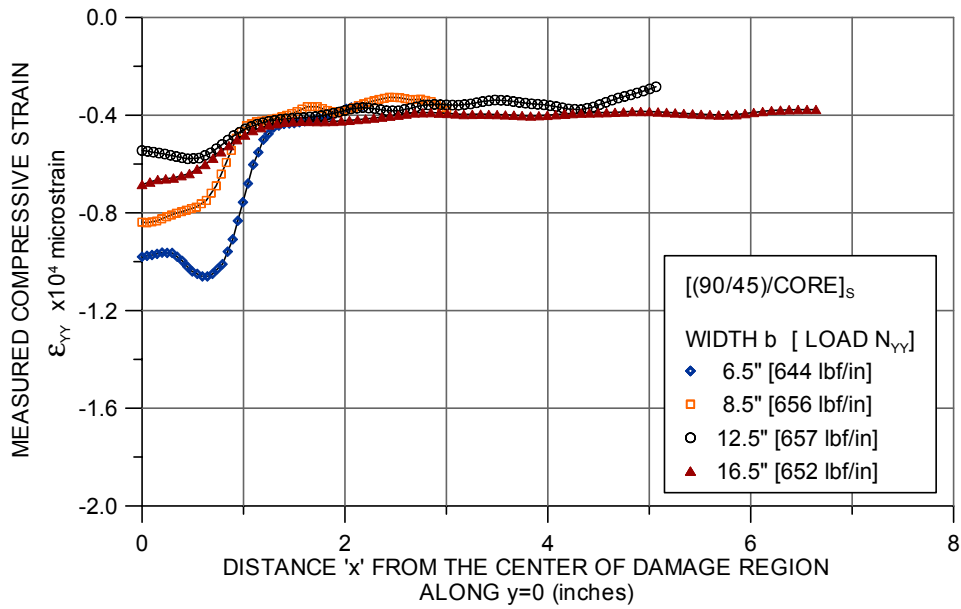


FIGURE 42c. STRAIN DISTRIBUTION IN [(90/45)/CORE]<sub>s</sub> SANDWICH PANELS AT NOMINAL LOAD OF 650 lbf/in

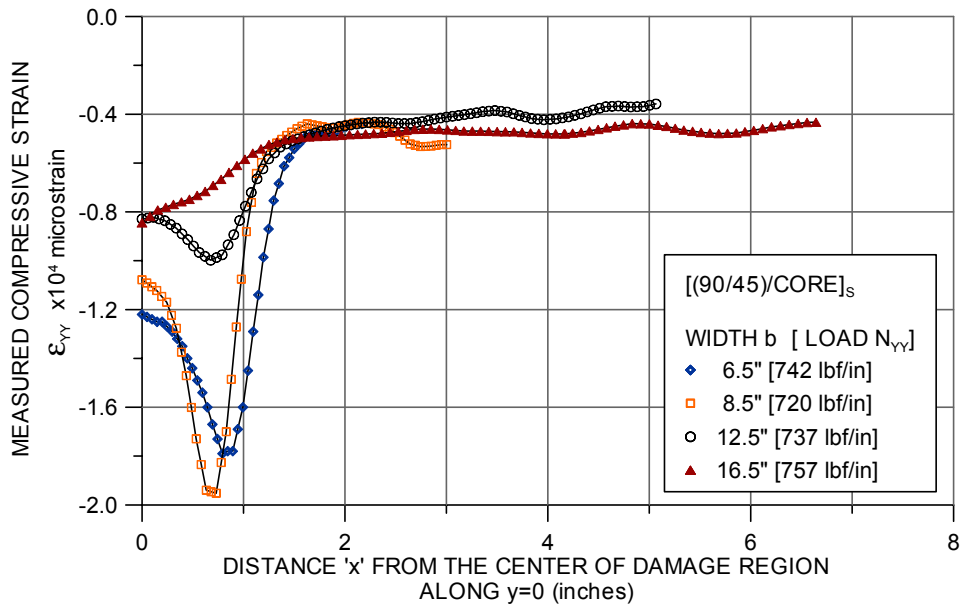


FIGURE 42d. STRAIN DISTRIBUTION IN [(90/45)/CORE]<sub>s</sub> SANDWICH PANELS AT NOMINAL LOAD OF 730 lbf/in

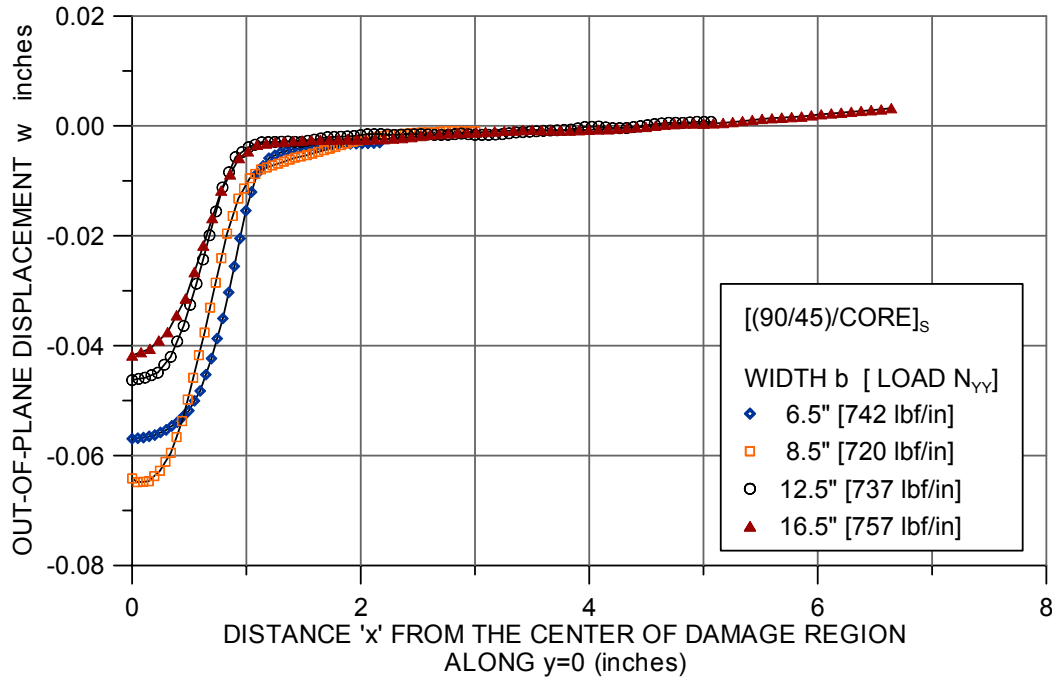


FIGURE 42e. OUT-OF-PLANE DISPLACEMENT DISTRIBUTION IN  $[(90/45)/CORE]_S$  SANDWICH PANELS AT NOMINAL LOAD OF 730 lbf/in

#### 4.2.2 Analysis of Displacement and Strain Distributions in $[(90/45)_2/CORE]_S$ Sandwich Panels.

The  $[(90/45)_2/CORE]_S$  sandwich panels exhibited trends similar to that of  $[(90/45)/CORE]_S$  panels when the strain distributions were compared for different specimen widths. The strain distributions along the horizontal section passing through the center of the damage region are shown in figures 43a through 43d. The  $[(90/45)_2/CORE]_S$  sandwich panels did not produce a strain peak at the edge of the damage region, indicating load transfer through the damage region in spite of the facesheet bending. A contrasting behavior of the sandwich specimens was observed as the width was increased. The 6.5" wide specimen exhibited an unstable dimple propagation across the width of the specimen resulting in a buckling failure, while the 16.5" wide specimen exhibited a dimple growth-arrest mechanism leading to the initiation of skin fracture and resulting in compressive failure of the facesheet. The bulging of the backside facesheet was visually observed in 6.5" wide specimens even at low load levels.

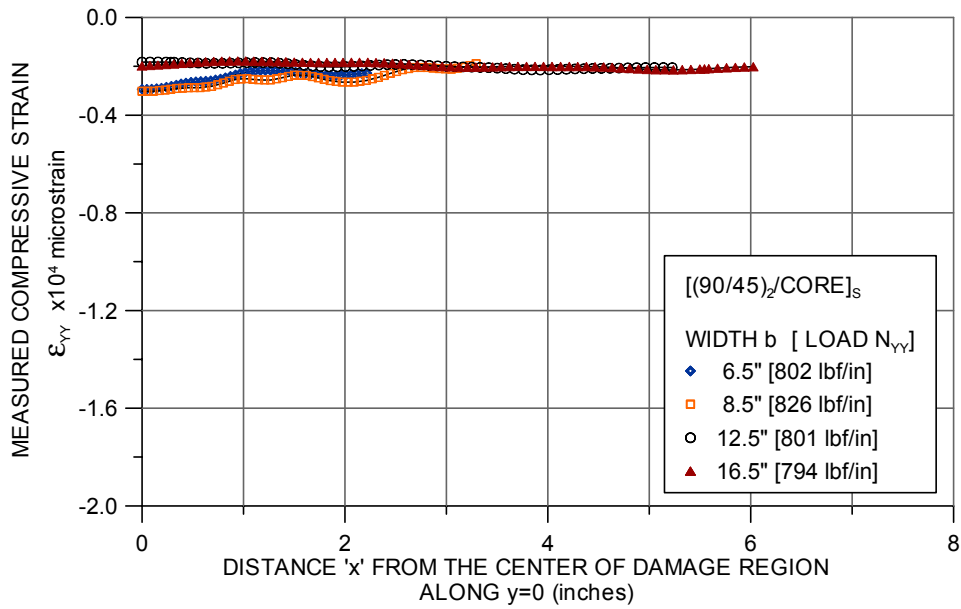


FIGURE 43a. STRAIN DISTRIBUTION IN [(90/45)<sub>2</sub>/CORE]<sub>s</sub> SANDWICH PANELS AT NOMINAL LOAD OF 800 lbf/in

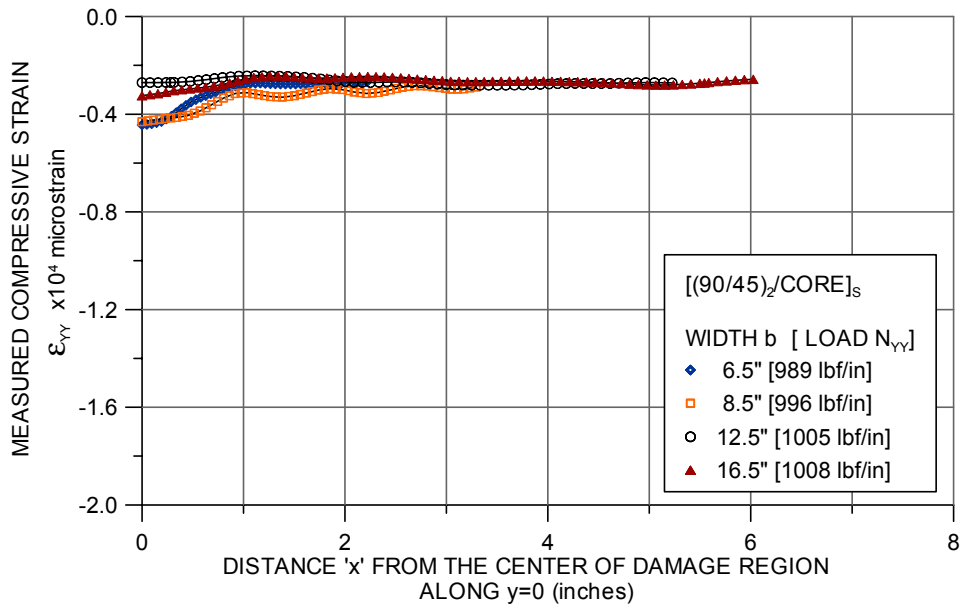


FIGURE 43b. STRAIN DISTRIBUTION IN [(90/45)<sub>2</sub>/CORE]<sub>s</sub> SANDWICH PANELS AT NOMINAL LOAD OF 1000 lbf/in

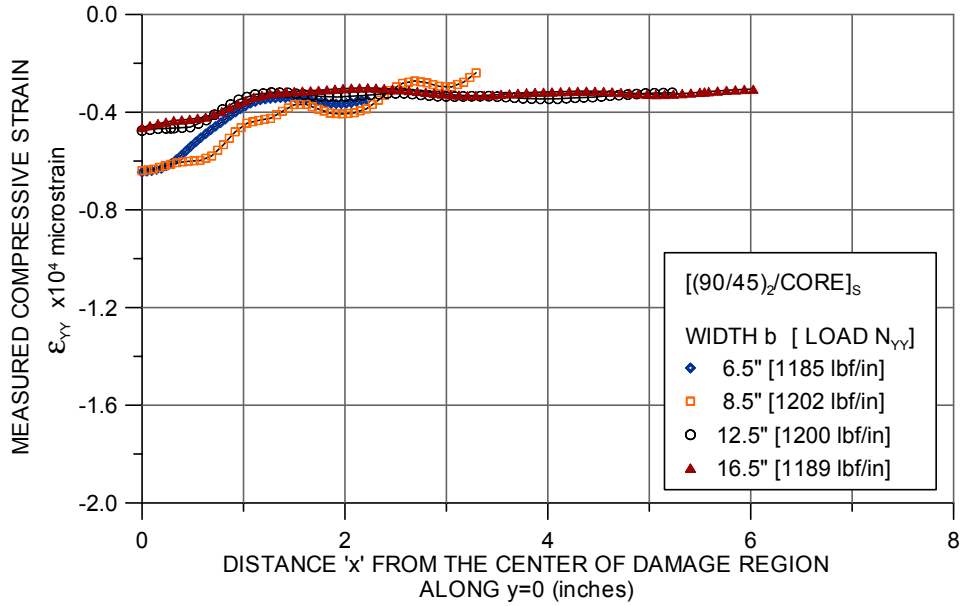


FIGURE 43c. STRAIN DISTRIBUTION IN  $[(90/45)_2/CORE]_s$  SANDWICH PANELS AT NOMINAL LOAD OF 1200 lbf/in

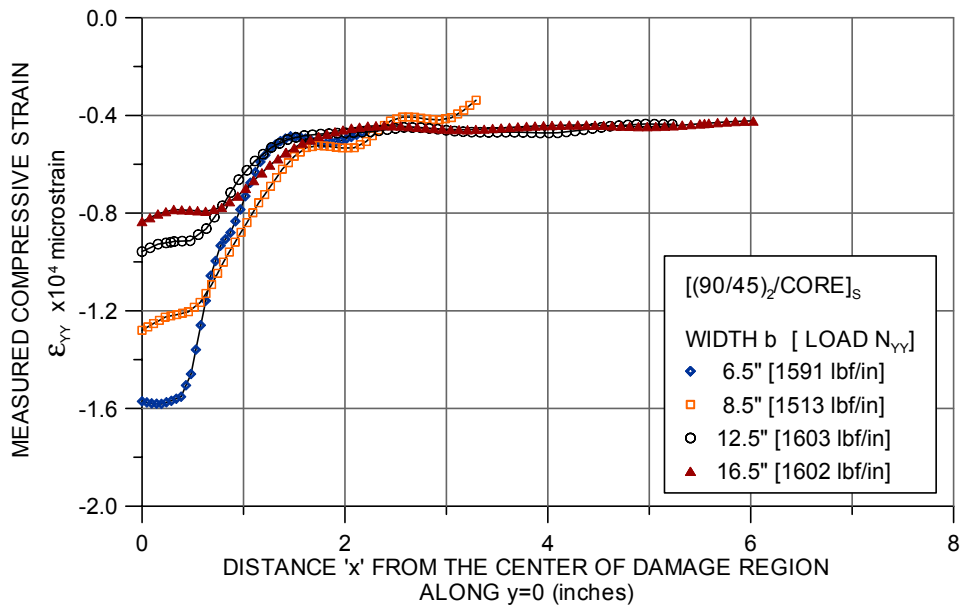


FIGURE 43d. STRAIN DISTRIBUTION IN  $[(90/45)_2/CORE]_s$  SANDWICH PANELS AT NOMINAL LOAD OF 1200 lbf/in

In summary, the effects of the specimen width to damage size ratio on the residual compression strength of two sandwich configurations were studied. The experimental results for  $[(90/45)/CORE]_s$  sandwich specimens indicated that the residual strength increased by 12% as the  $b/2R_{damage}$  ratio was increased from 4.6 to 12.4. Contrasting strain distributions were observed using the photogrammetry method, as the specimen width was increased. The impact

damage in  $[(90/45)/\text{CORE}]_s$  specimens tended to behave as an open hole, resulting in a strain concentration at the edge of the damage region. All  $[(90/45)/\text{CORE}]_s$  sandwich specimens failed by compressive fracture of facesheet, with the failure initiating at the edge of the damage region.

The  $[(90/45)_2/\text{CORE}]_s$  specimens exhibited contrasting failure modes when the width was increased. The 6.5" wide specimen failed due to unstable dimple propagation across the width resulting in buckling failure, while the 16.5" wide specimen failed due to a dimple growth-arrest mechanism that precipitated in compressive fracture of the facesheet. The strain distributions obtained using the photogrammetry method did not indicate a strain concentration at the edge of the damage region, but the strains were consistently higher within the damage region for narrower specimens. The residual strength was observed to decrease with increase in specimen height, for a constant width to damage size ratio. The reduction was about 5% and 7% for  $[(90/45)/\text{CORE}]_s$  and  $[(90/45)_2/\text{CORE}]_s$  sandwich panels respectively, when the height was increased from 10.5" to 16.5".

## 5. CONCLUSIONS.

The work presented in this report describes the effects of scaling on the impact damage resistance and damage tolerance of sandwich panels with thin quasi-isotropic facesheets and honeycomb cores. The effects of scaling the planar dimensions on the impact behavior and the resulting damage in honeycomb core sandwich panels were studied by conducting a limited number of experiments. A parametric study, using a finite element (FE) model, was conducted to investigate panel sizes that are not practical to test in the laboratory. A limited number of compression-after-impact tests were conducted on sandwich panels to investigate the dependence of residual strength on the specimen width to damage size ratio. Full-field photogrammetry methods were used to observe the displacement and strain distributions in the vicinity of the impact damage under compressive loading.

The effects of scaling the planar dimensions on the impact resistance of honeycomb core sandwich panels were investigated experimentally. The sandwich specimens were impacted using a 3" diameter impactor, at four impact energy levels, and the effects of scaling were characterized in terms of the impact response, planar damage size, and the residual dent depth. The experimental results indicated that the impact force decreased when both the planar dimensions of the panel were increased. However, the increase of a single dimension did not significantly change the impact response. The scaling of planar dimensions on the planar damage size exhibited trends similar to that of the impact force, with the exception of the sandwich specimens with rigid-base supports, which suffered more residual indentation than planar damage.

The off-center impacts conducted on a 16"  $\times$  16" panel indicated that the impact was more severe at locations closer to the boundary supports. The planar damage diameter and the residual indentation depth increased when the impact location approached the boundary. Further, the shape of the planar damage region was unsymmetrical for impact locations closest to the boundary supports.

The effects of scaling on the impact resistance were further investigated using an FE model using contact laws. The predication of the FE model compared satisfactorily with the experimental results. The parametric study using linearized contact laws indicated that the energy absorption in sandwich panels, due to impacts, depends on the dissipativeness of the contact behavior and the planar dimension of the plate. The effects of impactor mass to plate mass ratio have been highlighted using this study.

The damage tolerance of sandwich structures with subsurface impact damage from a 3" diameter impactor was investigated for possible scaling effects. The effects of varying the ratio of specimen width to planar damage diameter, for a fixed damage size, were studied by conducting compression tests. A full-field displacement and strain measurement photogrammetry system was used during the tests. The effects of the width to damage size ratio was characterized in terms of the residual strength, displacement distributions, and strain distributions. Based on the limited test data, the residual strength was observed to increase by 12% when the width of the specimen was increased from 6.5" to 16" for sandwich specimens with two-ply facesheets. No significant trend was however observed for sandwich specimens with four-ply facesheets. The displacement and strain distributions showed contrasting behavior of impact damage as the specimen width was increased. The results indicated higher component of facesheet bending within the damage region for narrow specimens when compared with the wider specimens.

This study showed that compressive residual strength results obtained experimentally are valid if the impact damage size and failure mechanisms are monitored to ensure the finite width effects of small specimens do not affect the outcome. As related to the impact event, it is important to realize that the larger specimen sizes will sustain less impact damage for equivalent impact energy levels unless the impact is close to a stiffener. Thus, it is valid to test smaller panels if the damage is simulated correctly from the larger specimens. The effects of specimen height were not investigated, but specimen height could affect the buckling response of the panels.

## 6. REFERENCES.

1. Tomblin, J.S., Raju, K.S., Liew, J., and Smith, B.L., "Impact Damage Characterization and Damage Tolerance of Composite Sandwich Airframe Structures," FAA report DOT/FAA/AR-00/44, January 2001.
2. Morton, J., "Scaling of Impact-Loaded Carbon Fiber Composites," *AIAA Journal*, 1988, **26**, pp. 989-994.
3. Swanson, S.R., "Scaling of Impact Damage in Fiber Composites From Laboratory Specimens to Structures," *Composite Structures*, 1993, **25**, pp. 249-255.
4. Qian, Y., Swanson, S.R., Nuismer, R.J., and Bucinell, R.B., "An Experimental Study of Scaling Rules for Impact Damage in Fiber Composites," *Journal of Composite Materials*, 1990, **24**, pp. 559-570.
5. Rhodes, M.D., "Impact Fracture of Composite Sandwich Panels," *AIAA Journal*, 1975.

6. Ferri, R. and Sankar, B.V., "Static Indentation and Low Velocity Impact Tests on Sandwich Plates," *Proceedings of the ASME Aerospace Division*, Ad-Vol. 55, ASME, 1997.
7. Dost, E.F., Avery, W.B., Finn, S.R., Grande, D.H., Huisken, A.B., Ilcewicz, L.B., Murphy, D.P., Scholz, D.B., Coxon, B.R., and Wishart, R.E., "Impact Damage Resistance of Composite Fuselage Structure," NASA-CR-4658, April 1997.
8. Williamson J.E. and Lagace P.A., "Response Mechanisms in the Impact of Graphite/Epoxy Honeycomb Sandwich Panels," *Proceedings of the American Society for Composites*, 1993.
9. McGowan, D.M. and Ambur, D.R., "Damage Characteristics and Residual Strength of Composite Sandwich Panels Impacted With and Without Compressive Loading," *AIAA 98-1783*.
10. Ambur, D.R. and Kemmerly, H.L., "Influence of Impactor Mass on the Damage Characteristics and Failure Strength of Laminated Composite Plates," *AIAA 98-1784*.
11. Ishai, O. and Hiel, C., "Damage Tolerance of a Composite Sandwich With Interleaved Foam Core," *Journal of Composites Technology and Research*, JCTRER, Vol. 14, No. 3, Fall 1992, pp. 274-284.
12. Palm, T.E., "Impact Resistance and Residual Compression Strength of Composite Sandwich Panels," *35<sup>th</sup> International SAMPE Symposium*, April 2-5, 1990.
13. Bernard, M.L. and Lagace, P.A., "Impact Resistance of Composite Sandwich Plates," *Journal of Reinforced Plastics and Composites*, Vol. 8, September 1989.
14. Tsang, P.H.W. and Dugundji, J., "Damage Resistance of Graphite/Epoxy Sandwich Panels Under Low Speed Impacts," *46<sup>th</sup> Annual Forum, American Helicopter Society*, Washington, DC, May 1990.
15. Chang, Fu-Kuo and Lessard, Larry B., "Damage Tolerance of Laminated Composites Containing an Open Hole and Subjected to Compressive Loadings: Part I—Analysis," *Journal of Composite Materials*, Vol. 25, No. 1, 1991.
16. Chang, Fu-Kuo and Lessard, Larry B., "Damage Tolerance of Laminated Composites Containing an Open Hole and Subjected to Compressive Loadings: Part II—Experiments," *Journal of Composite Materials*, Vol. 25, No. 1, 1991.
17. Raju, K.S., "The Static Indentation Behavior of Sandwich Panels With Quasi-Isotropic Skins," Ph.D. Dissertation, Dept. Aerospace Engineering, Wichita State University, December 2001.
18. Abrate, S., *Impact on Composite Structures*, Cambridge University Press, 1998.

19. Bucinell, R.B., Nuismer, R.J., and Koury, J.L., "Response of Composite Plates to Quasi-Static Impact Events," *Composite Materials: Fatigue and Fracture (3<sup>rd</sup> volume)*, ASTM STP 1110, T.K. O'Brien, ed., ASTM, Philadelphia, PA, 1991.
20. Whitney, J.M. and Pagano, N.J., "Shear Deformation in Heterogeneous Anisotropic Plates," *Journal of Applied Mechanics*, Vol. 37, 1970.
21. Sun, C.T. and Chattopadhyay, S., "Dynamic Response of Anisotropic Laminated Plates Under Initial Stress to Impact of a Mass," *Transactions of the ASME, Journal of Applied Mechanics*, Vol. 42, September 1975, pp. 693-698.
22. Dobyns, A.L., "Analysis of Simply-Supported Orthotropic Plates Subject to Static and Dynamic Loads," *AIAA 80-0688R*.
23. Tan, T.M., and Sun, C.T., "Use of Statistical Indentation Laws in the Impact Analysis of Laminated Composite Plates," *Transactions of the ASME, Journal of Applied Mechanics*, Vol. 52, March 1985, pp. 6-12.
24. Tracy, J.J., Dimas, D.J., and Pardoen, G.C., 1985, "The Effect of Impact Damage on the Dynamic Properties of Laminated Plates." *Proc. 5<sup>th</sup> Int. Conf. Composite Materials, ICCM-V*, San Diego, CA, July 29-August 1, 1985, 111-125.
25. Wang, J.T.S., Liu, Y.Y., and Gibby, J.A., "Vibrations of Split Beams," *Journal of Sound and Vibration* 84:491-502, 1982.
26. MSC Software Corporation, Los Angeles, CA 90041-1777.
27. MSC, Marc Volume B: Element Library, MSC Software Corporation, Los Angeles, CA 90041-1777.
28. Raju, K.S., and Tomblin, J.S., "Damage Characteristics in Sandwich Panels Subjected to Static Indentation Using Spherical Indentors," *42<sup>nd</sup> AIAA/ASME/ASCE/AHS/ASC Structures, Structural Dynamics and Materials Conference*, April 16-19, 2001, Seattle, WA.
29. Crook, A.W., "A Study of Some Impacts Between Metal Bodies by a Piezoelectric Method," *Proceedings of the Royal Society*, London, Series A, Vol. 212, 1952.
30. Christoforou, A.P., and Swanson, S.R., "Analysis of Impact in Composite Plates," *International Journal of Solids & Structures*, Vol. 27, No. 2, pp. 161-170, 1991.
31. Tomblin, J.S., Raju, K.S., Acosta, J., Smith, B.L., and Romine, N., "Impact Damage Characterization and Damage Tolerance of Composite Sandwich Airframe Structures—Phase-II," FAA report DOT/FAA/AR-02/80, October 2002.
32. GOM Optical Measuring Techniques, GOM mbH, Mittelweg 7-8, 38106 Braunschweig, Germany.

APPENDIX A—FORCE-TIME HISTORIES

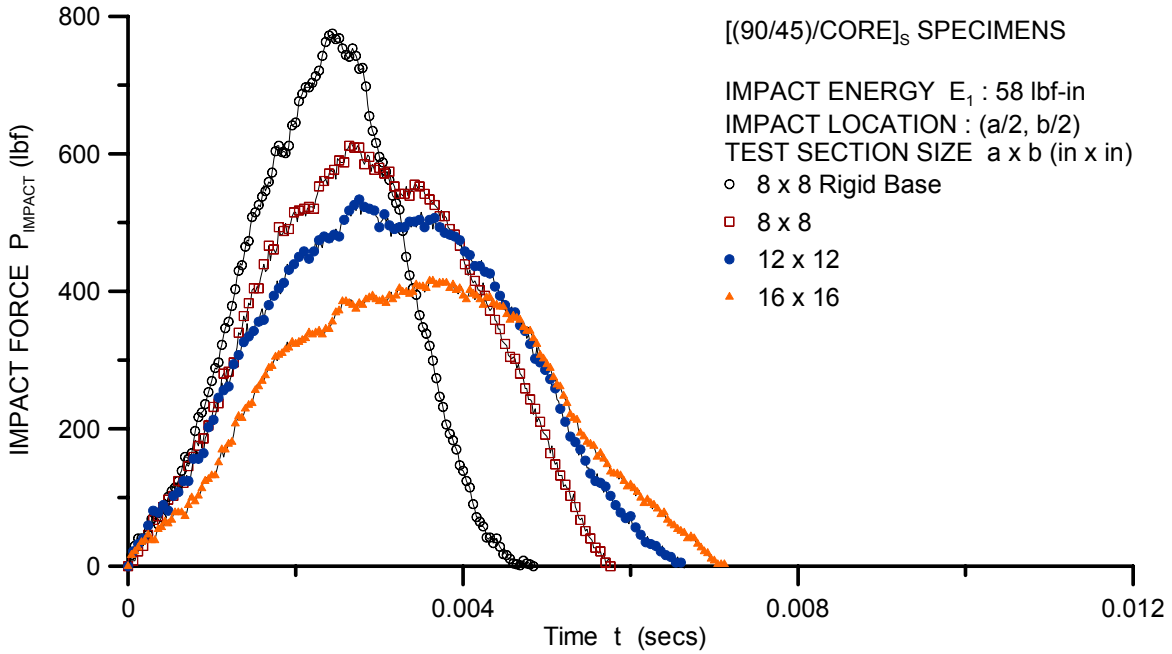


FIGURE A-1. FORCE-TIME HISTORY FOR [(90/45)/CORE]<sub>s</sub> SANDWICH PANELS IMPACTED AT ENERGY LEVEL  $E_1 = 58$  lbf-in

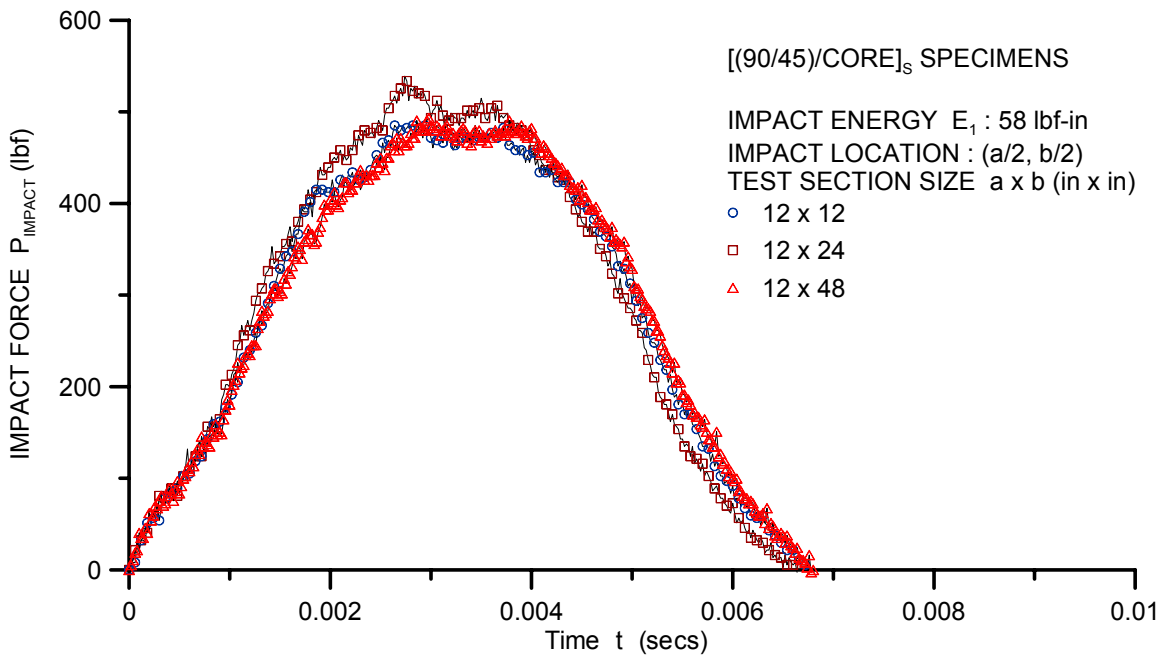


FIGURE A-2. FORCE-TIME HISTORY FOR [(90/45)/CORE]<sub>s</sub> SANDWICH PANELS IMPACTED AT ENERGY LEVEL  $E_1 = 58$  lbf-in FOR DIFFERENT WIDTHS

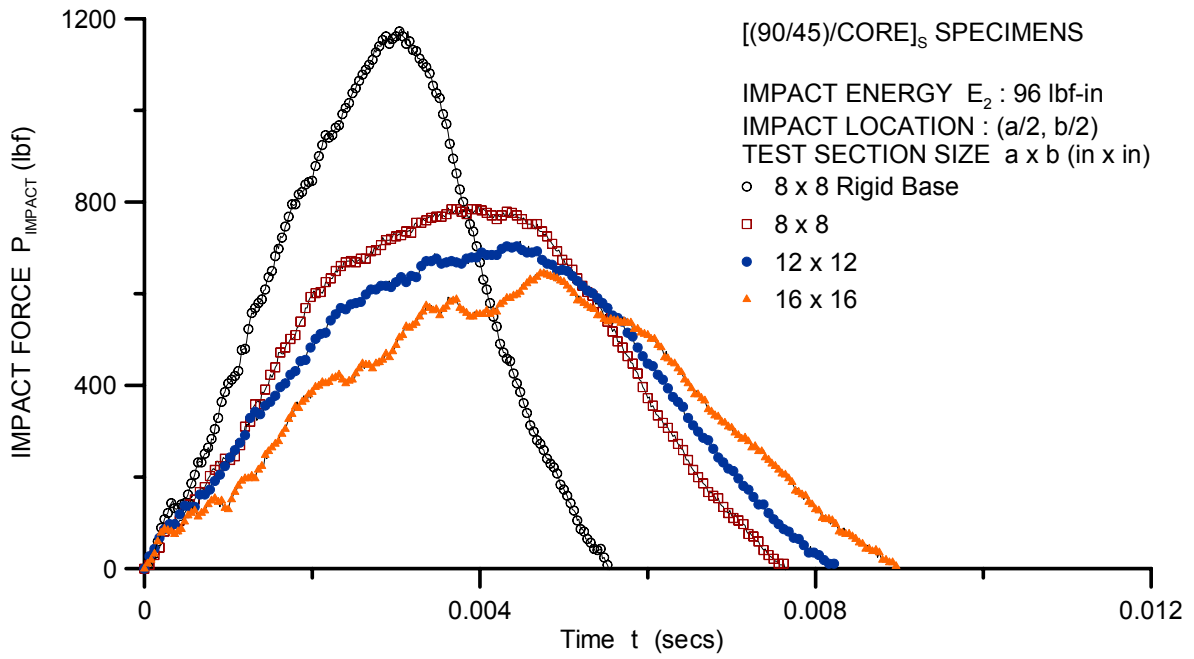


FIGURE A-3. FORCE-TIME HISTORY FOR [(90/45)/CORE]<sub>s</sub> SANDWICH PANELS IMPACTED AT ENERGY LEVEL  $E_2 = 96$  lbf-in

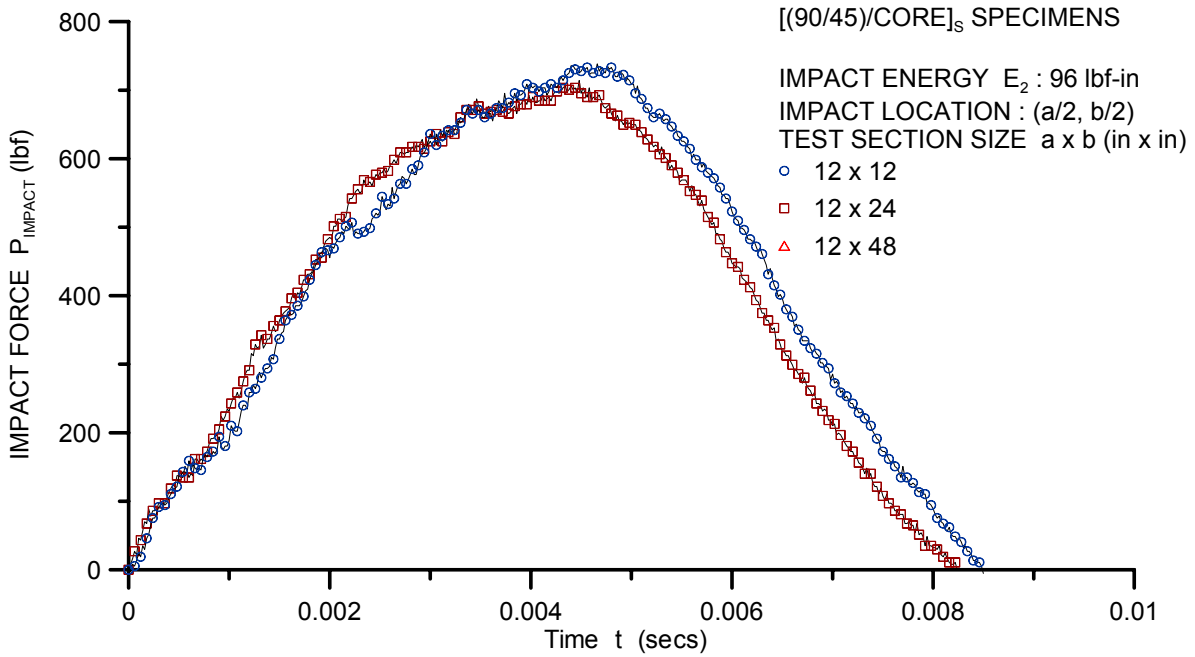


FIGURE A-4. FORCE-TIME HISTORY FOR [(90/45)/CORE]<sub>s</sub> SANDWICH PANELS IMPACTED AT ENERGY LEVEL  $E_2 = 96$  lbf-in FOR DIFFERENT WIDTHS

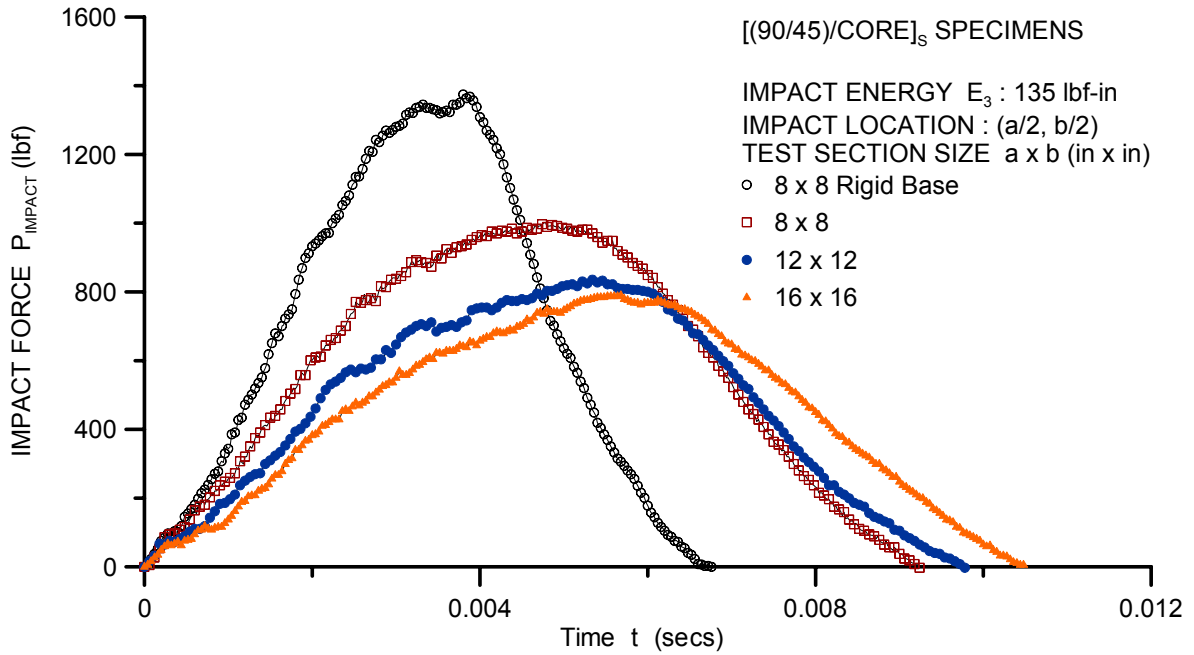


FIGURE A-5. FORCE-TIME HISTORY FOR [(90/45)/CORE]<sub>s</sub> SANDWICH PANELS IMPACTED AT ENERGY LEVEL  $E_3 = 135$  lbf-in

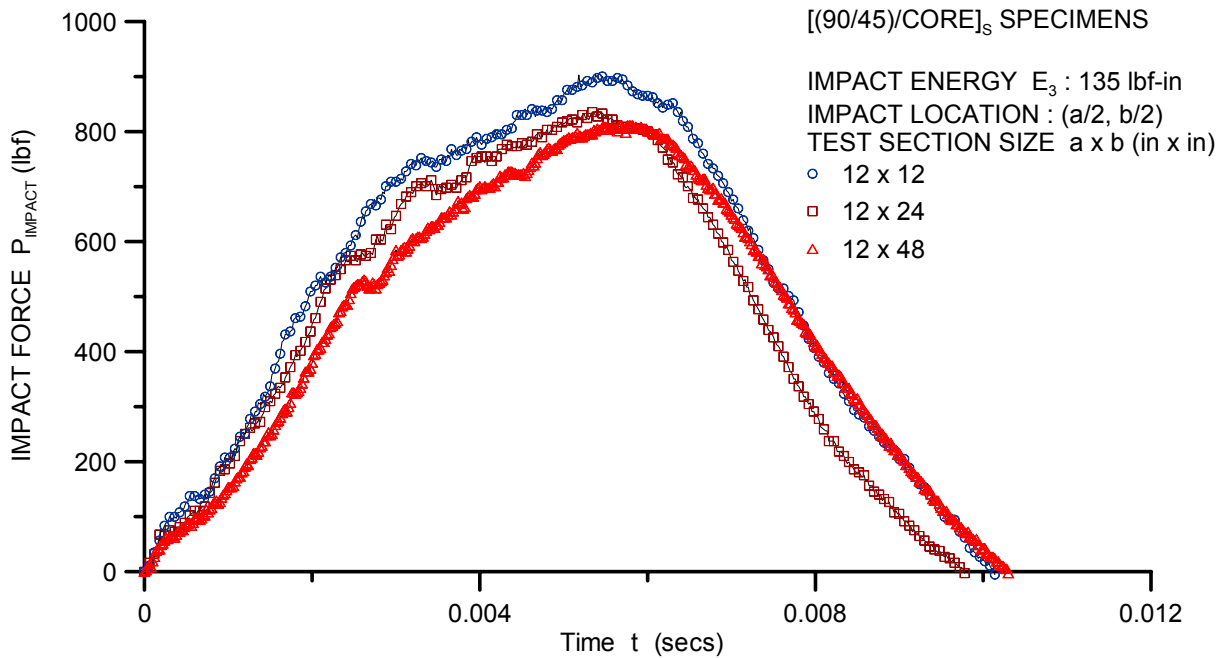


FIGURE A-6. FORCE-TIME HISTORY FOR [(90/45)/CORE]<sub>s</sub> SANDWICH PANELS IMPACTED AT ENERGY LEVEL  $E_3 = 135$  lbf-in FOR DIFFERENT WIDTHS

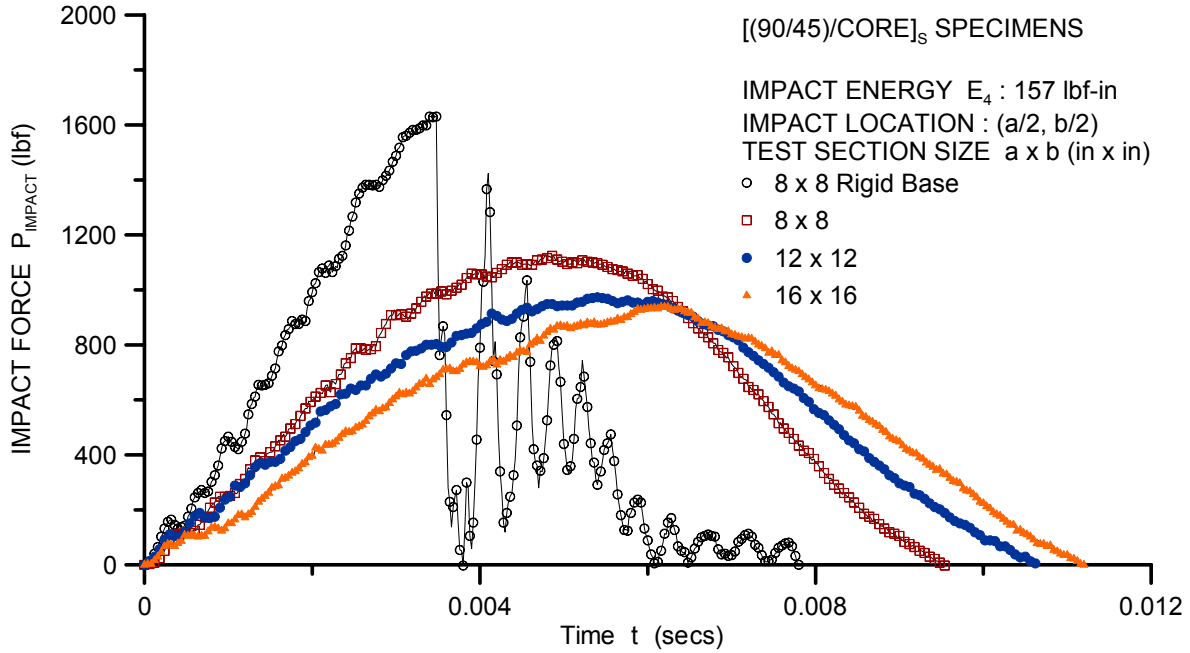


FIGURE A-7. FORCE-TIME HISTORY FOR [(90/45)/CORE]<sub>s</sub> SANDWICH PANELS IMPACTED AT ENERGY LEVEL  $E_4 = 157$  lbf-in

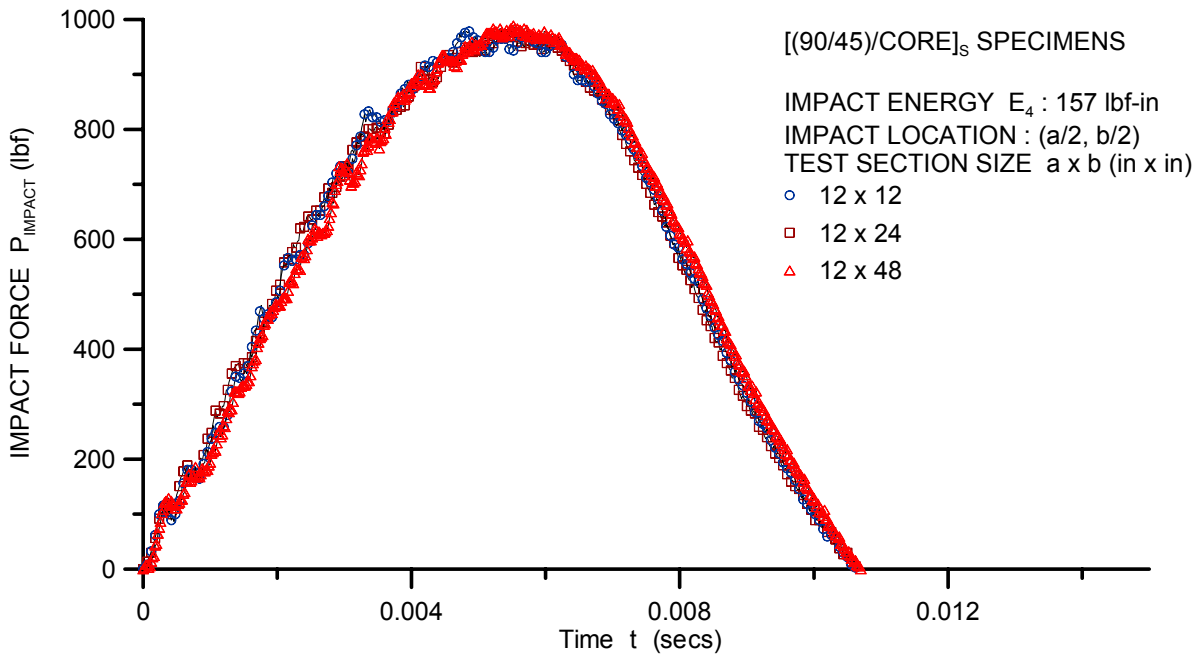


FIGURE A-8. FORCE-TIME HISTORY FOR [(90/45)/CORE]<sub>s</sub> SANDWICH PANELS IMPACTED AT ENERGY LEVEL  $E_4 = 157$  lbf-in FOR DIFFERENT WIDTHS

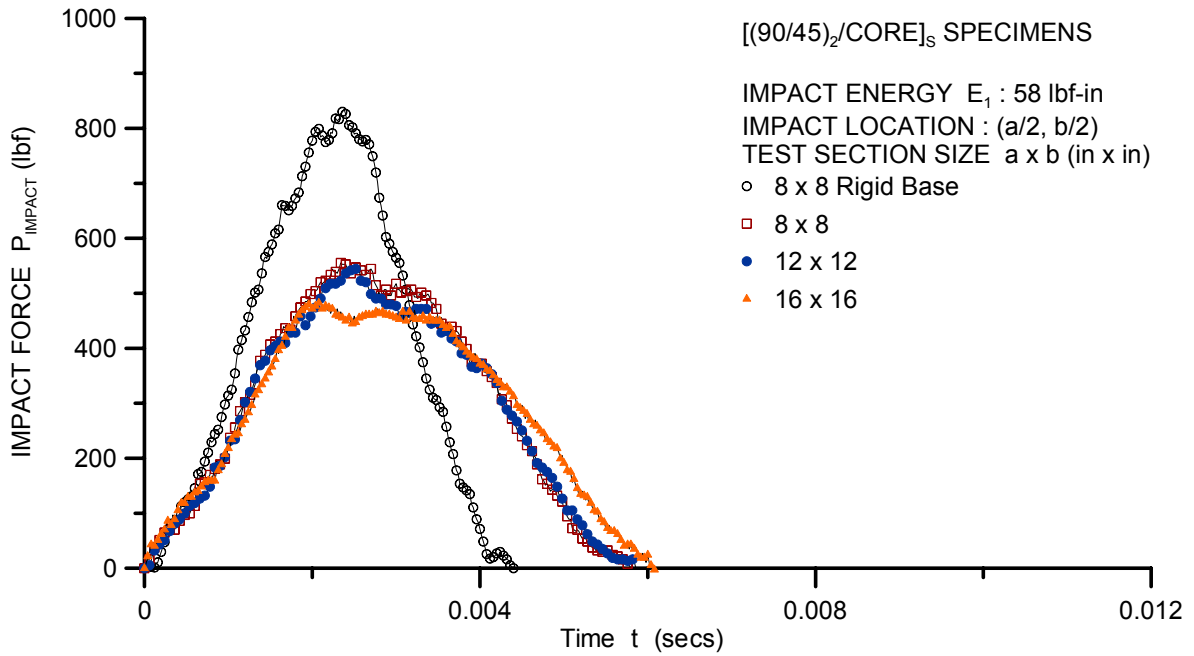


FIGURE A-9. FORCE-TIME HISTORY FOR [(90/45)<sub>2</sub>/CORE]<sub>s</sub> SANDWICH PANELS IMPACTED AT ENERGY LEVEL  $E_1 = 58$  lbf-in

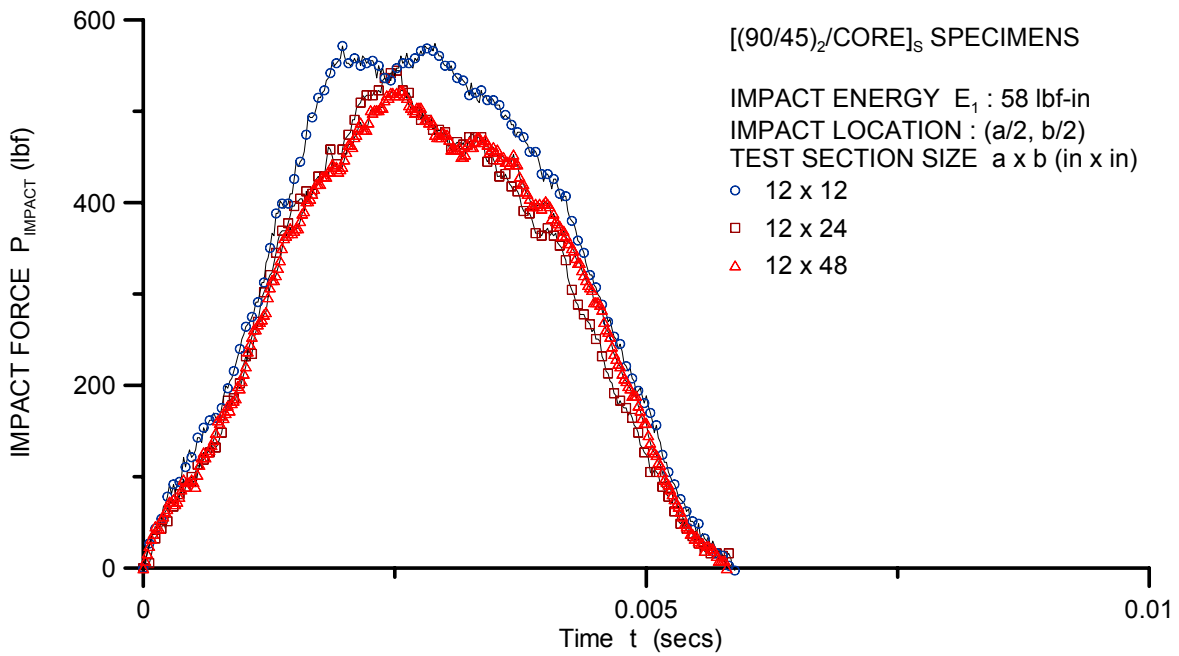


FIGURE A-10. FORCE-TIME HISTORY FOR [(90/45)<sub>2</sub>/CORE]<sub>s</sub> SANDWICH PANELS IMPACTED AT ENERGY LEVEL  $E_1 = 58$  lbf-in FOR DIFFERENT WIDTHS

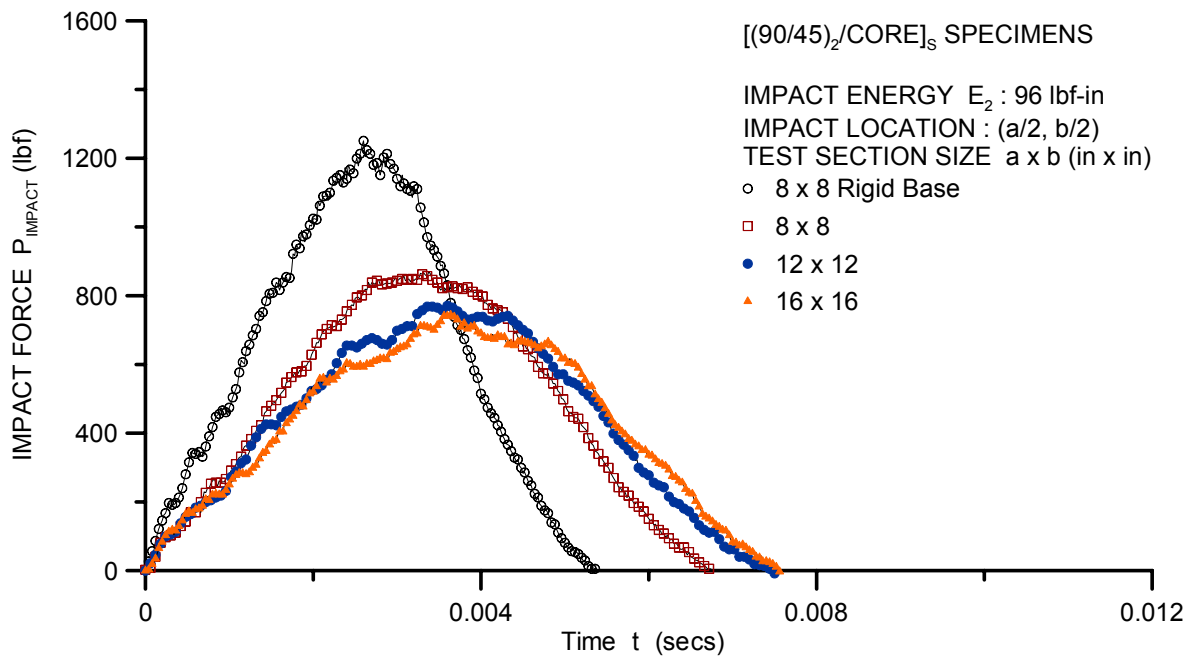


FIGURE A-11. FORCE-TIME HISTORY FOR [(90/45)<sub>2</sub>/CORE]<sub>s</sub> SANDWICH PANELS IMPACTED AT ENERGY LEVEL  $E_2 = 96$  lbf-in

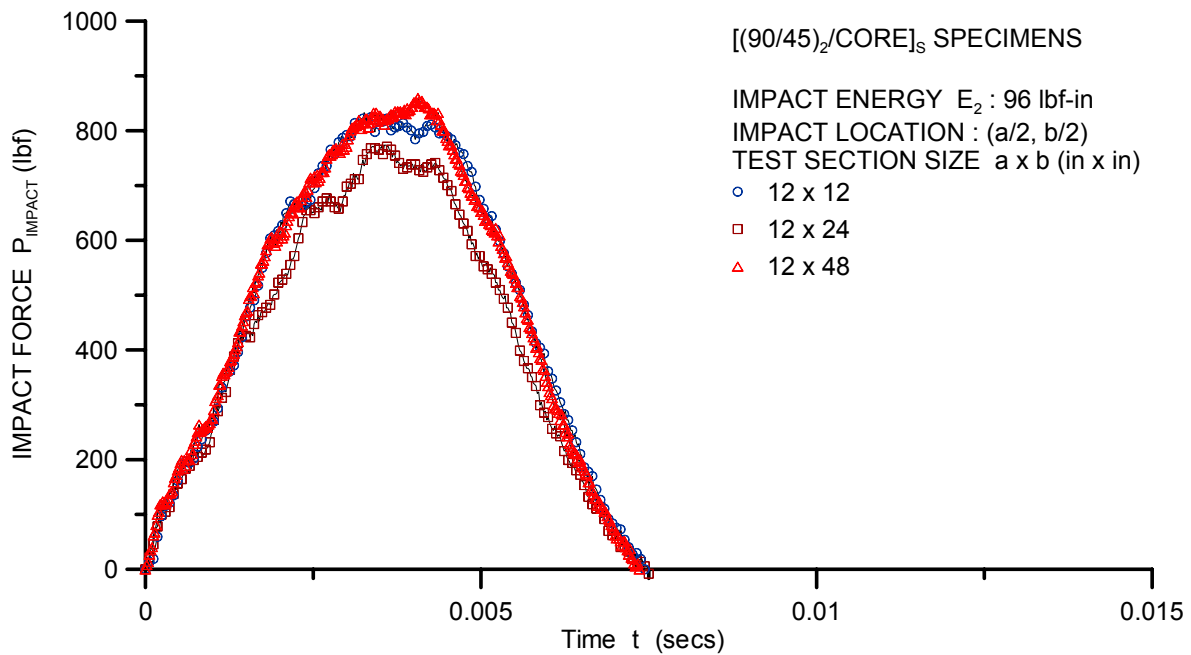


FIGURE A-12. FORCE-TIME HISTORY FOR [(90/45)<sub>2</sub>/CORE]<sub>s</sub> SANDWICH PANELS IMPACTED AT ENERGY LEVEL  $E_2 = 96$  lbf-in FOR DIFFERENT WIDTHS

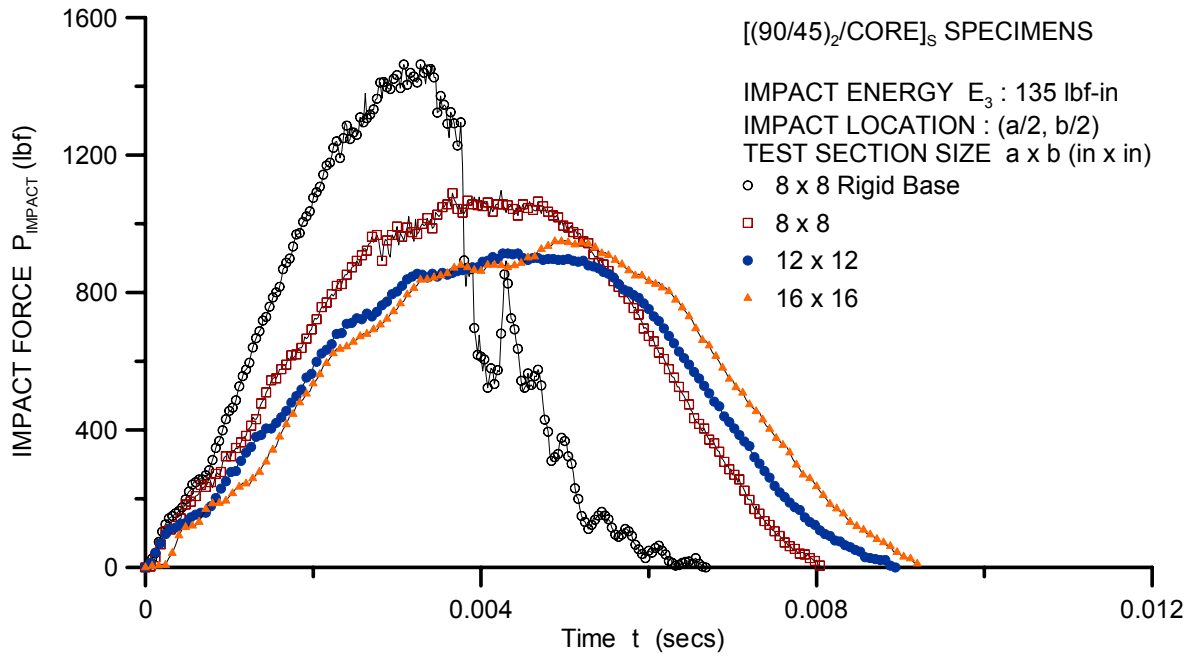


FIGURE A-13. FORCE-TIME HISTORY FOR [(90/45)<sub>2</sub>/CORE]<sub>s</sub> SANDWICH PANELS IMPACTED AT ENERGY LEVEL E<sub>3</sub> = 135 lbf-in

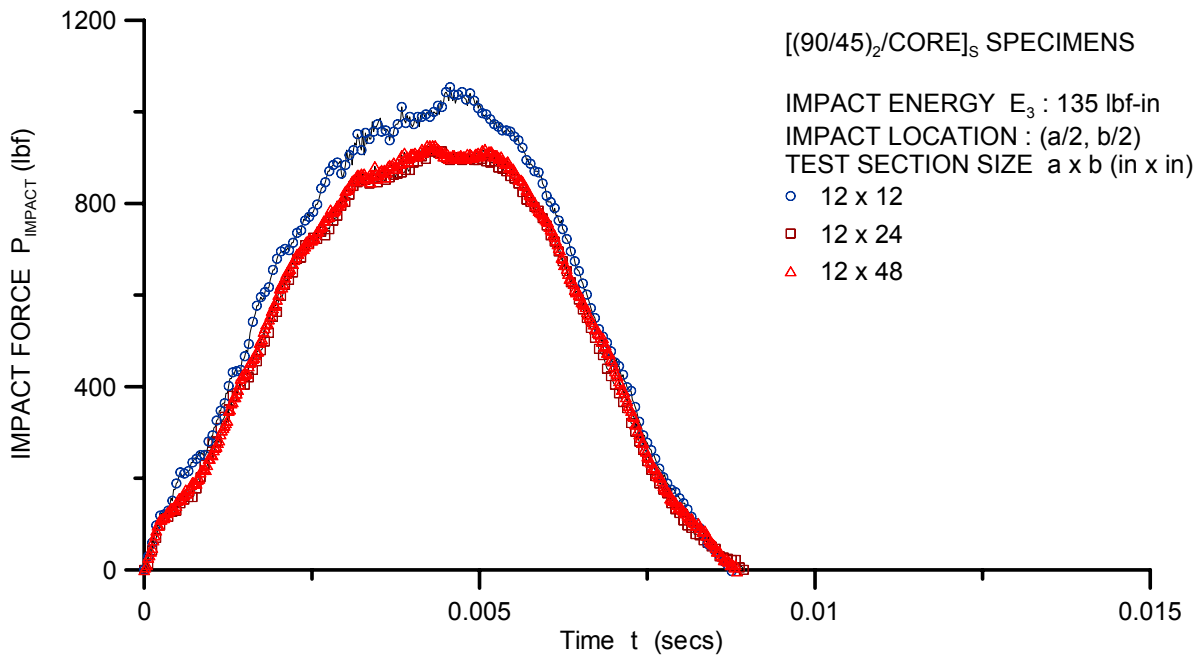


FIGURE A-14. FORCE-TIME HISTORY FOR [(90/45)<sub>2</sub>/CORE]<sub>s</sub> SANDWICH PANELS IMPACTED AT ENERGY LEVEL E<sub>3</sub> = 135 lbf-in FOR DIFFERENT WIDTHS

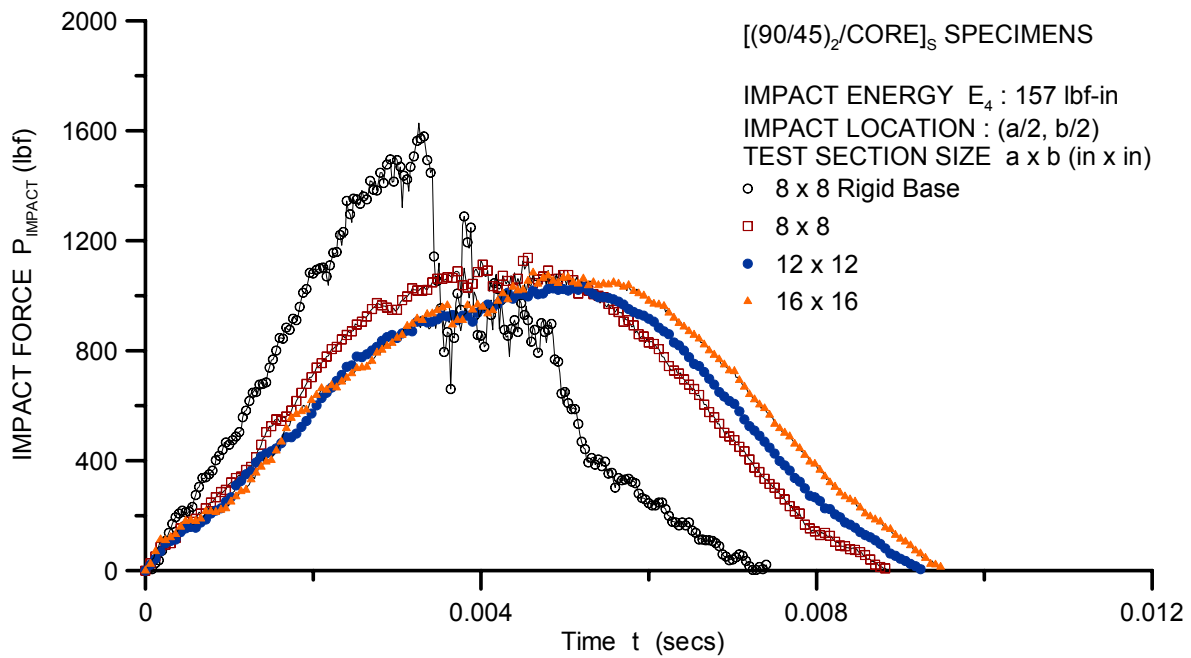


FIGURE A-15. FORCE-TIME HISTORY FOR [(90/45)<sub>2</sub>/CORE]<sub>s</sub> SANDWICH PANELS IMPACTED AT ENERGY LEVEL E<sub>4</sub> = 157 lbf-in

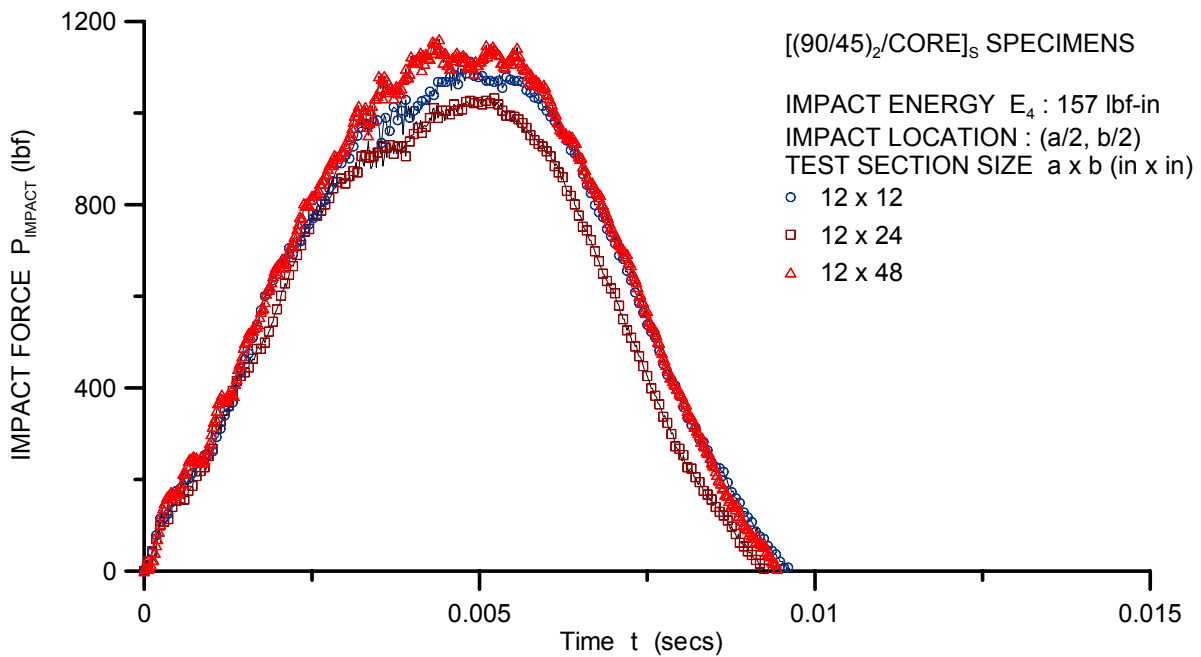


FIGURE A-16. FORCE-TIME HISTORY FOR [(90/45)<sub>2</sub>/CORE]<sub>s</sub> SANDWICH PANELS IMPACTED AT ENERGY LEVEL E<sub>4</sub> = 157 lbf-in FOR DIFFERENT WIDTHS

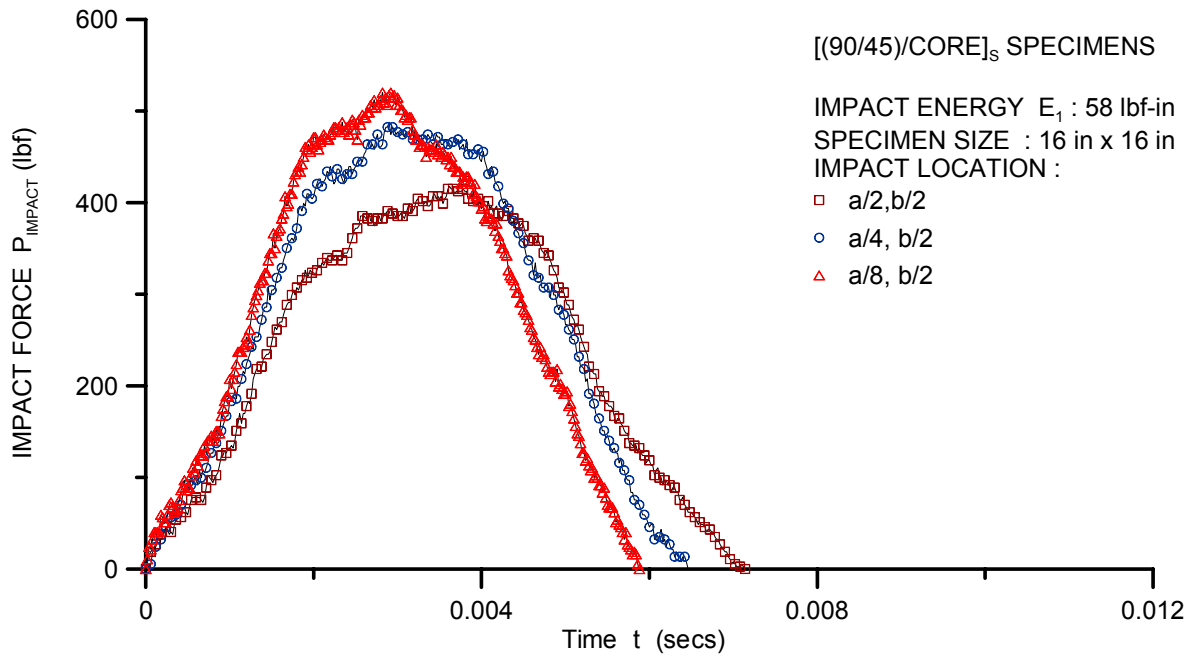


FIGURE A-17. FORCE-TIME HISTORY FOR [(90/45)/CORE]<sub>s</sub> SANDWICH PANELS IMPACTED AT ENERGY LEVEL  $E_1 = 58$  lbf-in (OFF-CENTER IMPACTS)

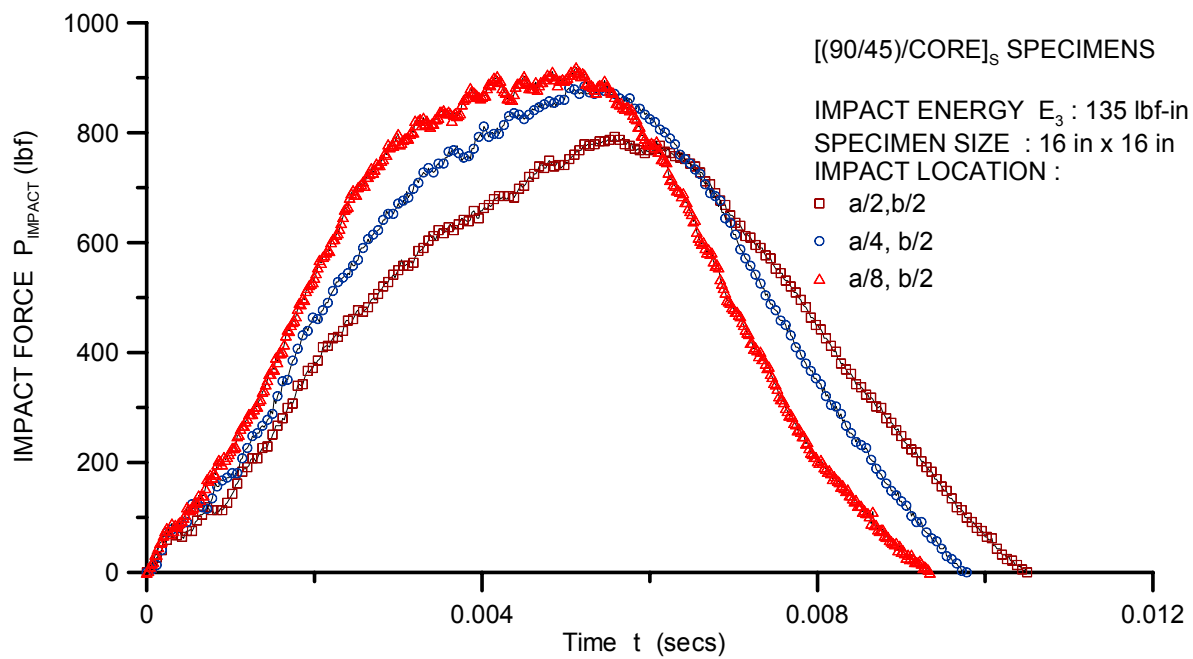


FIGURE A-18. FORCE-TIME HISTORY FOR [(90/45)/CORE]<sub>s</sub> SANDWICH PANELS IMPACTED AT ENERGY LEVEL  $E_3 = 135$  lbf-in (OFF-CENTER IMPACTS)

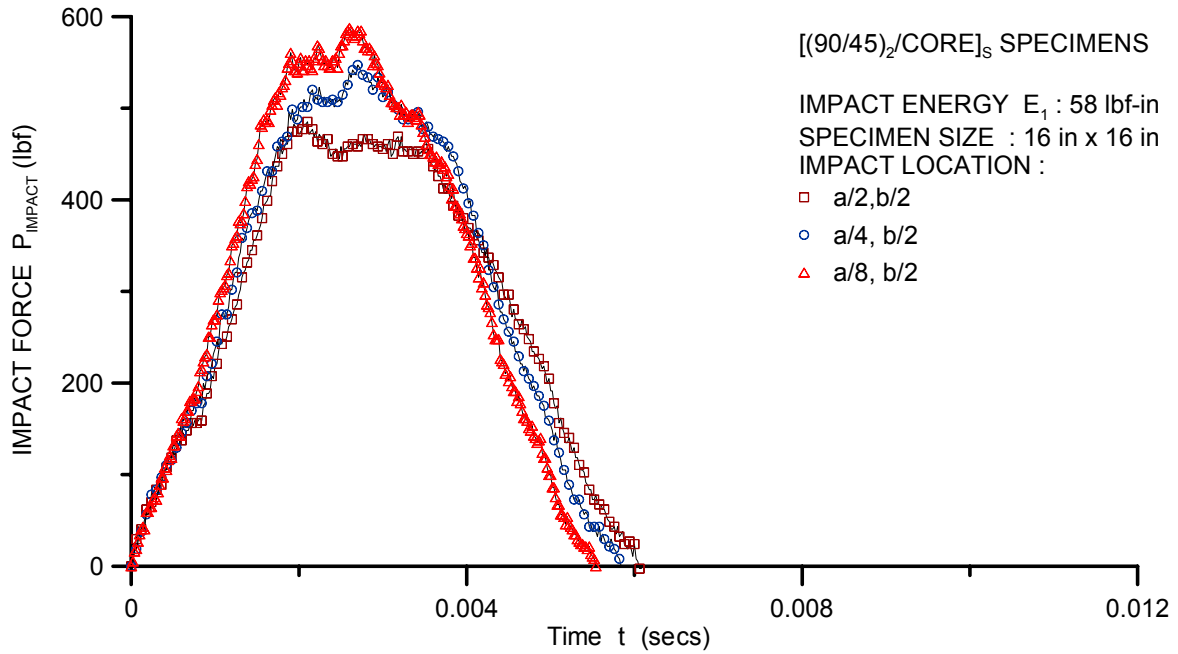


FIGURE A-19. FORCE-TIME HISTORY FOR [(90/45)<sub>2</sub>/CORE]<sub>s</sub> SANDWICH PANELS IMPACTED AT ENERGY LEVEL E<sub>1</sub> = 58 lbf-in (OFF-CENTER IMPACTS)

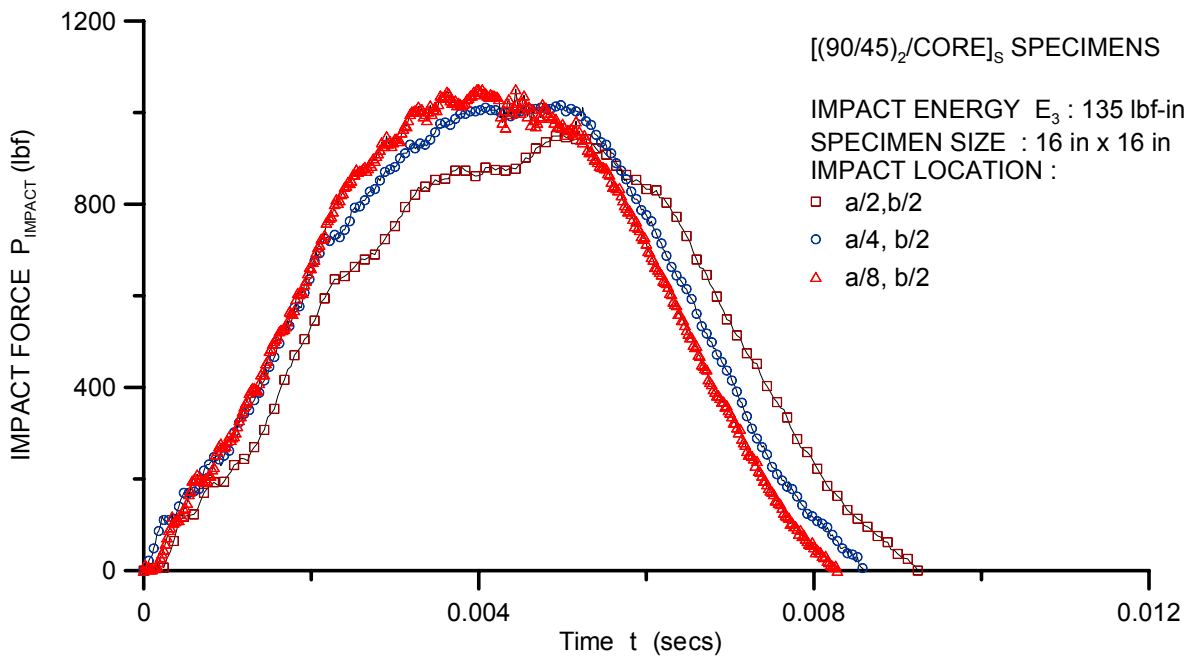


FIGURE A-20. FORCE-TIME HISTORY FOR [(90/45)<sub>2</sub>/CORE]<sub>s</sub> SANDWICH PANELS IMPACTED AT ENERGY LEVEL E<sub>3</sub> = 135 lbf-in (OFF-CENTER IMPACTS)

APPENDIX B—DISPLACEMENT AND STRAIN PROFILES USING ARAMIS

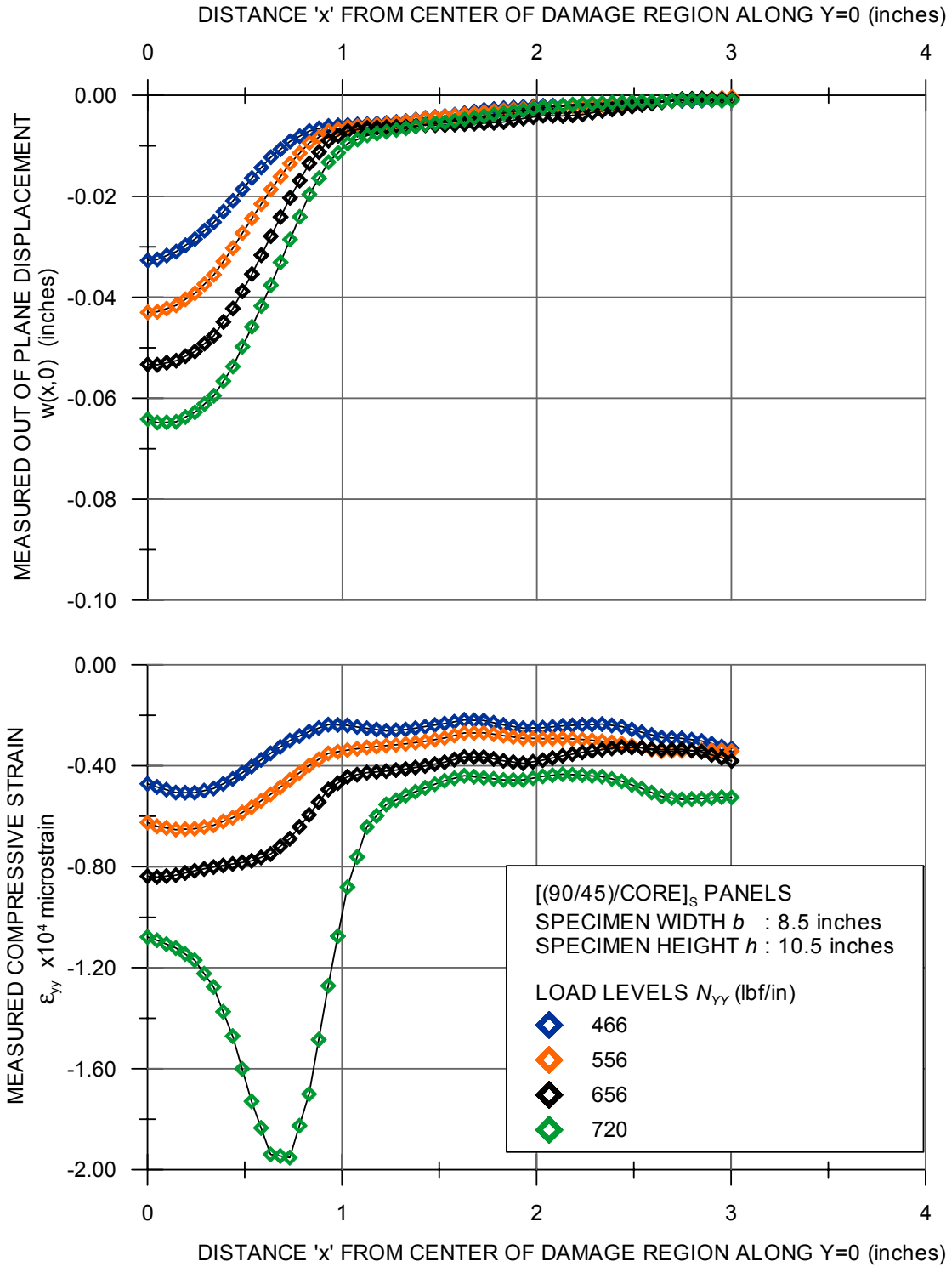


FIGURE B-1. DISPLACEMENT AND STRAIN PROFILES AT DIFFERENT LOAD LEVELS FOR [(90/45)/CORE]<sub>s</sub> SPECIMEN WITH WIDTH  $b = 8.5$  inches



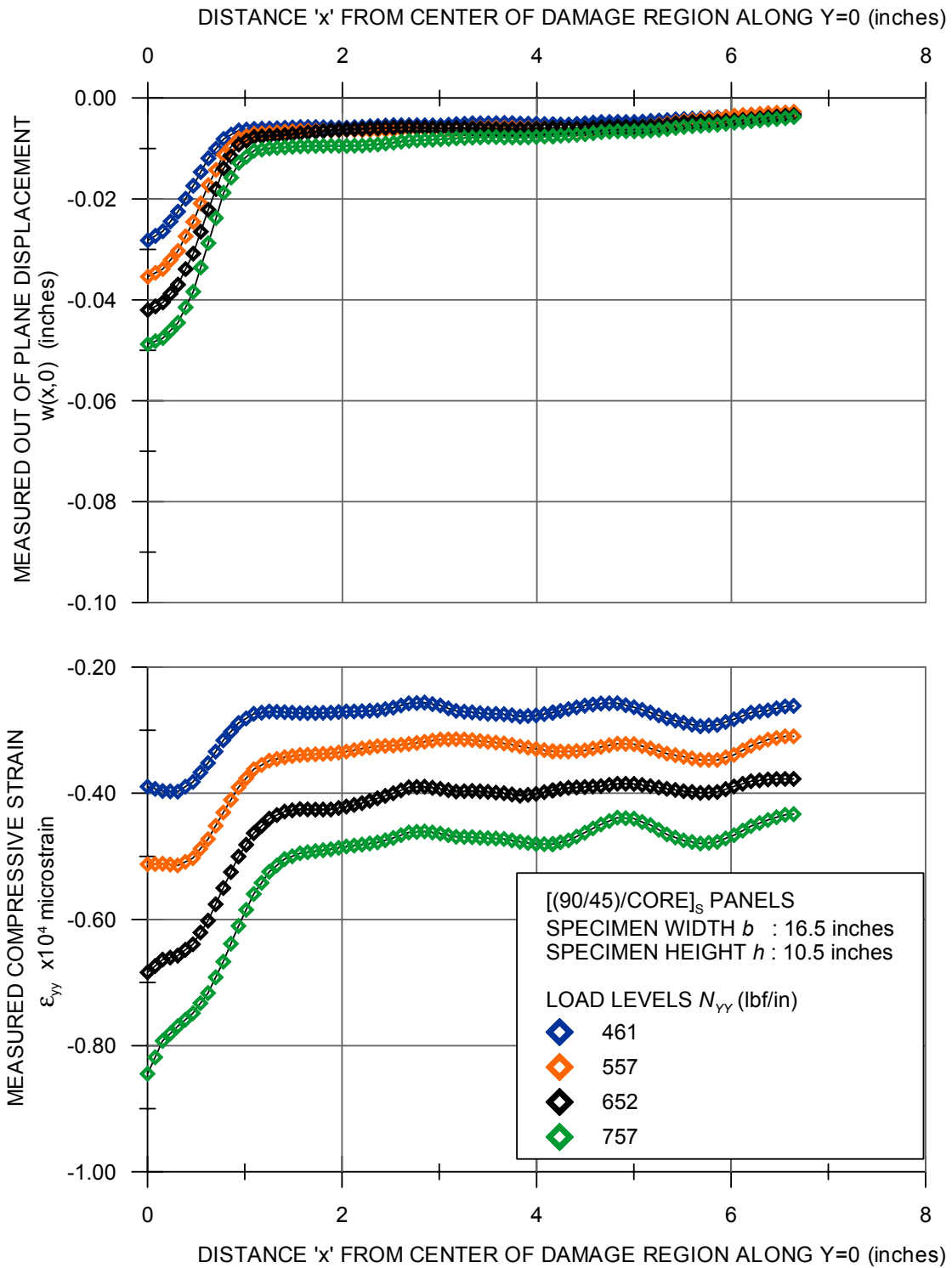


FIGURE B-3. DISPLACEMENT AND STRAIN PROFILES AT DIFFERENT LOAD LEVELS FOR [(90/45)<sub>2</sub>/CORE]<sub>s</sub> SPECIMEN WITH WIDTH  $b = 16.5$  inches

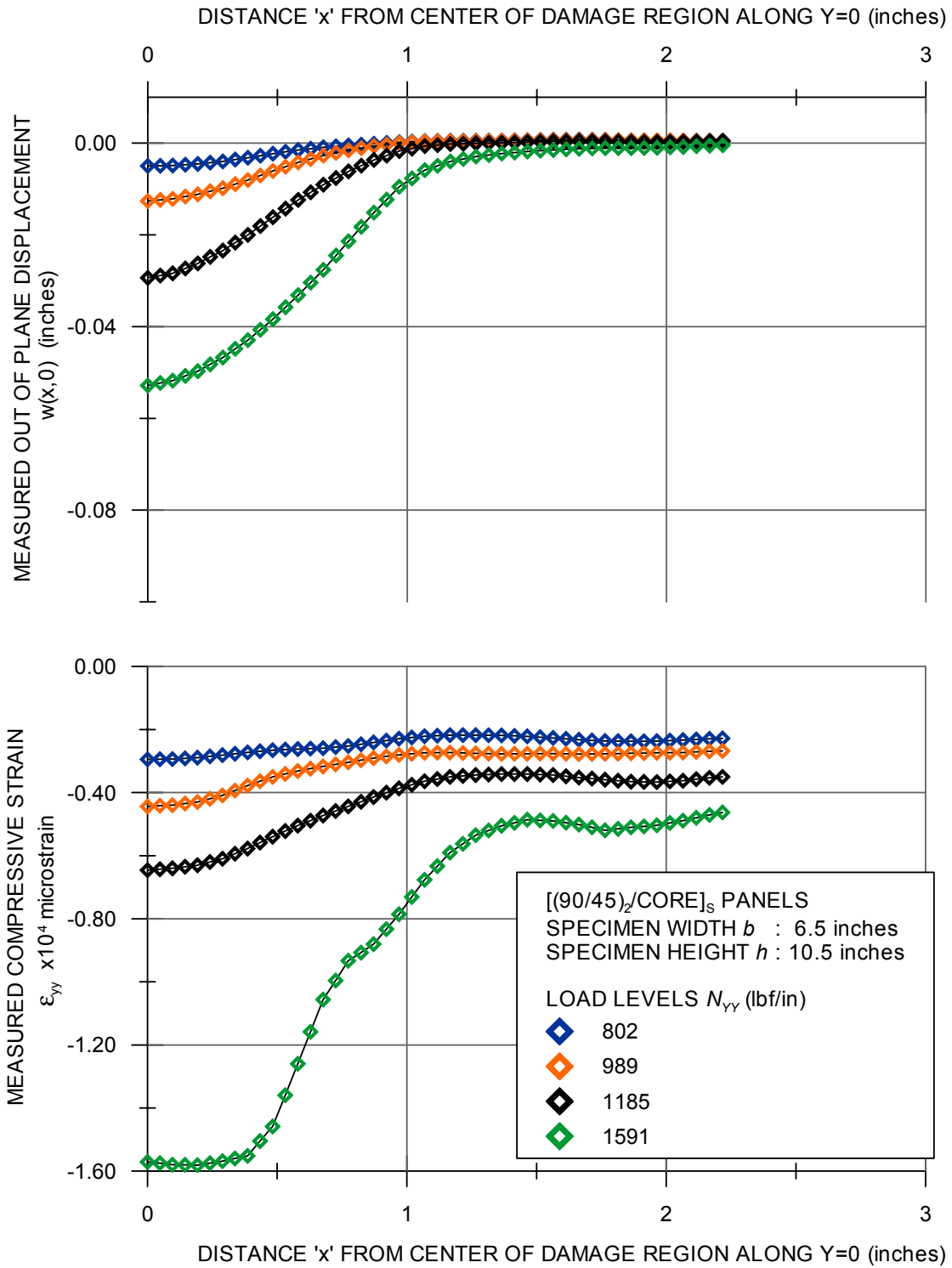


FIGURE B-4. DISPLACEMENT AND STRAIN PROFILES AT DIFFERENT LOAD LEVELS FOR [(90/45)<sub>2</sub>/CORE]<sub>s</sub> SPECIMEN WITH WIDTH  $b = 6.5$  inches

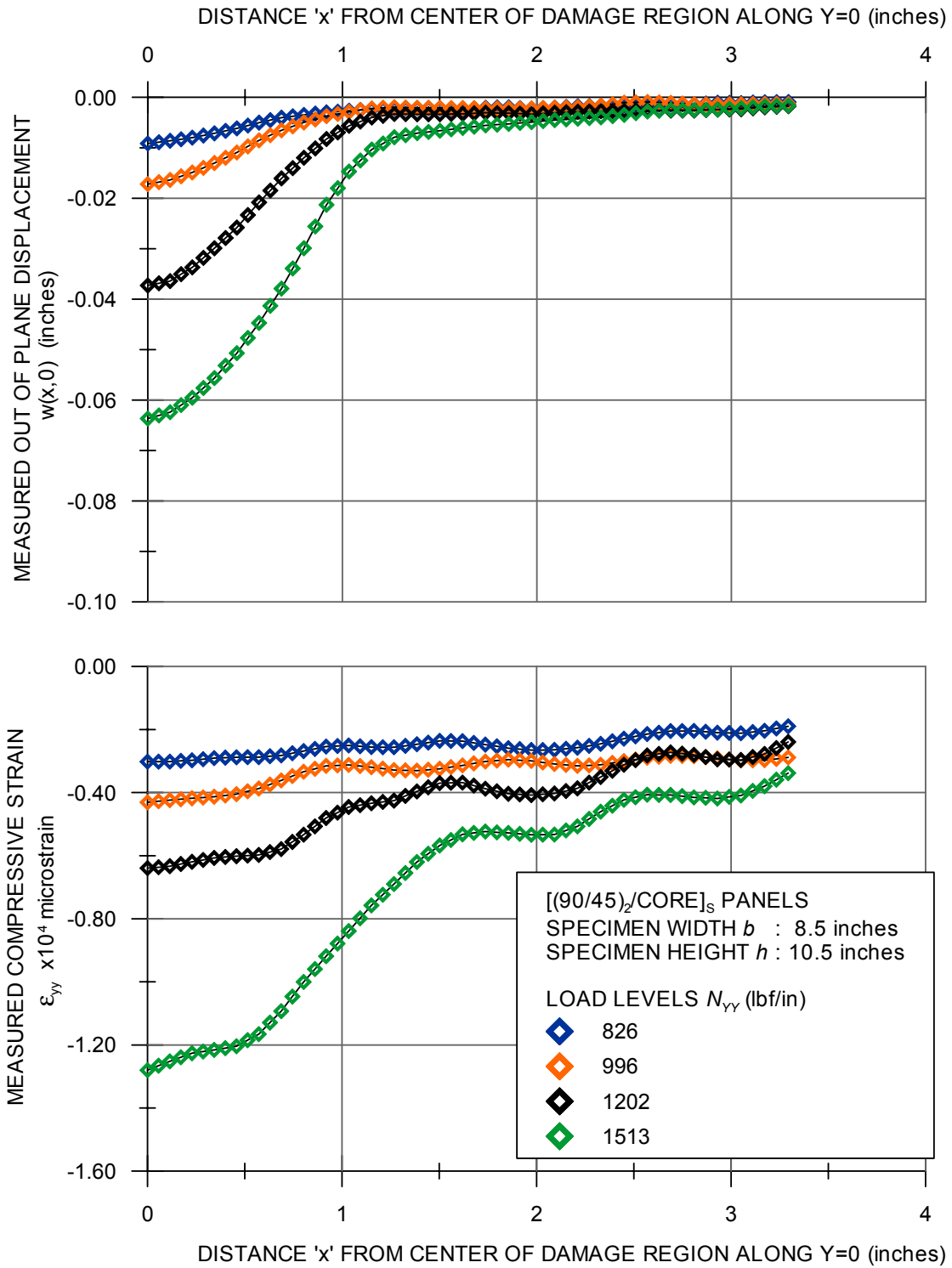


FIGURE B-5. DISPLACEMENT AND STRAIN PROFILES AT DIFFERENT LOAD LEVELS FOR [(90/45)<sub>2</sub>/CORE]<sub>s</sub> SPECIMEN WITH WIDTH  $b = 8.5$  inches



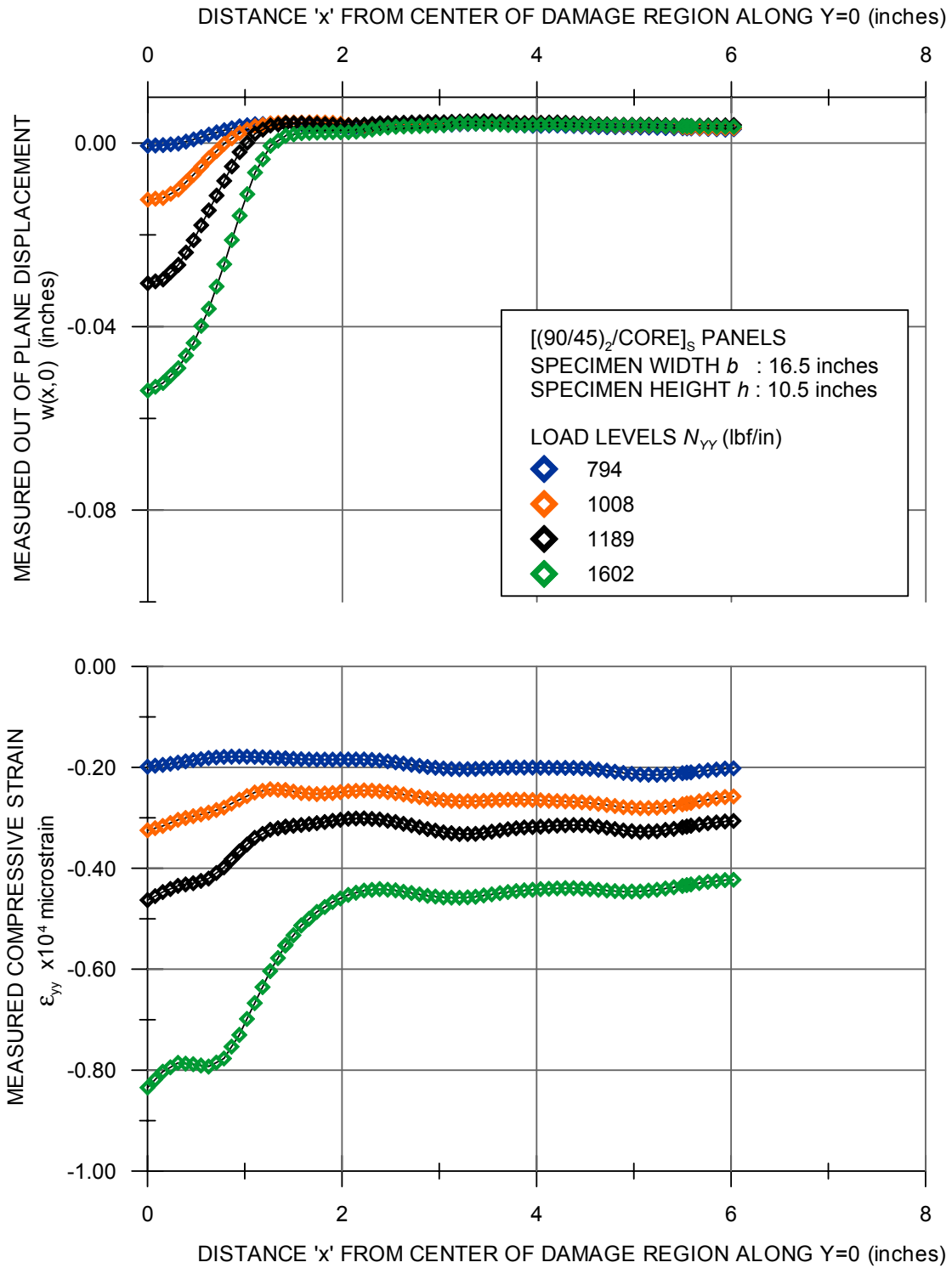


FIGURE B-7. DISPLACEMENT AND STRAIN PROFILES AT DIFFERENT LOAD LEVELS FOR [(90/45)<sub>2</sub>/CORE]<sub>s</sub> SPECIMEN WITH WIDTH  $b = 16.5$  inches